Optimization of a benzoylpiperidine class identifies a highly potent and selective reversible monoacylglycerol lipase (MAGL) inhibitor

Carlotta Granchi[a], *Margherita Lapillo*[a], *Sandra Glasmacher*[b], *Giulia Bononi*[a], *Cristina Licari*[a], *Giulio Poli*[a], *Maguie el Boustani*[c,d], *Isabella Caligiuri*[c], *Flavio Rizzolio*[c,e], *Jürg Gertsch*[b], *Marco Macchia*[a], *Filippo Minutolo*[a], *Tiziano Tuccinardi*[a,*], *Andrea Chicca*[b]

[a] Department of Pharmacy, University of Pisa, Via Bonanno 6, 56126 Pisa, Italy.

[b] Institute of Biochemistry and Molecular Medicine, NCCR TransCure, University of Bern, CH-3012 Bern, Switzerland.

[c] Pathology Unit, Department of Molecular Biology and Translational Research, National Cancer Institute and Center for Molecular Biomedicine, 33081 Aviano (PN), Italy.

[d] Doctoral School in Molecular Biomedicine, University of Trieste, 34100 Trieste, Italy.

[e] Department of Molecular Sciences and Nanosystems, Ca' Foscari University, 30123 Venezia, Italy.

* Corresponding author.

E-mail address: tiziano.tuccinardi@unipi.it

ABSTRACT

Monoacylglycerol lipase (MAGL) is the enzyme degrading the endocannabinoid 2-arachidonoylglycerol and it is involved in several physiological and pathological processes. The therapeutic potential of MAGL is linked to several diseases, including cancer. The development of MAGL inhibitors has been greatly limited by the side effects associated with the prolonged MAGL

inactivation. Importantly, it could be preferable to use reversible MAGL inhibitors *in vivo*, but nowadays only few reversible compounds have been developed. In the present study, structural optimization of a previously developed class of MAGL inhibitors led to the identification of compound **23**, which proved to be a very potent reversible MAGL inhibitor (IC_{50} = 80 nM), selective for MAGL over the other main components of the endocannabinoid system, endowed of a promising antiproliferative activity in a series of cancer cell lines and able to block MAGL both in cell-based as well as *in vivo* assays.

INTRODUCTION

The endocannabinoids system (ECS) is an endogenous system involved in many physiological and pathological processes. ECS is composed of two seven-transmembrane G protein-coupled receptors named cannabinoid receptors type 1 and type 2 (CB1, CB2),[1,2] a class of lipid signaling molecules called endocannabinoids (eCBs) and several biosynthetic and degrading enzymes that are involved in the production and transformation of these molecules. CB1 receptors are mainly expressed in the brain where they regulate the release of neurotransmitters from pre-synaptic neurons, whereas CB2 receptors are principally expressed in immune cells. Anandamide (AEA) and 2-arachidonoylglycerol (2-AG) are the two most abundant and well-studied eCBs,[3] which are biosynthesized on-demand from phospholipid precursors in the plasma membrane and released into the extracellular milieu.[4] After activating cannabinoid receptors, eCBs are transported into the cytoplasm via facilitated diffusion mediated by a putative endocannabinoid membrane transporter[5,6] and degraded by specific enzymes. AEA is hydrolyzed by fatty acid amide hydrolase (FAAH) in arachidonic acid and ethanolamine, whereas 2-AG is hydrolyzed into arachidonic acid and glycerol by monoacylglycerol lipase (MAGL) and α/β hydrolase-6 and -12 (ABHD6 and ABHD12). MAGL is the main degrading enzyme for 2-AG and it is responsible for approximately 85% of 2-AG hydrolysis in the brain, with a minor contribution of ABHD6 and ABHD12.[7,8] Several studies indicate the therapeutic potential of

selective FAAH and MAGL inhibitors in several disease models of inflammation, pain, anxiety and other neuroinflammatory diseases.[9–16] The inhibition of eCBs degradation represents a promising pharmacological strategy to activate the ECS limiting the potential side effects associated with direct receptor agonists.[7,17,18]

Many MAGL inhibitors were published[19] and patented[20] and some representative compounds are reported in Figure 1; however, most MAGL inhibitors reported to date in the literature are characterized by an irreversible binding mode. The irreversible mechanism of action shown by these inhibitors hampered their subsequent clinical development, since chronic administration of irreversible inhibitors, as well as genetic deletion of MAGL, provokes many negative effects *in vivo*. However, there are some recent noteworthy examples of irreversible inhibitors, endowed with a good pharmacokinetic profile and highly effective in reducing inflammation in vivo.[21,22] In some experimental studies reported in literature, sustained inactivation of MAGL by irreversible inhibition led to a loss of the therapeutic effects and a cross-tolerance to CB1 agonists in mice, accompanied by physical dependence. Moreover, prolonged MAGL inhibition provokes marked changes in some brain regions, such as CB1 receptor downregulation and desensitization, together with a reduction of the endocannabinoid-mediated synaptic plasticity. These effects are due to chronic MAGL inactivation in the central nervous system, provoking the maintenance of elevated 2-AG levels, which continuously activate and thus desensitize CB1 receptors in the brain, since this enzyme has a great impact on the brain ECS.[23] These just mentioned effects were observed *in vivo* by administration of irreversible inhibitors such as compound **1** (JZL184, 4-nitrophenyl-4-[bis(1,3-benzodioxol-5-yl)(hydroxy)methyl]piperidine-1-carboxylate, Figure 1), which is a very potent carbamate-based MAGL inhibitor.[24] Moreover, compound **2** (CAY10499, benzyl(4-(5-methoxy-2-oxo-1,3,4-oxadiazol-3(2*H*)-yl)-2-methylphenyl)carbamate, Figure 1) is a widely known irreversible MAGL inhibitor, used in many experimental studies concerning MAGL inhibition.[25] Despite the variety of irreversible MAGL inhibitors, at present their use is mainly limited as experimental tools in many studies. To the best of our knowledge, only a few reversible MAGL inhibitors are known and some

examples are reported in Figure 1. For example, natural terpenoids Euphol (compound **3**, Figure 1) and Pristimerin (compound **4**, Figure 1) were found to be potent MAGL inhibitors *in vitro* (IC_{50} values in the nanomolar range), although they were not selective, acting also on other targets different from MAGL.[26–28] Natural triterpenoid β-amyrin **5** (Figure 1) is a MAGL inhibitor structurally related to, although less potent than, Pristimerin and Euphol, but it also inhibits other enzymes that hydrolyse 2-AG, such as ABHDs.[29] In 2014, benzo[*d*][1,3]dioxol-5-ylmethyl 6-phenylhexanoate **6** (Figure 1) was reported by Hernández-Torres *et al.* as a potent, reversible and selective MAGL inhibitor. This compound was able to alleviate the clinical progression and the symptoms of a multiple sclerosis mouse model, without inducing catalepsy or other motor impairments, which were instead previously observed after the administration of irreversible MAGL inhibitors.[30] More recent examples of reversible MAGL inhibitors include derivative **7** (JZP-361, Figure 1), a nanomolar MAGL inhibitor that was characterized by a dual action, since it showed an anti-histaminergic activity, due to its high structural similarity to Loratadine, a histamine H_1 receptor antagonist.[31] Very recently, reversible MAGL inhibitor 1,5-diphenylpyrazole-3-carboxamide **8** (Figure 1) was reported to exert antiproliferative effects in cancer cell lines and to relieve the neuropathic hypersensitivity induced *in vivo* by oxaliplatin.[32] Moreover, compound **9** (Figure 2) is a benzoylpiperidine-based reversible MAGL inhibitor developed by our group in 2016 and it has been used as the starting point for the chemical optimization of the class of compounds reported in this paper.

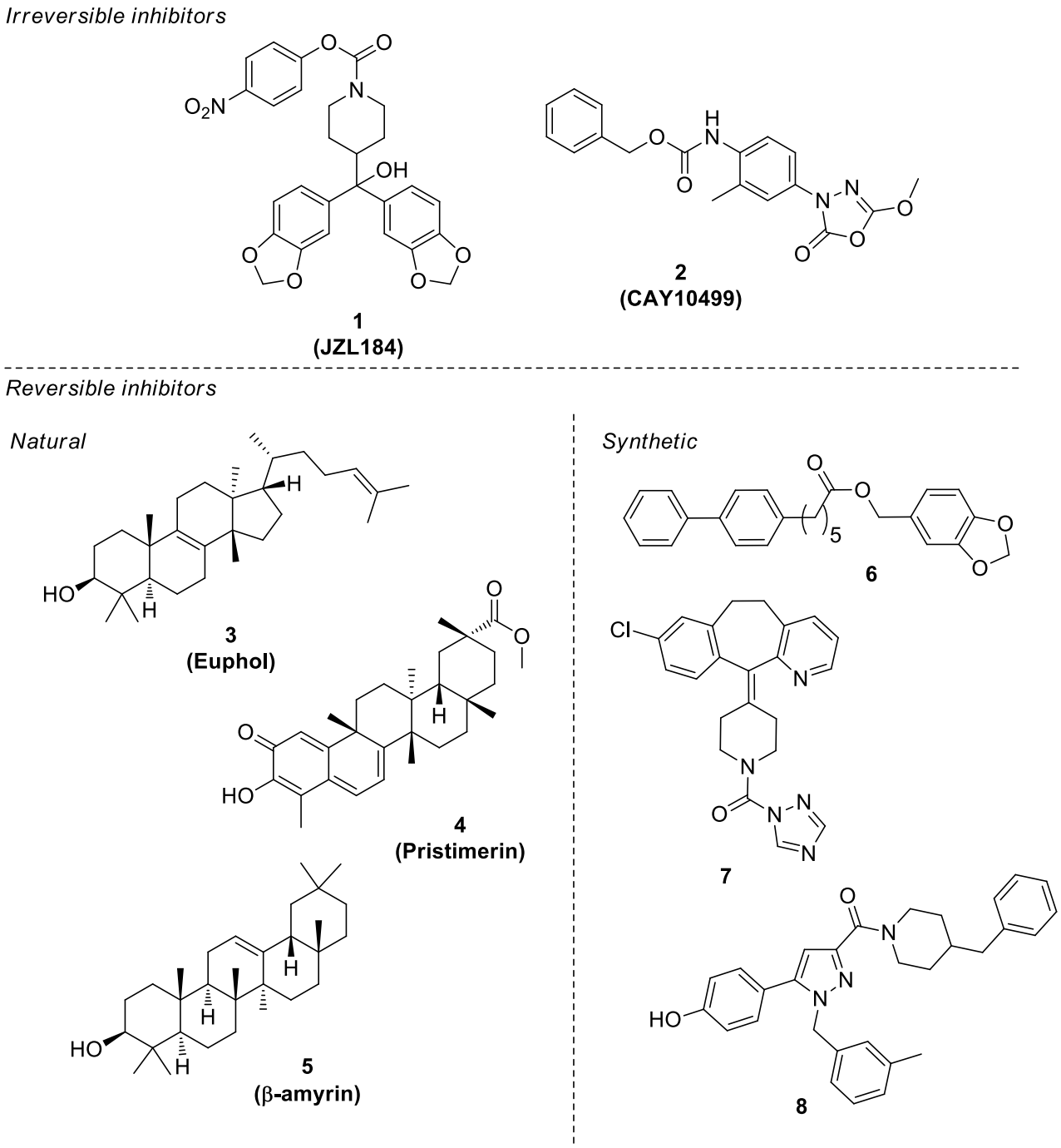

Figure 1. Structures of some of the most important known MAGL inhibitors.

RESULTS AND DISCUSSION

Design. In 2016, our group published the discovery of a chemical class of reversible MAGL inhibitors, based on a benzoylpiperidine scaffold, and within this class compound **9** (Figure 2) was

identified as the most potent inhibitor, showing an IC_{50} value of 0.84 μM, thus representing one of the first example of potent and selective reversible MAGL inhibitor.[33] The significant improvement of the inhibitory potency of this compound with respect to the other synthesized compounds is supposed to be due to a strategic hydrogen bond network established between the *meta*-hydroxyl group on the amidic phenyl ring of compound **9**, which replaces a structural water molecule observed in many MAGL X-ray structures, and a couple of active site residues (E53 and H272). Starting from this consideration, we were intrigued by the possibility to increase the acidity of the phenolic hydroxyl group of compound **9**, in order to strengthen the established hydrogen bonds and thus potentially lead to an increase in the inhibitory activity. At the same time, we took into account that this part of the molecule is located into a small pocket of the protein, where some polar residues are present, as suggested by modeling studies. Therefore, the insertion of bulky groups in the amidic phenyl ring is discouraged in order to avoid steric clashes and maintain the same binding disposition observed for compound **9**. On these bases, we started to modify compound **9** by adding halogen atoms (iodine, bromine, chlorine and fluorine atoms) in all the possible substitution positions of the amidic phenyl ring, due to their electron withdrawing properties and at the same time their different dimensions (Figure 2, panel A). This modification gave rise to compounds **10a-d**, **11a-d**, **12a-d** and **13a-d** (Figure 2, panel B) where iodine, bromine, chlorine and fluorine were inserted in the two possible *ortho* positions, in the *meta* or in the *para* positions with respect the phenolic hydroxyl group, still maintaining the 4-chlorobenzoylpiperidine portion on the other side of the molecule fixed. Regarding this last portion of compound **9**, molecular modeling studies suggested that the benzoyl moiety is directed toward the open cavity of the protein, pointing at the lipophilic channel of the enzyme (Figure 2, panel A). This consideration was confirmed by the good inhibition activity shown by a previously obtained analogue of **9**, where the *p*-Cl atom in the benzoyl ring was replaced by a second phenyl ring, which showed a 2-fold increase of inhibitory activity.[33] As an additional structural investigation, in the present work we have explored the possibility to fill the wide open enzymatic cavity, where the benzoyl part of compound **9** is located, with suitable groups. This purpose was achieved by removing

the chlorine atom from the benzoyl moiety (compound **14**, Figure 2, panel B) or replacing it with alkyl groups of different dimensions, such as methyl, ethyl, *n*-propyl, *i*-proyl or *n*-butyl (compounds **15-19**, Figure 2, panel B). Then, in order to verify whether this region preferentially hosts lipophilic groups, the *p*-Cl-phenyl was also replaced by more polar fragments, such as a phenolic ring, a benzodioxane and a 4-phenyl-morpholine moiety (compounds **20-22**, Figure 2, panel B).

Finally, we investigated the combinations of chemical modifications on both sides of the scaffold, such as: 1) the presence of a fluorine atom in *para* position to the phenolic hydroxyl group or to the amide carbonyl moiety, as in compounds **11d** and **13d**, respectively; 2) the presence of a *i*-propyl or *n*-butyl chain on the benzoyl ring, as in compounds **18** and **19**, respectively. The resulting compounds **23-26** (Figure 3) maintained the same central benzoylpiperidine scaffold and derived from the combination of different substituents in the two terminal portions of the parent compound **9** and they were synthesized accordingly.

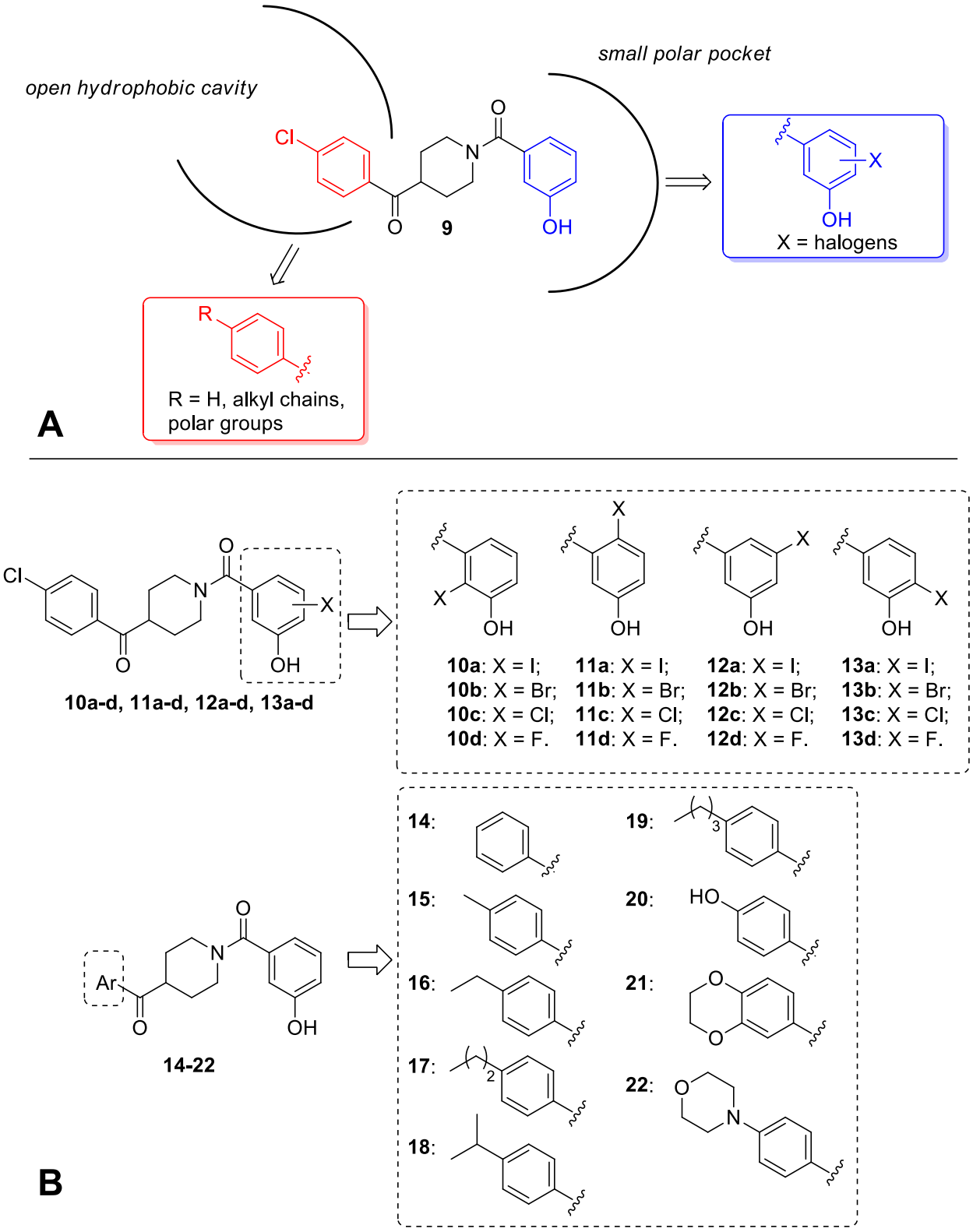

Figure 2. Design of new benzoylpiperidine derivatives. Upper panel (A): previously published starting compound **9** and its schematic location in the MAGL binding site: planned modifications of

the benzoyl part (in red) and the amidic moiety (in blue). Lower panel (B): newly synthesized compounds, modified in the amidic (**10a-d**, **11a-d**, **12a-d**, **13a-d**) and in the benzoyl (**14-22**) portions.

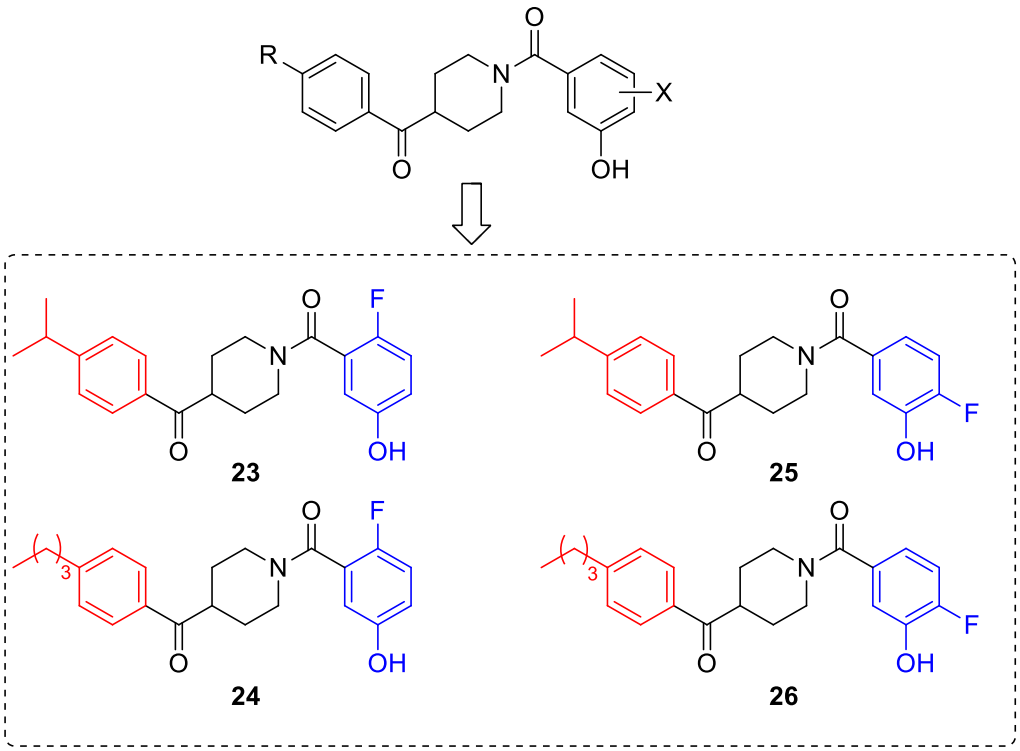

Figure 3. Design of new benzoylpiperidine derivatives: compounds **23-26** resulting from the combination of the best structural motifs present in compounds **10**-**22**.

Chemistry. For the synthesis of halogenated compounds, in most cases the starting halogenated carboxylic acids were commercially available and, therefore, they were directly submitted to the amidic condensation with the appropriate amine, as shown in Scheme 1. Basically, halogenated 3-methoxy-benzoic acids **27a**, **28** and **29a-f** were reacted with commercially available 4-(4-chlorobenzoyl)piperidine **30** in the presence of 1-[bis(dimethylamino)methylene]-1*H*-1,2,3-triazolo[4,5-*b*]pyridinium 3-oxid hexafluorophosphate (HATU) as the condensing agent, DIPEA as the base and dry *N*,*N*-dimethylformamide as the solvent, as previously reported,[33,34] to obtain the corresponding amidic derivatives **31**, **32** and **33a-f** (Scheme 1). Finally, the methoxy groups of these

intermediates were deprotected with boron tribromide to yield the final hydroxy-substituted compounds **10c**, **11b**, **12b-d** and **13b-d**. Just one case differs from the commonly adopted synthetic strategy, since we directly used the halogenated benzoic acid bearing the free phenolic group, in order to skip the last deprotection step. 2-Fluoro-3-hydroxybenzoic acid **27b** and piperidine derivative **30** straightforwardly furnished the final product **10d** (Scheme 1). However, the purification of this compound from the impurities formed in the reaction was not straightforward, finally resulting in a low reaction yield (23%). We believe that this problem was mainly due to the presence of a free phenolic OH group in precursor **27b**. Therefore, we slightly modified the synthetic strategy for the preparation of the other compounds of this series, by generally using the appropriate methoxylated benzoic acid in the amidic condensation reaction.

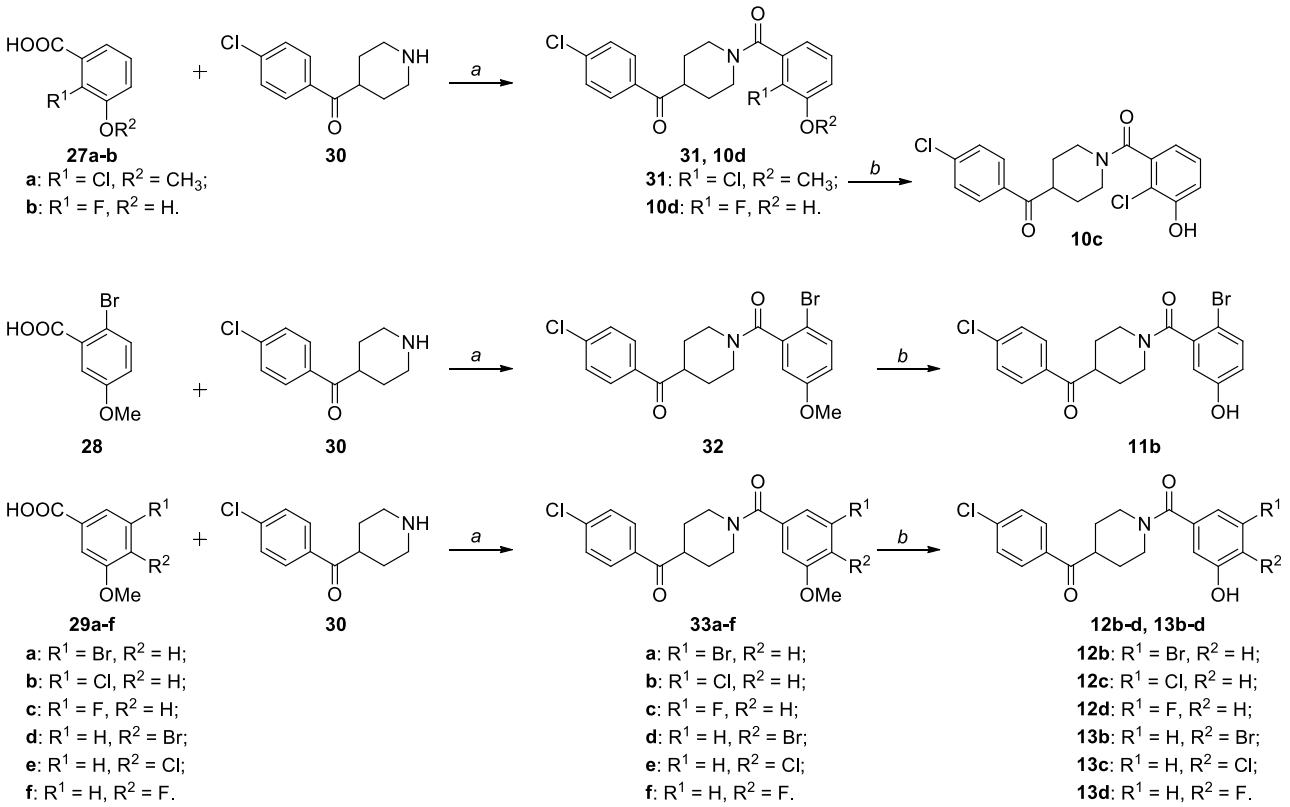

Scheme 1. Synthesis of halogenated derivatives **10c-d**, **11b**, **12b-d**, **13b-d**.

Reagents and conditions: (*a*) HATU, DIPEA, dry DMF, RT, 2-6.5 h [23-77%]; (*b*) 1M BBr_3, dry CH_2Cl_2, −10 to 0 °C, then RT, 1.5-4 h [40-81%].

In details, considering the just mentioned problems encountered with the amide formation starting from a hydroxy-substituted benzoic acid, and that in some cases benzoic acids or methyl benzoates bearing free phenolic hydroxyl groups were the only commercially available starting materials, we methylated the phenolic derivatives **34a-c** with methyl iodide by using potassium carbonate in DMF (Scheme 2). Under these conditions, both the carboxylic acid (if present, such as in compounds **34a,b**) and the hydroxyl groups were methylated and consequently, methoxylated methyl benzoates **35a-c** were hydrolyzed under aqueous basic conditions in order to obtain the free acids **36a-c**. At this point, the previously adopted reaction conditions were followed, which consisted in the amide condensation with compound **30** and the subsequent BBr_3-promoted deprotection of intermediates **37a-c** to obtain final compounds **11c-d** and **13a** (Scheme 2).

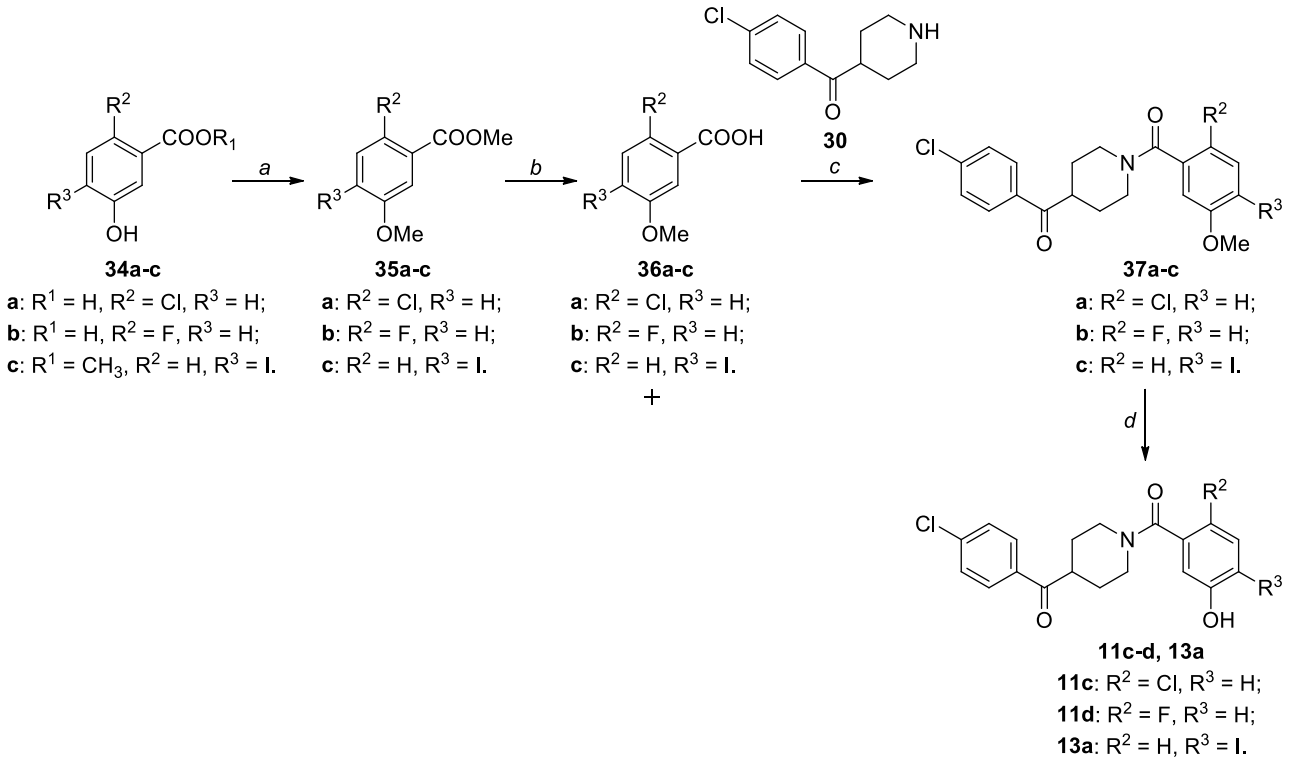

Scheme 2. Synthesis of halogenated derivatives **11c-d**, **13a**.

Reagents and conditions: (*a*) MeI, K_2CO_3, DMF, RT, 24 h [79-99%]; (*b*) aq. 2N LiOH, THF/MeOH 1:1 v/v, RT, overnight [95-99%]; (*c*) HATU, DIPEA, dry DMF, RT, 3-5 h [39-75%]; (*d*) 1M BBr_3, dry CH_2Cl_2, −10 to 0 °C, then RT, 1.5-7 h [33-88%].

An appropriate aniline derivative was used as the starting material instead of the halogenated precursor, when the latter was not commercially available. Hence, amino-substituted benzoic acids **38a-b** (Scheme 3) were converted to the corresponding methyl esters **39a-b** by refluxing them with thionyl chloride in methanol. Compounds **39a-b** and commercially available methyl-2-amino-5-methoxybenzoate **40** were reacted in a Sandmeyer reaction with the appropriate source of nucleophile (copper (I) bromide for compound **41b** or potassium iodide for compounds **41a, c, d**) to obtain halogenated compounds **41a-d**. Methyl esters **41a-d** were hydrolyzed to benzoic acids **42a-d**, which were then condensed with 4-(4-chlorobenzoyl)piperidine **30** to get amides **43a-d**. The final *O*-demethylation reaction furnished the last groups of halogenated benzoylpiperidine derivatives **10a-b**, **11a** and **12a** (Scheme 3).

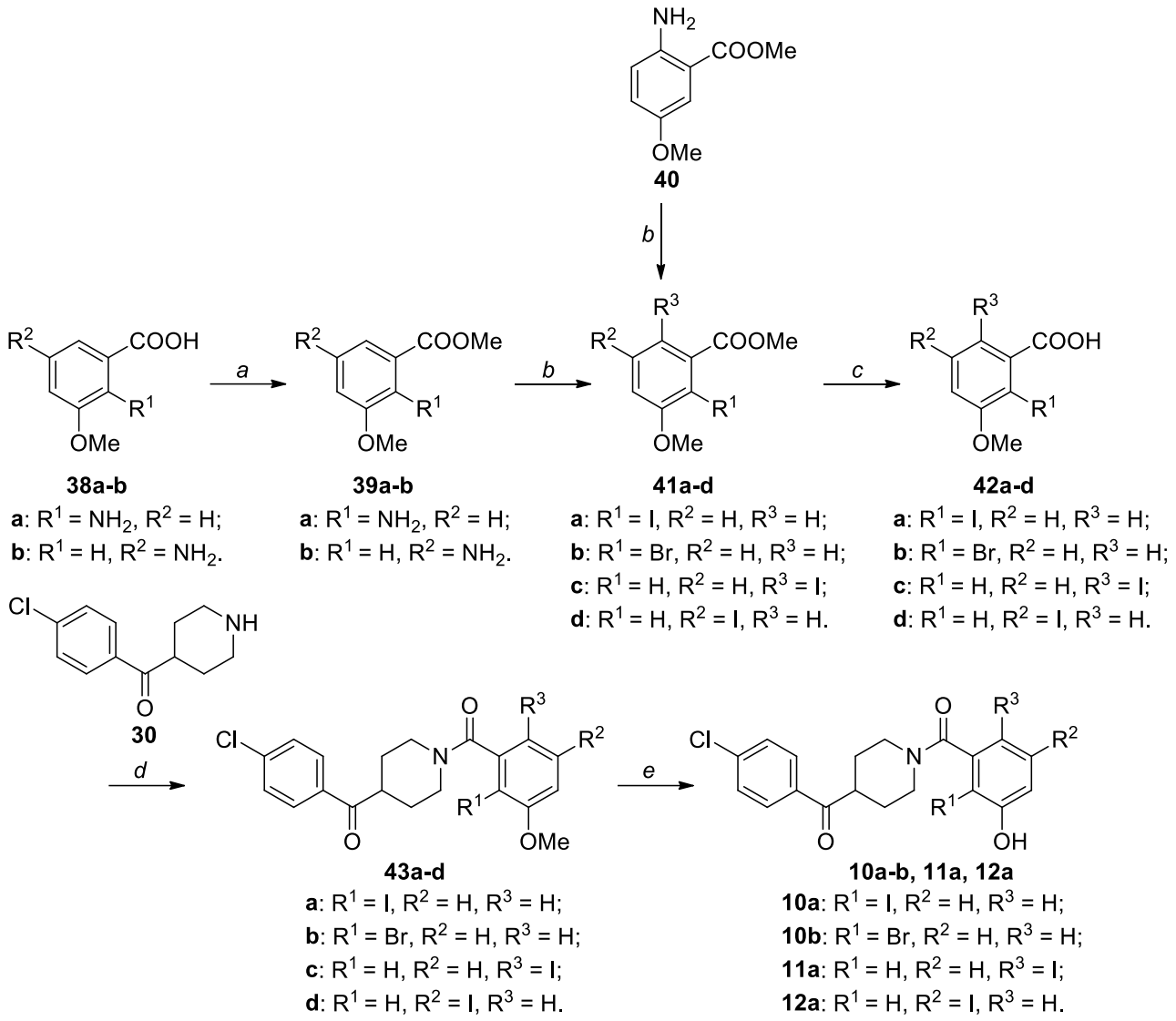

Scheme 3. Synthesis of halogenated derivatives **10a-b**, **11a**, **12a**.

Reagents and conditions: (*a*) $SOCl_2$, MeOH, reflux, 3-24 h [**39a**: 69%, **39b**: 97%]; (*b*) if R = I (**41a**, **c**, **d**): KI, $NaNO_2$, H_2SO_4, H_2O, - 5 °C to RT, 1-3 h; if R = Br (**41b**): CuBr, HBr 48%, $NaNO_2$, H_2O, dioxane, - 5 °C to RT, then 110 °C, 5 h [25-78%]; (*c*) aq. 2N LiOH, THF/MeOH 1:1 v/v, RT, overnight [64-99%]; (*d*) HATU, DIPEA, dry DMF, RT, 3-5 h [43-60%]; (*e*) 1M BBr_3, dry CH_2Cl_2, −10 to 0 °C, then RT, 1.5-4.5 h [24-94%].

Compounds **14-21** bearing different aromatic groups in the place of the *para*-chlorobenzoyl ring of the previous series of derivatives were obtained according to the synthetic pathway outlined in Scheme 4. Commercially available isonipecotic acid **44** was acetylated on the piperidine nitrogen

atom by using acetic anhydride in pyridine to obtain compound **45**, which was then converted to the corresponding acyl chloride by refluxing it with thionyl chloride in dichloroethane, and then reacted in a Friedel-Crafts reaction with the appropriate aromatic moiety, in the presence of aluminum chloride in dichloroethane. The aromatic systems utilized in this step were either a simple benzene ring (**46a**) or mono-substituted aromatic rings with alkyl chains of increasing length, such as toluene (**46b**), ethylbenzene (**46c**), *n*-propylbenzene (**46d**), cumene (**46e**) or *n*-butylbenzene (**46f**). More polar groups were also inserted, such as an anisole (**46g**) and a benzo-1,4-dioxane moiety (**46h**). After the different functionalization of the piperidine portion, hydrolysis under aqueous basic conditions and heating removed the acetyl group, thus making the piperidine nitrogen atom free to react with 3-methoxybenzoic acid **48** to get the corresponding amides **49a-h**. The final demethylation step afforded compounds **14-21**; in particular, it should be noticed that the two antipodal methoxy groups of compound **20**, one in *meta* position of the amidic phenyl ring and the other in *para* position of the benzoyl ring, were both converted to free hydroxyls.

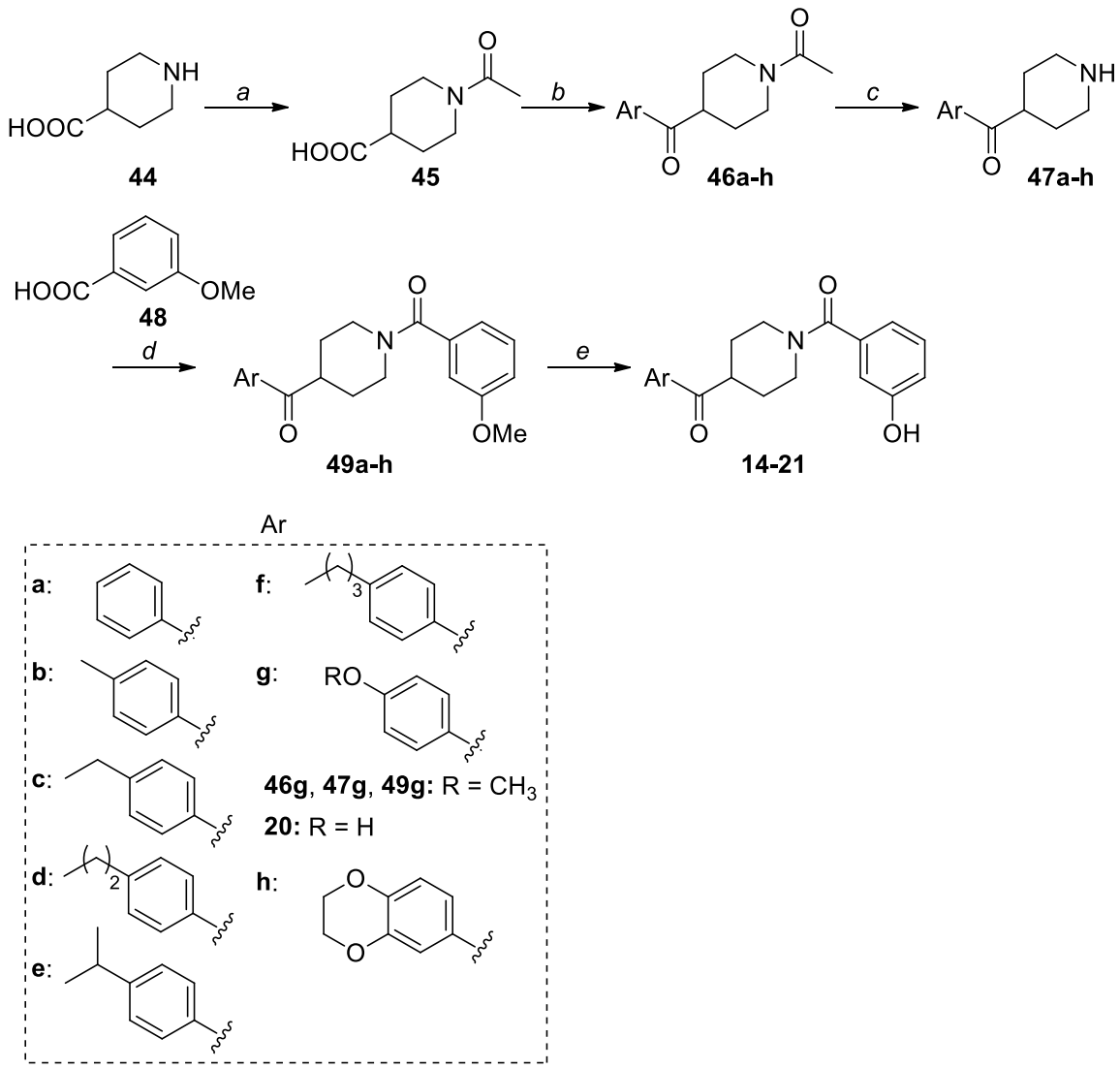

Scheme 4. Synthesis of aryl-substituted derivatives **14-21**.

Reagents and conditions: (*a*) Ac_2O, pyridine, 140 °C, 2 h [85%]; (*b*) *i.* $SOCl_2$, dry 1,2-DCE, 60 °C, 4 h; *ii.* appropriate aromatic system, $AlCl_3$, dry 1,2-DCE, 90 °C, overnight [43-76%]; (*c*) NaOH 1N, EtOH, 90 °C, overnight [66-95%]; (*d*) HATU, DIPEA, dry DMF, RT, 2-3 h [33-97%]; (*e*) 1M BBr_3, dry CH_2Cl_2, −10 to 0 °C, then RT, 1-2.5 h [43-76%].

Slight synthetic modifications were used for the preparation of morpholine-substituted derivative **22** (Scheme 5), when compared to the procedure used for the synthesis of compounds **14-21**. The piperidine nitrogen atom of isonipecotic acid **44** was protected by benzoylation and then its acyl chloride was reacted with bromobenzene in a Friedel-Crafts reaction to obtain compound **53**. This

bromo-derivative was subjected to a C-N coupling reaction with morpholine in the presence of tris(dibenzylideneacetone)dipalladium as the catalyst and XPhos as the ligand, by using potassium phosphate as the base under heating conditions, in order to replace the bromine atom with the morpholine ring. The protection of the piperidine nitrogen with a benzoyl group instead of the previous acetyl moiety was due to the harsh conditions in which this intermediate was subjected during the coupling reaction: our intent was to avoid the unwanted hydrolysis of the protecting amide group by using a quite resistant protecting group such as the benzoyl instead of the acetyl. Once the benzamide group was removed by basic hydrolysis for prolonged times, piperidine **55** was condensed with 3-methoxybenzoic acid **48** and finally the methoxy group was converted to the free phenolic OH to give final compound **22** (Scheme 5).

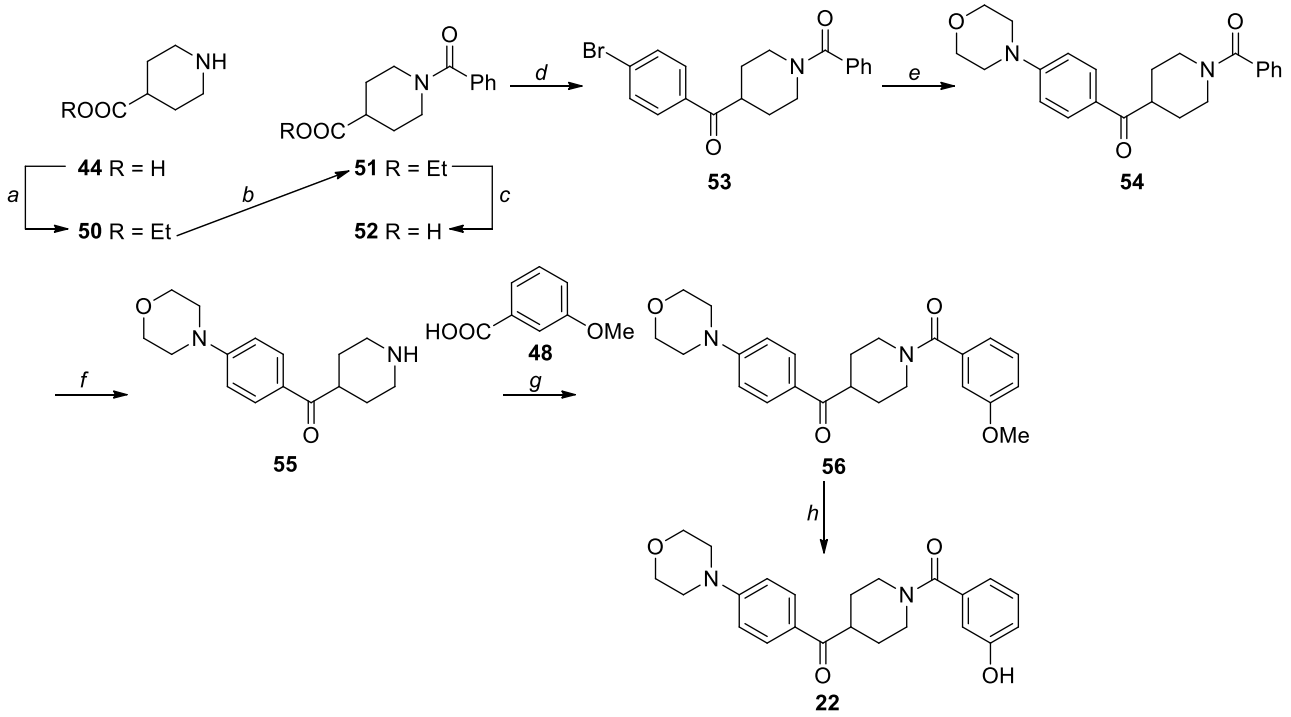

Scheme 5. Synthesis of derivative morpholine-substituted derivative **22**.

Reagents and conditions: (*a*) $SOCl_2$, EtOH, reflux, 3 h [74%]; (*b*) benzoyl chloride, Et_3N, dry DCM, RT, overnight [93%]; (*c*) NaOH, EtOH/H_2O, RT, overnight [99%]; (*d*) *i.* $SOCl_2$, dry 1,2-DCE, 60 °C, 4 h; *ii.* PhBr, $AlCl_3$, dry 1,2-DCE, 90 °C, overnight [43%]; (*e*) morpholine, $Pd_2(dba)_3$, XPhos, K_3PO_4,

toluene, 100 °C, 20 h [63%]; (*f*) NaOH 1N, EtOH, 95 °C, overnight [72%]; (*g*) HATU, DIPEA, dry DMF, RT, 3 h [99%]; (*h*) 1M BBr_3, dry CH_2Cl_2, −10 to 0 °C, then RT, 1.5 h [27%].

Finally, we combined the structural portions that gave the best results in enzymatic assays (see below): the *i*-propyl and *n*-butyl chains were favored as substituents in the benzoyl ring and *o*-/*p*-F-phenolic portions were chosen in the other terminal benzamide portion. Therefore, amines **47e** and **47f**, which were prepared as displayed in Scheme 4, were reacted either with benzoic acids **36b**, synthesized as outlined in Scheme 2, or with commercially available compound **29f** (Scheme 1), since it was observed that a fluorine atom in *para* to the phenolic hydroxyl group on the amidic phenyl ring or to the amide carbonyl group was beneficial for MAGL inhibition potency. The corresponding amides (**57**, **58** and **59**, **60**) were converted to the final compounds by BBr_3-promoted demethylation of the methoxy groups, to give compounds **23-26** (Scheme 6).

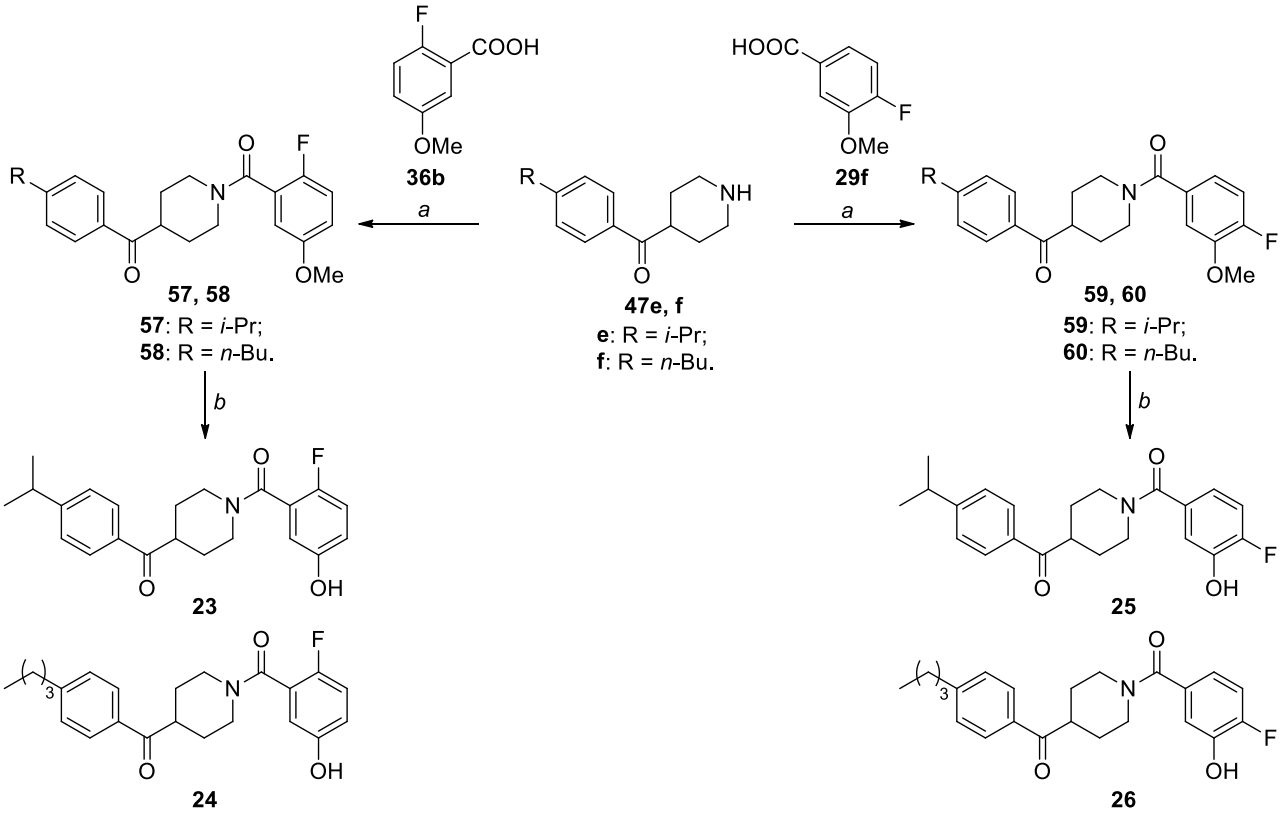

Scheme 6. Synthesis of compounds **23-26**.

Reagents and conditions: (*a*) HATU, DIPEA, dry DMF, RT, 3 h [86-93%]; (*b*) 1M BBr_3, dry CH_2Cl_2, −10 to 0 °C, then RT, 1-1.5 h [17-87%].

Analysis of ^1H and ^{13}C-NMR spectra of some of these benzoylpiperidine derivatives confirmed the presence of two rotational conformers generated by the hindered rotation around the C-C bond between the amidic phenyl ring and the carbonyl group nearby, as previously observed by us for similar compounds.[33] The splitting of ^1H and ^{13}C-NMR signals was observed for compounds bearing bulkier halogen atoms in the *ortho* position to the amidic carbonyl group, such as I (**10a** and **11a**), Br (**10b** and **11b**) and Cl (**10c** and **11c**). Conversely, the presence of a smaller fluorine atom in the same position, as in compounds **10d** and **11d**, led to the presence of a unique species detected by NMR, and this fact may be explained by considering the smaller size of the fluorine atom, which allows a free rotation around the above-mentioned C-C bond.

Enzymatic assays and molecular modeling. The newly synthesized compounds were evaluated for their inhibition potency in human MAGL by using an enzymatic assay in which 4-nitrophenylacetate was used as the substrate and the absorbance values relative to the amount of the formed product 4-nitrophenol were measured at 405 nm. The IC_{50} values obtained for the new series of compounds were compared with those of two reference inhibitors: the previously published (4-(4-chlorobenzoyl)piperidin-1-yl)(3-hydroxyphenyl)methanone (**9**), which represents the parent compound of this new class of derivatives, and the irreversible MAGL inhibitor CAY10499 (**2**), which is one of the most potent MAGL inhibitors present in literature. The MAGL inhibition activity data for the first series of compounds, halogenated derivatives **10a-d**, **11a-d**, **12a-d** and **13a-d**, are reported in Table 1. It is evident that the presence of the halogen atom in the *meta* or *ortho* position to both the amidic carbonyl moiety and the phenolic hydroxyl group (**12a-d** and **10a-d**, respectively) was not satisfactory for the MAGL inhibitory activity, because the IC_{50} values of these compounds

were only in the micromolar range. In particular, they were greater than 1 μM for compounds **12a-d** and even greater than 5 μM for compounds **10a-d**, thus resulting to be less active than original compound **9**. On the contrary, the other two substitution positions led to very positive effects in some cases. In fact, the shift of the halogen atom to the *para* position to either the amidic carbonyl moiety (**13a-d**) or the phenolic hydroxyl group (**11a-d**) generally produced more potent inhibitors and highlighted a possible trend: the inhibitory activity increased in parallel with the electron withdrawing property of the halogen present in the molecule, since it gradually increased going from iodine- (**11a, 13a**) to bromine- (**11b, 13b**), chlorine- (**11c, 13c**) and fluorine- (**11d, 13d**) substituted compounds. In particular, in the series of compounds **11a-d**, iodine and bromine led to IC_{50} values in the range of 2.4-2.5 μM, but when the halogen atom was a chlorine the activity of the resulting compound **11c** increased (IC_{50} value of 960 nM). This effect was even more pronounced in the presence of a fluorine atom, such as in compound **11d**, whose IC_{50} value was of 240 nM, thus reaching a higher inhibition potency than that of parent compound **9**. Similarly, in the series **13a-d** we observed an evident improvement by passing from iodine (IC_{50} = 1.3 μM) to bromine and chlorine (IC_{50} = 457 and 424 nM, respectively) and finally reaching the best inhibition activity in this group of halogenated benzoylpiperidines with the insertion of a fluorine atom in *para* to the amidic carbonyl group in compound **13d**, which showed an IC_{50} value of 389 nM (Table 1). The above-mentioned MAGL inhibition improvement given by fluorine atom in two specific positions of the amidic phenyl ring may rely on the small size and the powerful electron withdrawing property of fluorine. This atom is an isoster of hydrogen, but additionally it increases the acidity of the neighboring phenolic OH, stabilizing the anionic form, the phenoxide, thus leading to a highly polarized hydroxyl and, consequently, to the formation of stronger hydrogen bonds involving this group. The negative charge on the phenoxide can be delocalized on the carbons in *para* or *ortho* positions, that correspond to the same carbon atoms where the fluorine atom is bound (compounds **11d** and **13d**), thus contributing to a further stabilization of the charge. On the contrary, considering the two possible *ortho* positions to the phenolic OH, the one in which F is in the middle between the carbonyl and the phenolic OH leads

to negative results for the inhibition activity (compound **10d**). This effect could be rationalized by considering that the steric bulk in compound **10d** induces a plausible block of rotation around the adjacent C-C bond, thus preventing an ideal approach of the hydroxyl group to the protein residues involved in the hydrogen bond network.

Table 1. *In vitro* inhibitory activity on MAGL (IC_{50}, nM)[a] of halogenated derivatives **10a-d**, **11a-d**, **12a-d**, **13a-d**.

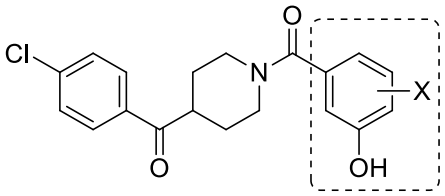

Compounds			X	IC_{50} (nM)
10	**a**	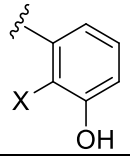	I	5300 ± 200
	b		Br	8200 ± 300
	c		Cl	8700 ± 500
	d		F	12300 ± 600
11	**a**	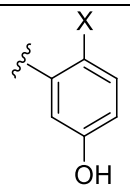	I	2500 ± 400
	b		Br	2400 ± 300
	c		Cl	960 ± 50
	d		F	240 ± 26
12	**a**	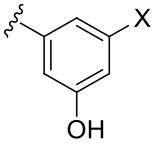	I	1400 ± 200
	b		Br	1300 ± 200
	c		Cl	1100 ± 100
	d		F	1300 ± 200
13	**a**	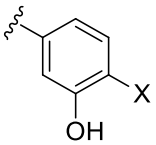	I	1300 ± 100
	b		Br	457 ± 6
	c		Cl	424 ± 46
	d		F	389 ± 15
9		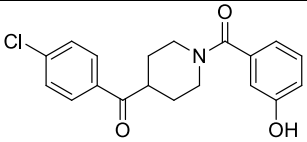		840 ± 40
CAY10499				134 ± 15
JZL184				49.3 ± 3.9
KML29				3.0 ± 0.1

[a] Enzymatic values are the mean of three or more independent experiments, performed in duplicate.

With the aim of investigating the effect of the introduction of halogen atoms in different positions of the amidic phenyl ring of the benzoylpiperidine derivatives, the compounds showing the most interesting structure-activity relationship (SAR) have been analyzed through molecular modeling studies, thus evaluating their binding mode within MAGL and the impact of their different substitution pattern on the ligand-protein interactions. In particular, compounds **11d** and **10d**, presenting the highest and lowest MAGL inhibitory activity, respectively, among the halogenated derivatives, were subjected to a robust docking procedure (see the Experimental section for details), which further confirmed the reliability of the binding mode already predicted for the parent inhibitor **9**. In fact, these two ligands shared a very similar disposition within the protein, with the 4-chlorobenzoyl moiety directed toward the entrance of the catalytic site and showing lipophilic interactions with L148, L205, L213 and L241 already observed for compound **9**.[33] Moreover, the carbonyl oxygen of **10d** and **11d** forms H-bonds with the backbone nitrogen of A51 and M123. The fluorophenol ring of the ligands is placed within the small pocket of the enzyme binding site, sandwiched between Y194 and V270 that form lipophilic interactions with the inhibitors (Figure 4). Interestingly, the docking calculations suggested that only compound **11d** was able to form the H-bond network with E53 and H272 through its hydroxyl group, as predicted for the parent compound **9**. In fact, the fluorophenol ring of compound **10d** was predicted to be about 180° rotated with respect to that of **11d**, with the hydroxyl group pointing toward the inner side of the binding site cavity, far from both E53 and H272. In this orientation, the hydroxyl group can only form an H-bond with the side chain of R57 (Figure 4B). This difference in the binding mode predicted for the two derivatives might be ascribed to the steric hindrance that would occur between the fluorine atom and the central piperidine core of **10d** if its fluorophenol ring assumed the opposite orientation in order to place the OH group in close proximity to the E53/H272 pair. Moreover, a repulsive electrostatic interaction between the highly electronegative fluorine atom and the close carboxylic group of E53 would need to be overcome for allowing the formation of the H-bond between E53 and the ligand hydroxyl group. Such steric and electrostatic factors could make this binding mode energetically unfavorable for **10d**,

compared to that displayed in Figure 4B. Therefore, the consequential loss of the H-bond network with E53 and H272 could explain the drop of activity observed for compound **10d** with respect to **11d**.

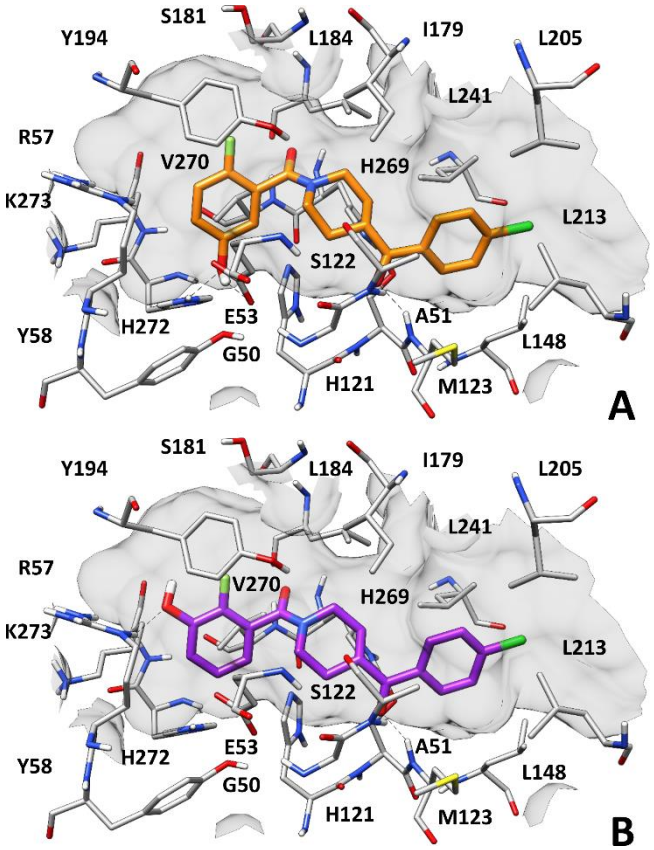

Figure 4. Docking results of compounds **11d** (A) and **10d** (B) into MAGL (PDB code 3PE6).

In order to analyze the binding modes proposed for the two compounds from an energetic point of view, the predicted **11d**-MAGL and **10d**-MAGL complexes were further studied through a 101 ns molecular dynamics (MD) simulation protocol followed by ligand-protein binding energy evaluations performed using the Molecular Mechanics-Generalized Born Surface Area (MM-GBSA) method (see the Experimental section for details). The MD studies confirmed the reliability of the predicted binding modes, as both compounds maintained their disposition within MAGL catalytic site during the simulations. The last 80 ns of MD simulation were employed to estimate the binding free energies

associated with the two ligand-protein complexes. The results of the energetic evaluations were found to be consistent with the experimental activities of the compounds and further confirmed the reliability of the predicted ligand binding modes. In fact, the ligand-protein binding energy calculated for compound **11d** (-61.3 kcal/mol) exceeded of about 11 kcal/mol the binding energy predicted for **10d** (-50.4 kcal/mol), in agreement with the remarkably higher MAGL inhibition activity of **11d** compared to **10d** (Table S1). The whole computational protocol including docking, MD simulations and binding free energy evaluations was then employed to evaluate and analyze the binding mode of compound **13d**, which showed an IC_{50} value for MAGL inhibition considerably close to that determined for compound **11d**. As expected, compound **13d** showed a binding disposition very similar to that predicted for **11d**, consistently with the very similar activity of the two compounds. In particular, compound **13d** was able to form the H-bond network with E53 and H272 through its hydroxyl group (Figure S1). In agreement with the experimental data, free energy evaluations performed on MAGL in complex with **13d** predicted a ligand-protein binding energy of -61.0 kcal/mol, comparable to that calculated for the **11d**-MAGL complex, thus supporting the reliability of the binding mode predicted for the *p*-fluoro derivative **13d**.

The inhibition activity results obtained for compounds **14-22**, which are variously substituted on the ketone part of the scaffold, are reported in Table 2. The removal of the chlorine atom of compound **9** led to compound **14**, possessing an unsubstituted benzoyl ring, but this modification was not beneficial for the inhibition activity on MAGL, resulting in an IC_{50} value of about 2.2 μM. On the other hand, the insertion of alkyl groups of increasing dimensions – going from a methyl group (compound **15**) to a *n*-butyl chain (compound **19**) – generated a progressive improvement of the inhibitory activity. However, this behavior was subjected to a sort of "plateau": after an initial decrease of the IC_{50} values from methyl, to ethyl and *n*-propyl chain of compounds **15**, **16** and **17** (IC_{50} = 368, 194 and 162 nM, respectively), the best results were reached by *i*-propyl (**18**) and *n*-butyl (**19**)-substituted compounds that showed nearly the same IC_{50} values (138 and 136 nM, respectively),

thus indicating a limit in the increase of the activity induced by the increase of the dimension of the alkyl chain. Moreover, it is worth noting that compounds **18** and **19** were not only more potent than parent compound **9**, but their IC_{50} values were comparable to that of irreversible inhibitor **CAY10499** and were only about 3-fold less active than **JZL184.** With regards to compound **KML29**,[35] it was about 46-fold more active than compounds **18** and **19**. The presence of polar groups in the place of the aliphatic chains, such as a phenol (**20**), a benzodioxane (**21**) or a morpholine ring (**22**), was detrimental for the enzyme inhibition activity of the resulted compound, which raised to values in the micromolar range (in the range of 1-10 μM), thus suggesting that the insertion of polar moieties in this position is strongly disadvantageous for MAGL inhibition.

Table 2. *In vitro* inhibitory activity on MAGL (IC_{50}, nM)[a] of compounds **14-22**.

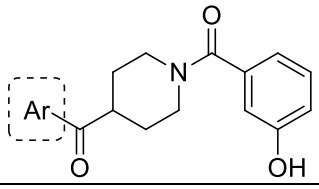

Compounds		IC_{50} (nM)
14	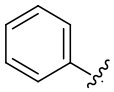	2200 ± 200
15	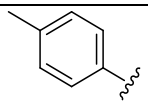	368 ± 25
16	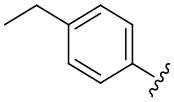	194 ± 19
17	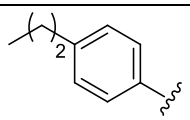	162 ± 5
18	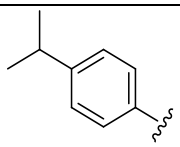	138 ± 9
19	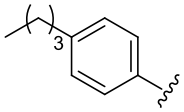	136 ± 9

20	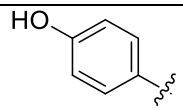	10200 ± 1100
21	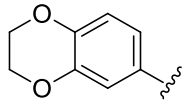	1000 ± 100
22	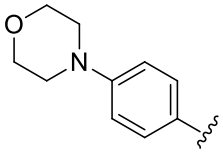	5000 ± 900
9	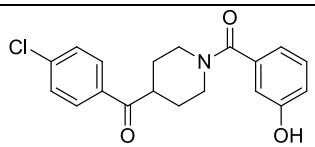	840 ± 40

[a] Enzymatic values are the mean of three or more independent experiments, performed in duplicate.

Considering the inhibitory activities of the compounds belonging to the two previous series of MAGL inhibitors (Table 1 and 2), we selected the more potent inhibitors with the aim of combining the best structural modifications in new molecules. Therefore, the presence of a fluorine atom in *para* position to the amidic carbonyl group (compound **13d**) or to the phenolic hydroxyl group (compound **11d**), as well as the insertion of a *n*-butyl (compound **19**) or *i*-propyl (compound **18**) chain on the ketone-type benzoyl ring were the most promising modifications, which were therefore combined to obtain "hybrid" compounds **23-26** (Table 3). These new four compounds showed IC_{50} values in the nanomolar range, which were comparable to, or even better than, those of the original compounds which inspired their design. In fact, compounds **25** and **26** (IC_{50} = 110 and 262 nM, respectively), bearing a common *p*-F,*m*-OH-benzamido motif, were more active than their simpler analogue **13d** (IC_{50} = 389 nM). However, **26** was less potent than its *n*-butyl-substituted non-fluorinated analogue **19** (IC_{50} values of 262 and 136 nM, respectively), whereas the inhibition potency of **25** was quite similar to that of its *i*-propyl-substituted non-fluorinated analogue **18** (IC_{50} values of 110 and 138 nM, respectively). The strongest synergistic effect was observed in compounds **23** and **24**, which both shared a common *o*-F,*m*-OH-benzamido portion. In fact, **23** and **24** gave IC_{50} values of 80 and 74 nM, respectively, thus being remarkably more active than their close analogues **11d**, **18** and **19**. These

two new compounds were also found to be more potent than both reference compounds **9** and **2**. Therefore, **23** and **24** currently represent the most active benzoylpiperidine-based MAGL inhibitors.

Table 3. *In vitro* inhibitory activity on MAGL (IC_{50}, nM)[a] of compounds **23-26**, **57**.

Compounds		IC_{50} (nM)
23	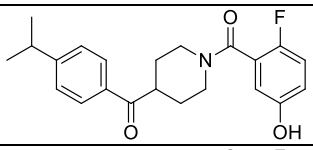	80 ± 12
24	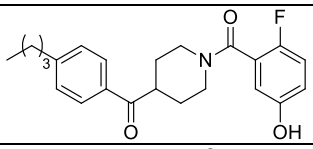	74 ± 1
25	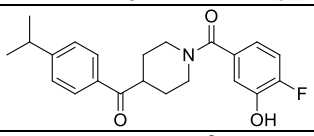	110 ± 8
26	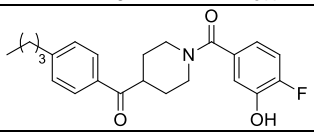	262 ± 26
57	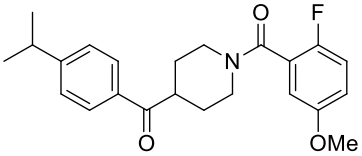	2600 ± 400
9	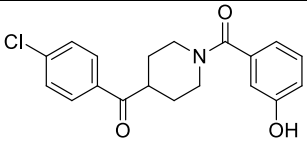	840 ± 40

[a] Enzymatic values are the mean of three or more independent experiments, performed in duplicate.

Finally, in order to confirm the importance of the phenolic hydroxyl group, which was maintained fixed in all synthesized derivatives, we tested the methoxylated precursor of compound **23**, compound **57** (Scheme 6, Table 3). The decrease of activity of compound **57** was evident, since it displayed an IC_{50} value of 2.6 μM, compared to its analogue **23** with the free OH (IC_{50} = 80 nM), thus confirming that the hydroxyl group is essential for the interaction with MAGL, as previously suggested by modeling studies.[33] In order to have information about the lipophilic properties of the herein reported

compounds, an evaluation of the log*P* has been carried out. Table S2 shows the consensus log*P* values obtained through the Chemicalize tool. None of the analyzed compounds showed a log*P* value higher than five and, furthermore, no evident correlation between log*P* and activity of the different compounds was observed; in fact, by plotting the log*P* values against the measured pIC_{50} values of the ligands a correlation (R^2) lower than 0.2 was obtained. In order to confirm the hypothesized reversible mechanism of inhibition, the effects of dilution and preincubation on the inhibitory activity of compound **23** were evaluated. In the presence of an irreversible mechanism of inhibition, the potency should not decrease after dilution, whereas for a reversible inhibition, the potency level should be strongly reduced after dilution.[36] Therefore, the inhibition produced by incubation with a 4000 nM concentration of **23** was measured after a 40X dilution and compared to the potency observed by a 4000 nM and a 100 nM of compound **23**. The results showed in Figure 5A supported a reversible mechanism of inhibition, since the inhibition produced by 100 nM of this compound was similar to that obtained after a 40X dilution and was considerably lower than that produced by the same compound at a concentration of 4000 nM. As a second assay, the inhibition activity of **23** was measured at different preincubation times with MAGL. Compound **23** was preincubated with the enzyme for 0, 30 and 60 min before adding the substrate to start the enzymatic reaction. An irreversible inhibition should produce a higher potency after longer incubation times, whereas a reversible inhibitor should produce a constant inhibition potency over all the different incubation times. As shown in Figure 5B, this test agreed with the reversible property of **23**, as it showed a very similar activity for the three different incubation times.

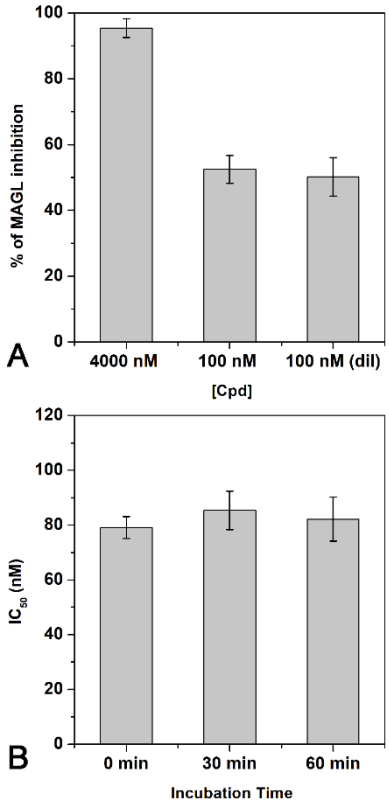

Figure 5. Analysis of the mechanism of MAGL inhibition by compound **23**-MAGL inhibition analysis. A) Dilution assay: the first two columns indicate the inhibition percentage of compound **23** at a concentration of 4000 nM and 100 nM. The third column indicates the inhibition percentage of compound **23** after dilution (final concentration = 100 nM). B) IC_{50} (nM) values of **23** at different preincubation times with MAGL (0 min, 30 min and 60 min).

Once we verified the reversible mechanism of inhibition of compound **23**, its mode of inhibition was then evaluated by measuring Michaelis–Menten kinetics at various inhibitor concentrations. The dataset was plotted as substrate concentration *versus* enzyme activity and analyzed by applying the mixed-model inhibition fit of GraphPad Prism 5.0, which includes competitive, uncompetitive, and noncompetitive inhibition terms. This model evaluates the V_{max}, K_m and the α parameter, which is indicative of the inhibition mechanism. When α corresponds to one, the inhibitor does not alter the binding of the substrate to the enzyme, and the mixed-model can be considered as a noncompetitive

inhibition. When α is a very large value, the inhibitor interaction prevents the substrate binding and the mixed-model corresponds to a competitive inhibition. Finally, when α is a very small value, the binding of the inhibitor increases the binding of the substrate and the mixed model corresponds to an uncompetitive model. Kinetic studies indicate for **23** a K_i value of 39 ± 4 nM and an α value greater than 10000, thus supporting a competitive behavior for this compound (Figure 6).

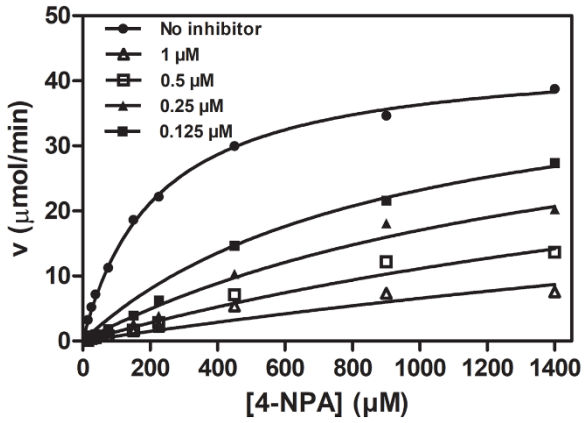

Figure 6. Inhibition of the activity of MAGL and competitive nature of compound **23** (K_i = 39 ± 4 nM, α >10000). 4-NPA = 4-nitrophenylacetate.

The binding mode of the most promising derivative of the series compound **23**, which showed the best activity in the cell-based assay and selectivity profile (see also following sections), was studied through the same robust docking procedure applied on **10d**, **11d** and **13d**. As expected, the predicted disposition of compound **23** within MAGL catalytic site, as well as its H-bond interactions with the binding site residues (Figure 7), were highly similar to those predicted for compound **11d**. The predicted MAGL-**23** complex was further studied through the same MD simulation protocol applied on the other derivatives, in order to evaluate the reliability of the predicted ligand-protein interactions (see the Experimental section for details). The ligand was found to maintain its binding disposition with remarkable stability during the whole simulation, showing an average root-mean-square

deviation (RMSD) from its initial coordinates about 1.4 Å (Figure S2 in the Supporting Information). The H-bond analysis revealed very stable H-bonds with A51 and E53, which were kept for more than 95% of the whole MD simulation, and a strong H-bond with H272 maintained for about 80% of the MD. Moreover, in agreement with the results obtained for compound **9**, compound **23** only partially maintained the interaction with M123 in favor of an additional H-bond with S181 that was formed for almost 90% of the MD (Table S3 in the Supporting Information). A deeper analysis of the ligand-protein interactions was then carried out with the aim of identifying which residues play a key role for the ligand inhibitory potency, thus providing a better interpretation of SAR data. For this purpose, the MM-GBSA approach was used to perform binding free energy evaluations with pairwise per-residue energy decomposition, thus calculating the contribution to the ligand binding affinity of each single amino acid constituting the MAGL catalytic site located in the surroundings of the ligand in its predicted binding mode.[37,38] This analysis, which was performed on the last 80 ns of MD simulation, highlighted E53 as a fundamental residue for the activity of the ligand (Figure 7), since the free energy contribute of the single **23**-E53 interaction corresponds to –9.6 kcal/mol out of an overall binding energy of –64.9 kcal/mol. These data further confirmed the importance of the hydroxyl group for the inhibitory potency of compound **23** and its analogues, in agreement with the experimental results herein reported. Other residues that mostly contribute to the total interaction energy were found to be A51 and Y194 (–4.6 kcal/mol), as well as L241 (around –4.0 kcal/mol): in fact, A51 forms a particularly stable H-bond with the carbonyl oxygen of the ligand (Table S3), the aromatic portion of Y194 shows a π-π stacking with the ligand benzamide moiety, whereas the side chain of L241 establishes extensive hydrophobic interactions with both the phenyl and the isopropyl group of the ligand oriented toward the solvent exposed region of the binding site. Finally, among the other residues showing a considerable impact on ligand-protein binding affinity we found other hydrophobic residues, such as I179 and V270, as well as polar residues S181 and H272, which form strong H-bonds with the inhibitor and appeared as key amino acids for the inhibitory potency of this series of compounds. Interestingly, none of the protein residues surrounding the ligand showed an

unfavorable contribute to the ligand-protein binding energy in the free energy decomposition calculation. The prediction of the pK_a value for the phenolic oxygen (pK_a = 8.6) confirmed that at physiological pH the undissociated form is the most prevalent (97.7% of the total population) with respect to the deprotonated one (2.3% of the total population).

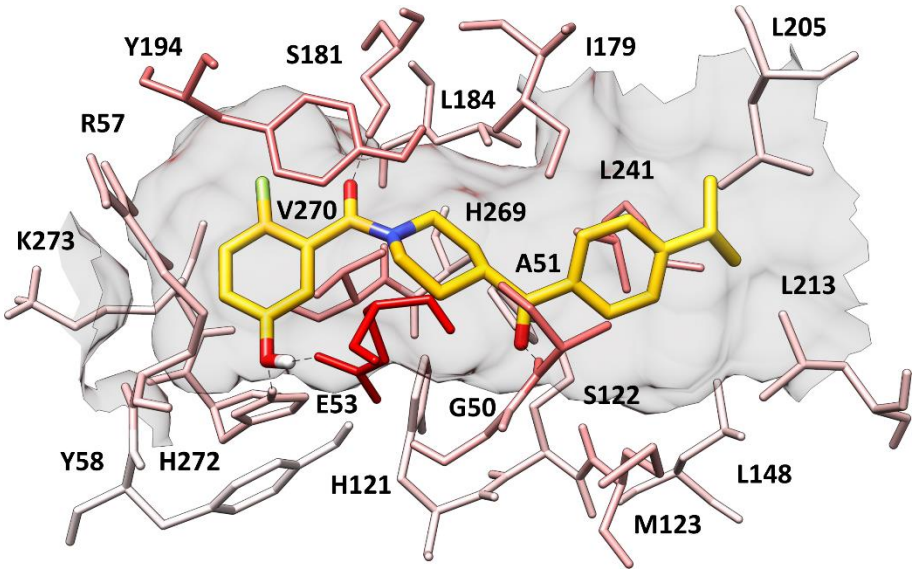

Figure 7. Minimized average structure of **23** within MAGL catalytic site. The residues are colored on the basis of their contribute to the ligand-protein binding affinity (red = highest, white = lowest) (PDB code 3PE6).

Finally, in order to verify the possible inhibition of cytochrome P450 (CYP) enzymes, compound **23** was analyzed by means of the CypRules prediction online server, which is able to predict the potential inhibition properties of ligands against CYP1A2, CYP2D6, CYP2C19, CYP2C9 and CYP3A4 that account for 90% of the xenobiotic and drug metabolism in human body.[39] From this prediction analysis the compound did not show to potentially inhibit any of the analyzed cytochromes. With regards to the main most probable atomic site of the molecule that will be modified during CYP-mediated metabolism, the analysis carried out by using the Xenosite prediction tool suggests that the isopropyl fragment is the most susceptible group to CYP-modifications (see Figure S3).[40]

Selectivity. Compound **23-26** were further profiled for their selectivity towards the other components of the ECS. As shown in Table 4, at 10 μM none of the compounds significantly bound to CB1 and CB2 receptors or inhibited ABHD6 and ABHD12. The most potent MAGL inhibitors **23** and **24** did not significantly inhibit FAAH activity at 10 μM, whereas **25** and **26** blocked AEA hydrolysis catalyzed by this enzyme with IC_{50} values of 1.0 ± 0.5 and 3.2 ± 0.6 μM, respectively (Table 4).

Table 4. Pharmacological characterization of compounds **23-26** towards the other components of the ECS. Data represent IC_{50} values (μM, mean ± SD) and the % of receptor binding/enzyme inhibition at the concentration of 10 μM (in brackets).

	IC_{50} values (μM, mean ± SD)				
Compound	**CB1**	**CB2**	**FAAH**	**ABHD6**	**ABHD12**
23	> 10 (4%)	> 10 (30%)	> 10 (18%)	> 10 (0%)	> 10 (21%)
24	> 10 (15%)	> 10 (13%)	> 10 (30%)	> 10 (0%)	> 10 (20%)
25	> 10 (9%)	> 10 (17%)	1.0 ± 0.5	> 10 (11%)	> 10 (12%)
26	> 10 (14%)	> 10 (24%)	3.2 ± 0.6	> 10 (16%)	> 10 (18%)

Cell-based assays of MAGL inhibition. In order to confirm the MAGL inhibition of **23** and **24** in a physiological system, we tested the compounds in the intact human monocytic cell line U937. As shown in Figure 8, both compounds inhibited [^{3}H]2-oleoyl glycerol (2-OG) hydrolysis in a concentration dependent manner. As expected, the inhibition of [^{3}H]glycerol formation (closed circles, solid line) is mirrored by the accumulation of non-hydrolyzed [^{3}H]2-OG (open circles, dotted line).

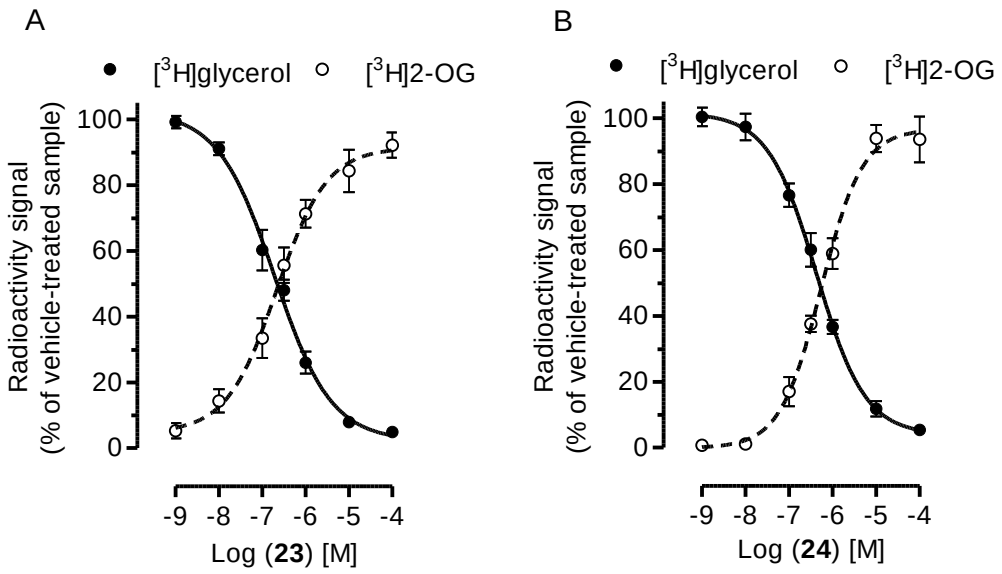

Figure 8. Concentration-dependent inhibition of [^{3}H]2-OG hydrolysis in intact U937 cells. Compound (A) **23** and (B) **24** were co-incubated with 1.0×10^6 cells and then 10 μM of 2-OG with a 0.5 nM of [^{3}H]2-OG as tracer was added to the cells. After 5 min of incubation at 37 °C, cells were centrifuged and the supernatants were extracted with a 1:1 mixture of $CHCl_3$:methanol. The radioactivity associated with the aqueous phase is associated with [^{3}H]glycerol formation (closed circles, solid line), while the organic phase is associated with [^{3}H]2-OG (open circles, dotted line).

In intact U937 cells, the IC_{50} value of compound **23** was approximately double (193 ± 41 nM) than that measured in the purified MAGL assay (80 ± 12 nM), while for compound **24** the IC_{50} value was approximately 6-times higher (431 ± 64 nM vs. 74 ± 1.0 nM). The lower potency observed for compound **24** in intact cells may depend on a suboptimal crossing of the plasma membrane or a potential interaction of the compound with other cellular components, thus reducing the actual concentration at the site of action (i.e. MAGL). On the basis of all these results, we decided to discard compound **24** focusing our attention on compound **23**: both compounds showed a similar inhibition potency on the isolated MAGL enzyme with compound **24** that showed a slightly higher activity (although the standard deviations measured for both compounds in enzymatic assays make them highly comparable). The selectivity assays suggested that both compounds are almost inactive against

CB1 and CB2 receptors FAAH, ABHD6 and ABHD12; however, the cell-based assays of MAGL inhibition clearly support the hypothesis that compound **23** is the best candidate as it shows an about two-fold higher potency with respect to **24**.

Activity-based protein profiling experiments. With the aim of assessing the effect of a reversible MAGL inhibition *in vivo*, we first performed competitive activity-based protein profiling (ABPP) experiments for compound **23** using mouse brain membrane preparations. ABPP is a functional proteomic technology, which exploits chemical probes that react with mechanistically related classes of enzymes.[41] TAMRA-fluorophosphonate (TAMRA-FP) is used to visualize serine hydrolases which includes the major eCB degrading enzymes.[42] An important advantage of ABPP relative to other approaches is that it can detect changes in activity of very low-abundance enzymes in highly complex samples and can simultaneously assess the potency and selectivity of an inhibitor towards the entire family of serine hydrolases in a specific tissue.

As shown in Figure 9, compound **23** inhibited MAGL in a concentration dependent manner (Figure 9, doublet band 3 and 4, and Table 5, MAGL migrates as double band in the ABPP),[43] without affecting other serine hydrolases in particular FAAH (Figure 9, band 1) and ABHD6 (Figure 9, band 5) up to 50 μM, indicating a high selectivity of compound **23** in mouse brain preparations. Unfortunately, we were not able to confirm the selectivity of **23** versus ABHD12 in ABPP assays because we could not clearly visualize the band associated with this serine hydrolase (approx. 46 kDa) possibly due to low expression/activity of the enzyme and the experimental conditions.

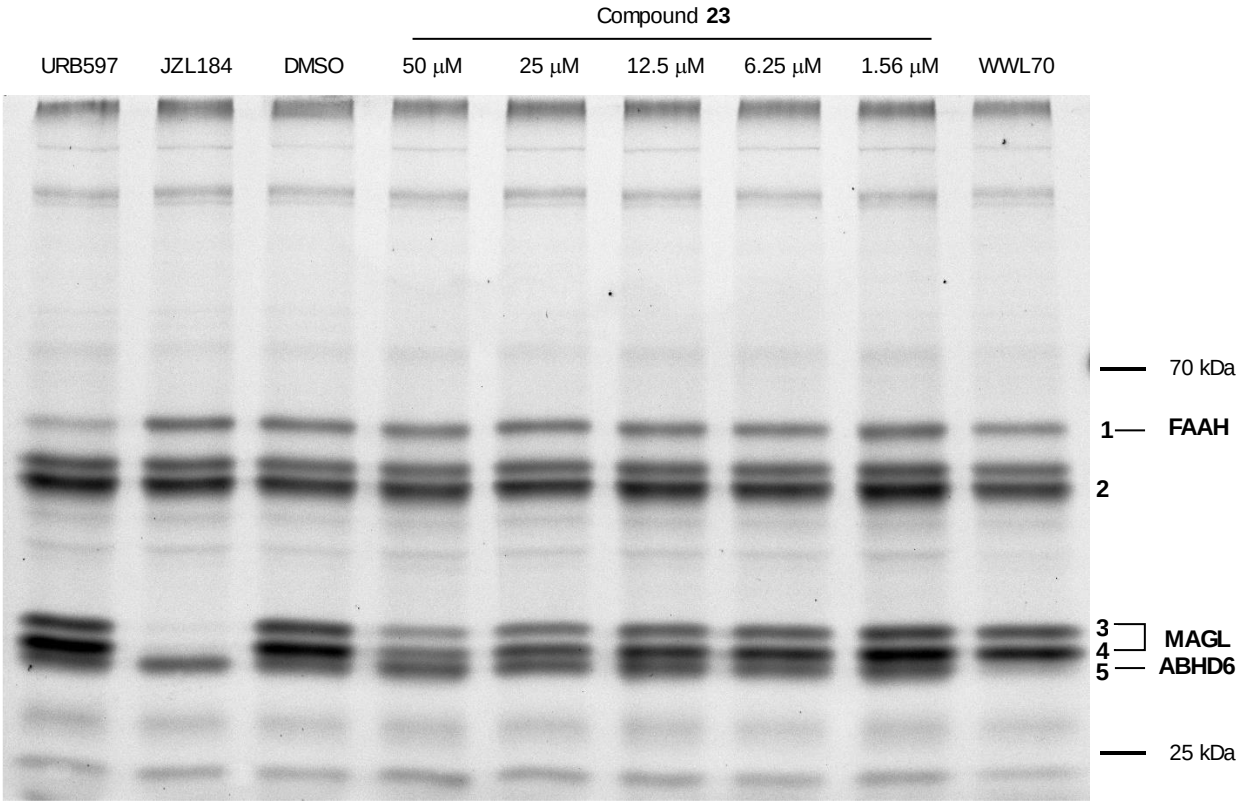

Figure 9. ABPP fluorescent screen of mouse brain membrane (MBM, 2 mg/mL) preparations with TAMRA-Fluorophosphonate serine hydrolase probe (TAMRA-FP). The MBM proteome was preincubated for 25 min with either DMSO, URB597 (4 μM), JZL184 (1 μM), WWL70 (10 μM*)* or compound **23** at different concentrations (50 μM, 25 μM, 12.5 μM, 6.25 μM, 1.56 μM) followed by 5 min labeling with TAMRA-FP (125 nM final concentration). Band 1 = FAAH, band 2 = used as a reference band for quantification, band 3 and 4 = doublet of MAGL, band 5 = ABHD6.

The quantification of the fluorescent bands confirmed a concentration dependent MAGL inhibition without showing any inhibition of FAAH and ABHD6 up to 50 μM (Table 5).

Table 5. Enzyme activity of FAAH, MAGL and ABHD6 calculated by quantifying of the intensity of band and expressed as % of vehicle control. The gels were analyzed using the software ImageJ and the quantification of band intensity was performed by normalizing the values obtained for FAAH

(band 1) MAGL (bands 3 and 4) and ABHD6 (band 5) with the reference band (2). The intensities were compared to DMSO sample, which reflects 100% of enzyme activity. Data are an average of three independent gels.

Enzyme	URB597	JZL184	WWL70	Compound **23**				
	4 μM	1 μM	10 μM	50 μM	25 μM	12.5 μM	6.25 μM	1.56 μM
FAAH	49	102	102	105	103	101	98	92
MAGL	92	9	95	**47**	**60**	**68**	**78**	**94**
ABHD6	96	116	50	123	116	112	103	90

Mouse membrane assays of MAGL inhibition. In order to further characterize the inhibition of MAGL activity in a functional assay, we tested compound **23** in mouse brain membrane preparations. As shown in Figure S4, compound **23** inhibited 2-OG hydrolysis in a concentration-dependent manner with an IC_{50} value of 2.1 ± 0.2 μM, in line with the data observed in ABPP experiments in the same biological matrix.

Antiproliferative assays. Compound **23** was also selected for further *in vitro* experiments to evaluate its antiproliferative potency against cancer cells. Compound CAY10499 (**2**) was used as the reference compound. Due to the key role that MAGL plays in the tumor progression of breast, colon and ovarian cancer, five tumor cell lines were chosen: human breast MDA-MB-231, colorectal HCT116 and ovarian CAOV3, OVCAR3 and SKOV3 cancer cells (Table 6).[44] Therefore, the antiproliferative activity of the two compounds was tested against these five cell lines, together with the noncancerous human fibroblast lung cells MRC5 (Table 6).[44] Derivative **23** produced an appreciable inhibition of cell viability in all the tested cancer cell lines, with IC_{50} values ranging from 7.9 to 57 μM. With respect to the covalent reference inhibitor **CAY10499**, the compound showed a more potent cytotoxic activity on HCT116, MDA-MB-231, CAOV3 and SKOV3, whereas the proliferation of the OVCAR3 tumor cells was similarly affected by the two compounds. Furthermore, both compounds proved to

be inactive against MRC5 (IC_{50} > 100 μM). We cannot exclude that the antiproliferative effects of compound **23** are not mediated by the inhibition of MAGL; however, we can exclude that these effects are mediated by the other main proteins of the ECS, as this compound showed a selectivity higher than 100-fold against the CB1 and CB2 receptors, FAAH, ABHD6 and ABHD12.

Table 6. Cell growth inhibitory activities (IC_{50} values) of **CAY10499** and compound **23**.

	IC_{50} (μM, mean ± SD)					
Compound	**HCT116**	**MDA-MB-231**	**CAOV3**	**OVCAR3**	**SKOV3**	**MRC5**
CAY10499	42 ± 2	89 ± 4	92 ± 5	50 ± 3	34 ± 3	> 100
23	21 ± 1	7.9 ± 1.2	25 ± 3	57 ± 2	15 ± 2	> 100

***In Vivo* Experiments.** In order to evaluate the ability of compound **23** to inhibit MAGL *in vivo*, we injected this compound to C57BL6 mice and quantified the levels of 2-AG and other related lipids in brain and plasma after 1 h and 2 h. The results showed that 2-AG levels were significantly increased in plasma (after 1 h and 2 h by 55%, Figure 10A) and in brain (after 1 h by 30%, Figure 10C). In agreement with the selectivity over FAAH observed in cellular system and mouse brain homogenates (ABPP experiments), compound **23** did not show any modification of AEA levels in plasma (Figure 10B) and brain (Figure 10D). Similarly, compound **23** did not significantly alter arachidonic acid and prostaglandin levels in plasma and brain as compared to vehicle (Figure S5 in the Supporting Information).

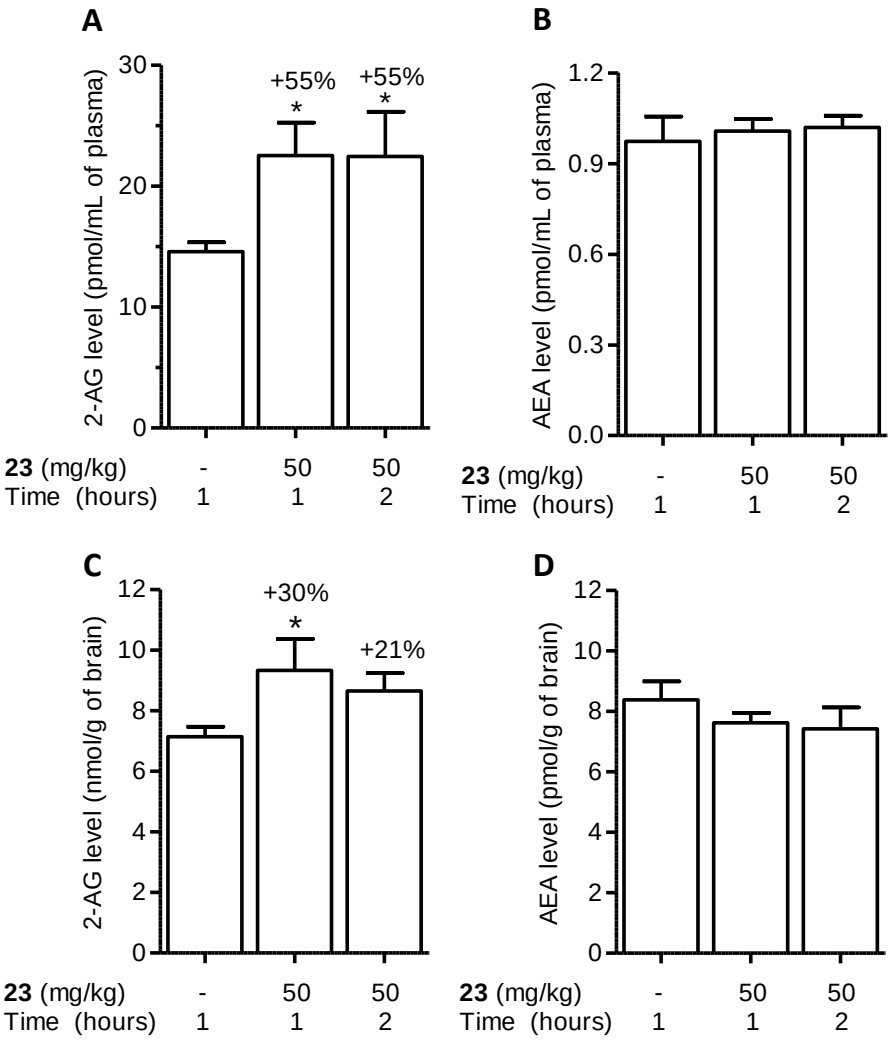

Figure 10. Quantification of 2-AG and AEA levels in plasma (A and B) and in brain (C and D) of C57BL6 mice treated with compound **23** at the dose of 50 mg/kg (i.p.). The animals were sacrificed after 1 h and 2 h post-injection. Male C57BL6 mice, 8-10 weeks old, n= 5-15. Data show mean ± SE. Statistical analysis was performed with one-way ANOVA followed by Tukey post-hoc test. *$p<0.05$ versus vehicle.

CONCLUSIONS

In the present work, starting from (4-(4-chlorobenzoyl)piperidin-1-yl)(3-hydroxyphenyl)methanone (**9**), a structural optimization has been performed leading to the identification of compound **23**, which

displayed a high MAGL inhibition activity with an IC_{50} value of 80 nM and a reversible mode of action, as well as a high selectivity for MAGL *vs.* CB1, CB2, FAAH, ABHD6 and ABHD12 (IC_{50} value > 10 μM in all cases). This reversible inhibitor was also tested in intact human monocytic cell line U937, where it inhibited 2-OG hydrolysis, with an IC_{50} value of 193 nM. Furthermore, **23** showed antiproliferative activities in human breast MDA-MB-231, colorectal HCT116 and ovarian CAOV3, OVCAR3 and SKOV3 cancer cells at micromolar concentrations. Finally, after intraperitoneal injection into C57BL6 mice, compound **23** induced a significant increase of 2-AG levels in brain and plasma confirming its MAGL inhibition *in vivo*. These preliminary *in vivo* studies suggest that the effects of this compound could be further explored. In particular, a wide *in silico* and *in vitro* ADME evaluation will be developed and, in case of potential problems, compound's modifications supported by molecular modeling will be carried out to maintain the potency and selectivity and to overcome any potential ADME problems. Taken together these results suggest that, to the best of our knowledge, compound **23** is one of the most active and selective MAGL reversible inhibitors so far reported in literature and may thus open new perspectives to study the therapeutic potential of reversible MAGL inhibition. The biological characterization of reversible MAGL inhibition *in vivo* will be addressed in a future work focused on the pharmacology of this new class of compounds. Compound **23** is the most potent inhibitor of this series, but it may need to be further optimized to become a lead candidate for drug development.

EXPERIMENTAL SECTION

1. Synthesis. General Procedures and Materials. All solvents and chemicals were used as purchased without further purification. Chromatographic separations were performed on silica gel columns by flash chromatography (Kieselgel 40, 0.040−0.063 mm; Merck). Reactions were followed by thin layer chromatography (TLC) on Merck aluminum silica gel (60 F254) sheets that were visualized under a UV lamp. Evaporation was performed in vacuo (rotating evaporator). Sodium

sulfate was always used as the drying agent. Proton (^{1}H) and carbon (^{13}C) NMR spectra were obtained with a Bruker Avance III 400 MHz spectrometer using the indicated deuterated solvents. Chemical shifts are given in parts per million (ppm) (δ relative to residual solvent peak for ^{1}H and ^{13}C). ^{1}H-NMR spectra are reported in this order: multiplicity and number of protons. Standard abbreviation indicating the multiplicity were used as follows: s = singlet, d = doublet, dd = doublet of doublets, ddd = doublet of doublet of doublets, t = triplet, tt = triplet of triplets, dt = doublet of triplets, td = triplet of doublets, q = quartet, quint = quintet, sext = sextet, sept = septet, m = multiplet, bm = broad multiplet and bs = broad signal. HPLC analysis was used to determine purity: all target compounds (i.e., assessed in biological assays) were ≥ 95% pure by HPLC, as confirmed via UV detection (λ = 254 nm). Analytical reversed-phase HPLC was conducted using a Kinetex EVO C18 column (5 μm, 150 × 4.6 mm, Phenomenex, Inc.); eluent A, water; eluent B, CH_3CN; after 5 min. at 25% B, a gradient was formed from 25% to 75% of B in 5 min and held at 75% of B for 10 min; flow rate was 1 mL/min. HPLC analyses were performed at 254 nm. Elemental analysis was used to further characterize the final compounds; analytical results are within ± 0.4% of the theoretical value. Yields refer to isolated and purified products derived from non-optimized procedures. Compound **2** was purchased from Cayman Chemical and compound **9** was synthesized as previously reported.[33]

1.1. General procedure for the synthesis of amide derivatives 10d, 31, 32, 33a-f, 37a-c, 43a-d, 49a-h, 56-60. HATU (1.05 equiv) was added to a solution of the appropriate benzoic acid (1 equiv) in dry DMF (2.1 mL), then DIPEA (4 equiv) was added dropwise. The resulting mixture was stirred at room temperature for 30 min and then 4-(4-chlorobenzoyl)piperidine **30** or substituted piperidines **47a-h**, **55** (100 mg, 1 equiv) was added and left under stirring at room temperature until consumption of starting material (TLC). After this time, the residue was diluted with water and extracted with EtOAc. The organic layer was repeatedly washed with brine, dried over Na_2SO_4 and the solvent was removed under reduced pressure. The residue was purified with a flash column chromatography (silica gel, appropriate mixture of *n*-hexane/ethyl acetate) or with a preparative TLC (only for

compound **10d**, mixture $CHCl_3$/MeOH) and pure fractions containing the desired compound were evaporated to dryness affording the amides.

1.2. General procedure for the synthesis of *O*-deprotected benzoylpiperidines 10a-c, 11a-d, 12a-d, 13a-d, 14-26. A solution of pure *O*-methylated amides (0.23 mmol) in anhydrous CH_2Cl_2 (2.7 mL) was cooled to −10 °C and treated dropwise with a 1.0 M solution of BBr_3 in CH_2Cl_2 (0.73 mL) under argon. The mixture was left under stirring at the same temperature for 5 min and then at 0 °C for 1 h and finally at RT until starting material was consumed (TLC). For compound **20**, further 0.36 mL BBr_3 were added. The mixture was then diluted with water and extracted with ethyl acetate. The organic phase was washed with brine, dried and concentrated. The crude product was purified by flash chromatography over silica gel. Elution with *n*-hexane/EtOAc mixtures afforded the desired compounds.

1.3. General procedure for the synthesis of methyl 3-methoxybenzoates 35a-c. A solution of phenolic derivatives **34a-c** (300 mg, 1 equiv) in 6 mL of DMF was treated with anhydrous K_2CO_3 (2.2 equiv) and iodomethane (3 equiv) and the reaction mixture was stirred at room temperature for 24 h. The mixture was diluted with water and extracted into ethyl acetate. The organic extract was repeatedly washed with brine, and the organic solvent was removed under vacuum on a rotary evaporator. The crude product afforded the pure desired compounds **35a-c**, that were used in the next step without further purification.

1.4. General procedure for the synthesis of 3-methoxybenzoic acids 36a-c, 42a-d. Methyl esters **35a-c** (200 mg) were dissolved in a 1:1 v/v mixture of THF/methanol (7 mL) and treated with 2.1 mL of 2 N aqueous solution of LiOH. The reaction was stirred overnight, then the solvents were evaporated, and the residue was treated with 1 N aqueous HCl and extracted with EtOAc. The organic phase was dried and evaporated to afford the pure desired carboxylic acid derivatives.

1.5. General procedure for the synthesis of methyl 3-methoxybenzoates 39a-b. Under argon atmosphere, thionyl chloride (2.5 equiv) was added dropwise to a solution of commercially available benzoic acids **38a-b** (400 mg, 1 equiv) in dry methanol (17 mL) cooled in an ice bath and then the

mixture was refluxed at 80 °C until starting material was not more present (TLC). The reaction mixture was cooled to room temperature and then carefully diluted with water and ethyl acetate and the organic phase was washed with saturated aqueous $NaHCO_3$ solution. The organic layer was dried over Na_2SO_4 and concentrated. Pure methyl esters **39a-b** were obtained and used in the next step without any further purification.

1.6. General procedure for the synthesis of iodinated derivatives 41a, c, d. To a solution of **39a-b**, commercially available methyl 2-amino-5-methoxybenzoate **40** (200 mg, 1 equiv) in H_2SO_4 (0.2 mL) and water (1.5 mL) cooled to -5 °C, a solution of sodium nitrite (1.05 equiv) in water (1.1 mL) was added dropwise. The mixture was stirred for 30 min, then a solution of potassium iodide (1.5 eq) in water (1.1 mL) was added dropwise. The reaction was stirred for 1-3 h at room temperature and then extracted with EtOAc. The combined organic extracts were washed with saturated aqueous $Na_2S_2O_3$, dried with anhydrous Na_2SO_4, filtered and concentrated. The crude product was purified by flash column chromatography to obtain the title compounds.

1.7. General procedure for the synthesis of compounds 46a-h, 53. To a cooled suspension of 1-acetylpiperidine-4-carboxylic acid **45** or 1-benzoylpiperidine-4-carboxylic acid **52** (500 mg, 1 equiv) in 2.7 mL of anhydrous 1,2-dichloroethane was slowly added $SOCl_2$ (2.3 equiv). The mixture was stirred at 60 °C for 4 h (the mixture turned from white to orange) and then evaporated under vacuum. Under argon atmosphere, the residue acyl chloride was dissolved in 2.2 mL of anhydrous 1,2-dichloroethane, then the reddish solution was cooled and $AlCl_3$ (2 equiv) was slowly added. Finally, a solution of the aromatic reagent (1 equiv; benzene, toluene, ethylbenzene, *n*-propylbenzene, cumene, *n*-butylbenzene, anisole, benzo-1,4-dioxane or bromobenzene) in anhydrous 1,2-dichloroethane (1.3 mL) was added dropwise. The mixture was stirred at 90 °C overnight. The solution was cooled to room temperature and poured into ice. The water layer was extracted with EtOAc, the combined organic phase was washed with brine, dried over anhydrous sodium sulfate and concentrated in vacuo. The residue was purified by silica gel chromatography using appropriate *n*-hexane/EtOAc mixtures.

1.8. General procedure for the synthesis of piperidine derivatives 47a-h and 55. To a solution of *N*-acetylated intermediates **46a-h** or *N*-benzoylated intermediate **54** (400 mg) in 17 mL of EtOH, 1 N aqueous solution of NaOH was added (17 mL). The reaction mixture was heated at 90 °C (for **47a-h**) or 95 °C (for **55**) overnight. The solution was cooled to room temperature, then concentrated under reduced pressure, diluted with water and extracted with EtOAc. The organic layer was washed with brine, dried over Na_2SO_4 and concentrated to dryness to obtain the pure desired compounds **47a-h**, **55** that were used in the next step without further purification.

(4-(4-Chlorobenzoyl)piperidin-1-yl)(3-hydroxy-2-iodophenyl)methanone (10a). Light grey solid; 94% yield from **43a**, eluent *n*-hexane/EtOAc 1:1. ^{1}H-NMR (acetone-d_6; asterisk denotes isomer peaks) δ (ppm): 1.52-2.02 (m, 4H), 2.98-3.08 (m, 1H), 3.16-3.33 (m, 1H), 3.41-3.53 (m, 1H), 3.74-3.84 (m, 1H), 4.64-4.72 (m, 1H), 6.68* (dd, 1H, J = 7.5, 1.4 Hz), 6.77 (dd, 1H, J = 7.4, 1.4 Hz), 6.94* (dd, 1H, J = 8.1, 1.4 Hz), 6.94 (dd, 1H, J = 8.0, 1.4 Hz), 7.26* (t, 1H, J = 7.7 Hz), 7.27 (t, 1H, J = 7.7 Hz), 7.54-7.59 (m, 2H), 8.06* (AA'XX', 2H, J_{AX} = 8.6 Hz, $J_{AA'/XX'}$ = 2.2 Hz), 8.07 (AA'XX', 2H, J_{AX} = 8.7 Hz, $J_{AA'/XX'}$ = 2.3 Hz), 9.20-9.35 (exchangeable bs, 1H). ^{13}C-NMR (acetone-d_6; asterisk denotes isomer peaks) δ (ppm): 28.84, 29.10*, 29.34, 41.26, 41.33*, 43.83, 43.98*, 46.54, 47.09*, 83.29, 83.58*, 115.23, 118.74*, 118.98, 129.78 (2C), 130.53*, 130.70, 130.95* (2C), 130.97 (2C), 135.45*, 135.48, 139.53, 139.57*, 145.66, 145.80*, 157.77, 157.95*, 169.32*, 169.53, 201.25. HPLC analysis: retention time = 11.702 min; peak area, 95% (254 nm). Elemental analysis for $C_{19}H_{17}ClINO_3$, calculated: % C, 48.58; % H, 3.65; % N, 2.98; found: % C, 48.90; % H, 4.01; % N, 2.59.

(1-(2-Bromo-3-hydroxybenzoyl)piperidin-4-yl)(4-chlorophenyl)methanone (10b). Light yellow solid; 43% yield from **43b**, eluent *n*-hexane/EtOAc 1:1. ^{1}H-NMR (acetone-d_6; asterisk denotes isomer peaks) δ (ppm): 1.52-1.87 (bm, 4H), 3.04 (tt, 1H, J = 13.0, 3.6 Hz), 3.16-3.34 (bm, 1H), 3.43-3.55 (bm, 1H), 3.73-3.84 (bm, 1H), 4.63-4.72 (bm, 1H), 6.74* (dd, 1H, J = 7.4, 1.5 Hz), 6.84 (dd, 1H, J = 7.4, 1.5 Hz), 7.01* (dd, 1H, J = 8.1, 1.4 Hz), 7.02 (dd, 1H, J = 8.1, 1.5 Hz), 7.25* (t, 1H, J = 7.1 Hz), 7.27 (t, 1H, J = 7.4 Hz), 7.54-7.59 (m, 2H), 8.06* (AA'XX', 2H, J_{AX} = 8.6 Hz, $J_{AA'/XX'}$ = 2.2 Hz),

8.07 (AA'XX', 2H, J_{AX} = 8.6 Hz, $J_{AA'/XX'}$ = 2.0 Hz), 9.07* (exchangeable bs, 1H), 9.10 (exchangeable bs, 1H). ^{13}C-NMR (acetone-*d*$_6$; asterisk denotes isomer peaks) δ (ppm): 29.04, 29.14*, 32.28, 41.16, 41.27*, 43.86, 43.97*, 46.35, 47.00*, 107.40*, 107.60, 116.79*, 116.83, 119.12*, 119.33, 129.64*, 129.78, 129.80 (2C), 130.98 (2C), 135.48, 135.51*, 139.55, 139.59*, 141.36, 141.48*, 155.20, 155.33*, 167.34, 167.59*, 201.24. HPLC analysis: retention time = 11.589 min; peak area, 98% (254 nm). Elemental analysis for $C_{19}H_{17}BrClNO_3$, calculated: % C, 53.99; % H, 4.05; % N, 3.31; found: % C, 54.15; % H, 3.88; % N, 3.03.

(1-(2-Chloro-3-hydroxybenzoyl)piperidin-4-yl)(4-chlorophenyl)methanone (10c). White solid; 74% yield from **31**, eluent *n*-hexane/EtOAc 1:1. ^{1}H-NMR (DMSO-*d*$_6$; asterisk denotes isomer peaks) δ (ppm): 1.34-1.62 (bm, 2H), 1.66-1.77 (bm, 1H), 1.85-1.95 (bm, 1H), 2.93-3.03 (m, 1H), 3.09-3.25 (bm, 2H), 3.66-3.80 (bm, 1H), 4.46-4.58 (bm, 1H), 6.72 (dd, 1H, *J* = 7.5, 1.4 Hz), 6.76* (dd, 1H, *J* = 7.5, 1.5 Hz), 6.95-7.05 (m, 1H), 7.19 (t, 1H, *J* = 7.8 Hz), 7.61 (AA'XX', 2H, J_{AX} = 8.7 Hz, $J_{AA'/XX'}$ = 2.3 Hz), 8.02 (AA'XX', 2H, J_{AX} = 8.7 Hz, $J_{AA'/XX'}$ = 2.2 Hz), 10.43 (exchangeable s, 1H). ^{13}C-NMR (DMSO-*d*$_6$; asterisk denotes isomer peaks) δ (ppm): 28.03, 28.17*, 28.45, 40.21, 42.28, 42.34*, 45.15, 45.83*, 115.86, 115.95*, 116.35*, 116.41, 117.33*, 117.36, 128.09*, 128.19, 128.93 (2C), 130.16 (2C), 134.04, 137.37*, 137.49, 138.18, 153.32, 153.39*, 165.46, 165.68*, 200.78, 200.83*. HPLC analysis: retention time = 11.513 min; peak area, 98% (254 nm). Elemental analysis for $C_{19}H_{17}Cl_2NO_3$, calculated: % C, 60.33; % H, 4.53; % N, 3.70; found: % C, 60.57; % H, 4.90; % N, 3.96.

(4-(4-Chlorobenzoyl)piperidin-1-yl)(2-fluoro-3-hydroxyphenyl)methanone (10d). White solid; 23% yield from 2-fluoro-3-hydroxybenzoic acid **27b** and **30**, eluent $CHCl_3$/MeOH 99:1. ^{1}H-NMR (DMSO-*d*$_6$) δ (ppm): 1.38-1.56 (bm, 2H), 1.69-1.80 (bm, 1H), 1.86-1.95 (bm, 1H), 2.94-3.05 (m, 1H), 3.15-3.27 (bm, 1H), 3.42-3.51 (m, 1H), 3.69-3.80 (m, 1H), 4.47-4.56 (m, 1H), 6.69-6.76 (m, 1H), 6.99 (td, 1H, *J* = 8.2, 1.9 Hz), 7.04 (t, 1H, *J* = 7.8 Hz), 7.61 (AA'XX', 2H, J_{AX} = 8.7 Hz, $J_{AA'/XX'}$ = 2.2 Hz), 8.02 (AA'XX', 2H, J_{AX} = 8.6 Hz, $J_{AA'/XX'}$ = 2.1 Hz), 10.01 (exchangeable bs, 1H). ^{13}C-NMR (DMSO-*d*$_6$) δ (ppm): 28.11, 28.46, 40.49, 42.28, 45.82, 117.42 (d, *J* = 2.3 Hz), 118.33 (d, *J* =

2.9 Hz), 124.84 (d, *J* = 4.1 Hz), 125.32 (d, *J* = 15.6 Hz), 128.94 (2C), 130.18 (2C), 134.07, 138.18, 145.03 (d, *J* = 11.9 Hz), 146.72 (d, *J* = 242.5 Hz), 163.94, 200.80. HPLC analysis: retention time = 11.417 min; peak area, 96% (254 nm). Elemental analysis for $C_{19}H_{17}ClFNO_3$, calculated: % C, 63.08; % H, 4.74; % N, 3.87; found: % C, 62.69; % H, 5.10; % N, 4.13.

(4-(4-Chlorobenzoyl)piperidin-1-yl)(5-hydroxy-2-iodophenyl)methanone (11a). Amber solid; 24% yield from **43c**, eluent *n*-hexane/EtOAc 1:1. ^{1}H-NMR (acetone-d_6; asterisk denotes isomer peaks) δ (ppm): 1.54-2.03 (bm, 4H), 2.97-3.08 (m, 1H), 3.17-3.35 (m, 1H), 3.44-3.55 (m, 1H), 3.74-3.85 (m, 1H), 4.62-4.69 (m, 1H), 6.69 (dd, 1H, *J* = 8.6, 3.0 Hz), 6.72* (d, 1H, *J* = 2.7 Hz), 6.81 (d, 1H, *J* = 3.0 Hz), 7.54-7.59 (m, 2H), 7.64 (d, 1H, *J* = 8.6 Hz), 7.66* (d, 1H, *J* = 8.4 Hz), 8.03-8.10 (m, 2H), 8.86 (exchangeable s, 1H). ^{13}C-NMR (acetone-d_6; asterisk denotes isomer peaks) δ (ppm): 28.87*, 29.13, 39.71, 41.27, 43.85, 43.98*, 46.57, 47.08*, 79.45, 79.66*, 115.20*, 115.43, 118.64*, 118.75, 129.81 (2C), 130.98 (2C), 131.01* (2C), 135.46, 135.49*, 139.56*, 139.61, 140.72, 140.95*, 144.86, 145.03*, 158.74*, 158.86, 168.82*, 168.94, 201.25. HPLC analysis: retention time = 12.107 min; peak area, 95% (254 nm). Elemental analysis for $C_{19}H_{17}ClINO_3$, calculated: % C, 48.58; % H, 3.65; % N, 2.98; found: % C, 48.86; % H, 3.90; % N, 2.69.

(1-(2-Bromo-5-hydroxybenzoyl)piperidin-4-yl)(4-chlorophenyl)methanone (11b). White solid; 69% yield from **32**, eluent *n*-hexane/EtOAc 1:1. ^{1}H-NMR (acetone-d_6; asterisk denotes isomer peaks) δ (ppm): 1.53-2.01 (m, 4H), 2.98-3.08 (m, 1H), 3.19-3.35 (m, 1H), 3.47-3.56 (m, 1H), 3.73-3.85 (m, 1H), 4.61-4.70 (m, 1H), 6.75* (d, 1H, *J* = 3.0 Hz), 6.81 (d, 1H, *J* = 3.0 Hz), 6.82-6.85 (m, 1H), 7.42* (d, 1H, *J* = 8.9 Hz), 7.43 (d, 1H, *J* = 8.7 Hz), 7.54-7.59 (m, 2H), 8.05* (AA'XX', 2H, J_{AX} = 8.6 Hz, $J_{AA'/XX'}$ = 2.3 Hz), 8.07 (AA'XX', 2H, J_{AX} = 8.7 Hz, $J_{AA'/XX'}$ = 2.5 Hz), 8.86 (exchangeable s, 1H). ^{13}C-NMR (DMSO-d_6; asterisk denotes isomer peaks) δ (ppm): 27.96*, 28.09, 28.19*, 28.36, 40.23, 42.28, 42.37*, 45.29*, 45.88, 106.45*, 106.51, 114.30, 114.33*, 117.62*, 117.76, 128.98 (2C), 130.21* (2C), 130.22 (2C), 133.31*, 133.45, 134.04*, 134.06, 138.21*, 138.24, 138.81*, 138.97, 157.03*, 157.10, 166.04*, 166.21, 200.82, 200.85*. HPLC analysis: retention time = 11.946 min;

peak area, 95% (254 nm). Elemental analysis for $C_{19}H_{17}BrClNO_3$, calculated: % C, 53.99; % H, 4.05; % N, 3.31; found: % C, 54.35; % H, 4.26; % N, 3.58.

(1-(2-Chloro-5-hydroxybenzoyl)piperidin-4-yl)(4-chlorophenyl)methanone (11c). Light grey solid; 88% yield from **37a**, eluent *n*-hexane/EtOAc 55:45. ^{1}H-NMR (DMSO-d_6; asterisk denotes isomer peaks) δ (ppm): 1.38-1.65 (m, 2H), 1.69-1.78 (m, 1H), 1.86-1.94 (m, 1H), 2.93-3.04 (m, 1H), 3.10-3.27 (m, 1H), 3.35-3.40 (m, 1H), 3.65-3.81 (m, 1H), 4.45-4.55 (m, 1H), 6.65* (d, 1H, J = 2.9 Hz), 6.71 (d, 1H, J = 2.9 Hz), 6.80* (dd, 1H, J = 8.7, 2.8 Hz), 6.81 (dd, 1H, J = 8.8, 2.9 Hz), 7.27 (d, 1H, J = 8.8 Hz), 7.28* (d, 1H, J = 8.7 Hz), 7.58-7.64 (m, 2H), 7.99-8.05 (m, 2H), 9.94 (exchangeable bs, 1H). ^{13}C-NMR (DMSO-d_6; asterisk denotes isomer peaks) δ (ppm): 28.02, 28.07*, 28.21*, 28.40, 40.23, 42.25, 42.30*, 45.22*, 45.83, 114.04, 117.21*, 117.37, 118.26, 118.30*, 128.94 (2C), 130.17 (2C), 130.24, 130.33*, 134.02, 134.05*, 136.60, 136.77*, 138.18*, 138.21, 156.50*, 156.55, 165.21*, 165.39, 200.78, 200.82*. HPLC analysis: retention time = 11.868 min; peak area, 99% (254 nm). Elemental analysis for $C_{19}H_{17}Cl_2NO_3$, calculated: % C, 60.33; % H, 4.53; % N, 3.70; found: % C, 60.50; % H, 4.80; % N, 3.50.

(4-(4-Chlorobenzoyl)piperidin-1-yl)(2-fluoro-5-hydroxyphenyl)methanone (11d). Light grey solid; 85% yield from **37b**, eluent *n*-hexane/EtOAc 1:1. ^{1}H-NMR (DMSO-d_6) δ (ppm): 1.38-1.53 (bm, 2H), 1.71-1.80 (bm, 1H), 1.85-1.94 (bm, 1H), 2.93-3.04 (m, 1H), 3.14-3.28 (bm, 1H), 3.44-3.53 (bm, 1H), 3.69-3.80 (m, 1H), 4.45-4.54 (m, 1H), 6.64-6.70 (m, 1H), 6.80 (ddd, 1H, J = 8.9, 4.3, 3.1 Hz), 7.08 (t, 1H, J = 9.1 Hz), 7.61 (AA'XX', 2H, J_{AX} = 8.7 Hz, $J_{AA'/XX'}$ = 2.2 Hz), 8.02 (AA'XX', 2H, J_{AX} = 8.7 Hz, $J_{AA'/XX'}$ = 2.2 Hz), 9.64 (exchangeable s, 1H). ^{13}C-NMR (DMSO-d_6) δ (ppm): 28.11, 28.45, 40.53, 42.26, 45.82, 113.94 (d, J = 3.7 Hz), 116.40 (d, J = 23.0 Hz), 117.21 (d, J = 7.7 Hz), 124.64 (d, J = 20.3 Hz), 128.95 (2C), 130.19 (2C), 134.06, 138.20, 150.71 (d, J = 235.3 Hz), 153.74 (d, J = 2.0 Hz), 163.80, 200.81. HPLC analysis: retention time = 11.575 min; peak area, 98% (254 nm). Elemental analysis for $C_{19}H_{17}ClFNO_3$, calculated: % C, 63.08; % H, 4.74; % N, 3.87; found: % C, 62.70; % H, 5.09; % N, 4.22.

(4-(4-Chlorobenzoyl)piperidin-1-yl)(3-hydroxy-5-iodophenyl)methanone (12a). Off-white solid; 84% yield from **43d**, eluent *n*-hexane/EtOAc 6:4. ^{1}H-NMR (acetone-d_6) δ (ppm): 1.60-1.72 (m, 2H), 1.84-2.00 (bm, 2H), 2.96-3.38 (bm, 2H), 3.79 (tt, 1H, J = 11.2, 3.7 Hz), 4.42-4.67 (bm, 2H), 6.89 (dd, 1H, J = 2.3, 1.3 Hz), 7.24 (t, 1H, J = 1.4 Hz), 7.29 (dd, 1H, J = 2.3, 1.5 Hz), 7.57 (AA'XX', 2H, J_{AX} = 8.8 Hz, $J_{AA'/XX'}$ = 2.2 Hz), 8.06 (AA'XX', 2H, J_{AX} = 8.8 Hz, $J_{AA'/XX'}$ = 2.2 Hz), 8.95 (exchangeable s, 1H). ^{13}C-NMR (acetone-d_6) δ (ppm): 43.94, 94.60, 114.38, 126.08, 127.57, 129.83 (2C), 131.00 (2C), 135.56, 139.62, 140.86, 159.04, 168.30, 201.27. HPLC analysis: retention time = 12.419 min; peak area, 99% (254 nm). Elemental analysis for $C_{19}H_{17}ClINO_3$, calculated: % C, 48.58; % H, 3.65; % N, 2.98; found: % C, 48.90; % H, 3.99; % N, 3.16.

(1-(3-Bromo-5-hydroxybenzoyl)piperidin-4-yl)(4-chlorophenyl)methanone (12b). Light grey solid; 40% yield from **33a**, eluent *n*-hexane/EtOAc 6:4. ^{1}H-NMR (acetone-d_6) δ (ppm): 1.60-1.72 (m, 2H), 1.84-2.00 (bm, 2H), 2.96-3.40 (bm, 2H), 3.69-3.93 (bm, 1H), 3.79 (tt, 1H, J = 11.1, 3.7 Hz), 4.41-4.70 (bm, 1H), 6.87 (dd, 1H, J = 2.2, 1.4 Hz), 7.05 (t, 1H, J = 1.5 Hz), 7.09 (t, 1H, J = 2.0 Hz), 7.57 (AA'XX', 2H, J_{AX} = 8.8 Hz, $J_{AA'/XX'}$ = 2.3 Hz), 8.06 (AA'XX', 2H, J_{AX} = 8.7 Hz, $J_{AA'/XX'}$ = 2.2 Hz), 9.04 (exchangeable s, 1H). ^{13}C-NMR (acetone-d_6) δ (ppm): 43.93, 113.82, 120.10, 121.56, 123.12, 129.83 (2C), 131.00 (2C), 135.55, 139.62, 140.79, 159.35, 168.50, 201.26. HPLC analysis: retention time = 12.281 min; peak area, 97% (254 nm). Elemental analysis for $C_{19}H_{17}BrClNO_3$, calculated: % C, 53.99; % H, 4.05; % N, 3.31; found: % C, 54.22; % H, 4.37; % N, 3.64.

(1-(3-Chloro-5-hydroxybenzoyl)piperidin-4-yl)(4-chlorophenyl)methanone (12c). Light yellow solid; 78% yield from **33b**, eluent *n*-hexane/EtOAc 6:4. ^{1}H-NMR (DMSO-d_6) δ (ppm): 1.42-1.56 (m, 2H), 1.70-1.95 (bm, 2H), 2.90-3.05 (bm, 1H), 3.10-3.26 (bm, 1H), 3.52-3.67 (bm, 1H), 3.74 (tt, 1H, J = 11.3, 3.5 Hz), 4.35-4.52 (bm, 1H), 6.70 (dd, 1H, J = 2.2, 1.3 Hz), 6.81-6.88 (m, 2H), 7.62 (AA'XX', 2H, J_{AX} = 8.7 Hz, $J_{AA'/XX'}$ = 2.2 Hz), 8.02 (AA'XX', 2H, J_{AX} = 8.8 Hz, $J_{AA'/XX'}$ = 2.3 Hz), 10.22 (exchangeable bs, 1H). ^{13}C-NMR (DMSO-d_6) δ (ppm): 42.40, 112.33, 116.11, 116.89, 129.00 (2C), 130.24 (2C), 133.71, 134.12, 138.22, 139.05, 158.48, 167.38, 200.89. HPLC analysis: retention

time = 12.152 min; peak area, 98% (254 nm). Elemental analysis for $C_{19}H_{17}Cl_2NO_3$, calculated: % C, 60.33; % H, 4.53; % N, 3.70; found: % C, 60.01; % H, 4.14; % N, 3.95.

(4-(4-Chlorobenzoyl)piperidin-1-yl)(3-fluoro-5-hydroxyphenyl)methanone (12d). White solid; 77% yield from **33c**, eluent *n*-hexane/EtOAc 6:4. ^{1}H-NMR (DMSO-d_6) δ (ppm): 1.43-1.58 (m, 2H), 1.65-1.95 (bm, 2H), 2.85-3.30 (bm, 2H), 3.50-3.69 (bm, 1H), 3.74 (tt, 1H, J = 11.2, 3.4 Hz), 4.32-4.57 (bm, 1H), 6.57-6.65 (m, 3H), 7.61 (AA'XX', 2H, J_{AX} = 8.8 Hz, $J_{AA'/XX'}$ = 2.3 Hz), 8.02 (AA'XX', 2H, J_{AX} = 8.8 Hz, $J_{AA'/XX'}$ = 2.2 Hz), 10.17 (exchangeable s, 1H). ^{13}C-NMR (DMSO-d_6) δ (ppm): 42.37, 103.37 (d, J = 23.7 Hz), 103.40 (d, J = 23.2 Hz), 109.71 (d, J = 2.6 Hz), 128.95 (2C), 130.19 (2C), 134.08, 138.18, 138.85 (d, J = 9.5 Hz), 159.02 (d, J = 11.8 Hz), 162.7 (d, J = 243.65 Hz), 167.59 (d, J = 3.0 Hz), 200.85. HPLC analysis: retention time = 11.749 min; peak area, 98% (254 nm). Elemental analysis for $C_{19}H_{17}ClFNO_3$, calculated: % C, 63.08; % H, 4.74; % N, 3.87; found: % C, 62.70; % H, 5.10; % N, 4.22.

(4-(4-Chlorobenzoyl)piperidin-1-yl)(3-hydroxy-4-iodophenyl)methanone (13a). White solid; 33% yield from **37c**, eluent *n*-hexane/EtOAc 1:1. ^{1}H-NMR (acetone-d_6) δ (ppm): 1.59-1.71 (m, 2H), 1.82-2.01 (bm, 2H), 2.91-3.38 (bm, 2H), 3.71-3.97 (bm, 1H), 3.80 (tt, 1H, J = 11.3, 3.7 Hz), 4.45-4.71 (bm, 1H), 6.71 (dd, 1H, J = 8.0, 1.9 Hz), 7.00 (d, 1H, J = 1.8 Hz), 7.57 (AA'XX', 2H, J_{AX} = 8.8 Hz, $J_{AA'/XX'}$ = 2.3 Hz), 7.79 (d, 1H, J = 8.0 Hz), 8.07 (AA'XX', 2H, J_{AX} = 8.8 Hz, $J_{AA'/XX'}$ = 2.2 Hz), 9.41 (exchangeable bm, 1H). ^{13}C-NMR (DMSO-d_6) δ (ppm): 42.38, 85.94, 112.99, 119.15, 128.99 (2C), 130.23 (2C), 134.08, 137.39, 138.21, 138.94, 156.59, 168.12, 200.92. HPLC analysis: retention time = 12.430 min; peak area, 97% (254 nm). Elemental analysis for $C_{19}H_{17}ClINO_3$, calculated: % C, 48.58; % H, 3.65; % N, 2.98; found: % C, 48.25; % H, 3.30; % N, 2.66.

(1-(4-Bromo-3-hydroxybenzoyl)piperidin-4-yl)(4-chlorophenyl)methanone (13b). White solid; 70% yield from **33d**, eluent *n*-hexane/EtOAc 1:1. ^{1}H-NMR (acetone-d_6) δ (ppm): 1.59-1.72 (m, 2H), 1.80-2.01 (bm, 2H), 2.93-3.35 (bm, 2H), 3.73-3.97 (bm, 1H), 3.80 (tt, 1H, J = 11.2, 3.7 Hz), 4.40-4.68 (bm, 1H), 6.85 (dd, 1H, J = 8.2, 1.8 Hz), 7.06 (d, 1H, J = 1.8 Hz), 7.53-7.60 (m, 3H), 8.06 (AA'XX', 2H, J_{AX} = 8.6 Hz, $J_{AA'/XX'}$ = 2.2 Hz), 9.16 (exchangeable bs, 1H). ^{13}C-NMR (acetone-d_6)

δ (ppm): 43.98, 111.46, 115.84, 120.34, 129.84 (2C), 131.01 (2C), 134.00, 135.55, 138.40, 139.63, 154.93, 169.18, 201.32. HPLC analysis: retention time = 12.168 min; peak area, 98% (254 nm). Elemental analysis for $C_{19}H_{17}BrClNO_3$, calculated: % C, 53.99; % H, 4.05; % N, 3.31; found: % C, 54.22; % H, 4.27; % N, 3.65.

(1-(4-Chloro-3-hydroxybenzoyl)piperidin-4-yl)(4-chlorophenyl)methanone (13c). Off-white solid; 81% yield from **33e**, eluent *n*-hexane/EtOAc 1:1. ^{1}H-NMR (acetone-d_6) δ (ppm): 1.60-1.71 (m, 2H), 1.85-2.00 (bm, 2H), 2.95-3.36 (bm, 2H), 3.73-4.00 (bm, 1H), 3.80 (tt, 1H, J = 11.3, 3.7 Hz), 4.40-4.70 (bm, 1H), 6.92 (dd, 1H, J = 8.1, 1.9 Hz), 7.07 (d, 1H, J = 1.8 Hz), 7.40 (d, 1H, J = 8.1 Hz), 7.57 (AA'XX', 2H, J_{AX} = 8.8 Hz, $J_{AA'/XX'}$ = 2.3 Hz), 8.07 (AA'XX', 2H, J_{AX} = 8.8 Hz, $J_{AA'/XX'}$ = 2.2 Hz), 9.10 (exchangeable s, 1H). ^{13}C-NMR (acetone-d_6) δ (ppm): 43.96, 116.23, 119.97, 122.21, 129.83 (2C), 130.82, 131.00 (2C), 135.54, 137.64, 139.62, 153.86, 169.20, 201.30. HPLC analysis: retention time = 12.014 min; peak area, 98% (254 nm). Elemental analysis for $C_{19}H_{17}Cl_2NO_3$, calculated: % C, 60.33; % H, 4.53; % N, 3.70; found: % C, 60.54; % H, 4.13; % N, 3.45.

(4-(4-Chlorobenzoyl)piperidin-1-yl)(4-fluoro-3-hydroxyphenyl)methanone (13d). Yellow solid; 65% yield from **33f**, eluent *n*-hexane/EtOAc 6:4. ^{1}H-NMR (DMSO-d_6) δ (ppm): 1.42-1.55 (m, 2H), 1.65-1.96 (bm, 2H), 2.87-3.27 (bm, 2H), 3.50-3.80 (bm, 1H), 3.74 (tt, 1H, J = 11.2, 3.5 Hz), 4.31-4.55 (bm, 1H), 6.81 (ddd, 1H, J = 8.3, 4.3, 2.1 Hz), 6.96 (dd, 1H, J = 8.5, 2.0 Hz), 7.18 (dd, 1H, J = 11.3, 8.3 Hz), 7.62 (AA'XX', 2H, J_{AX} = 8.7 Hz, $J_{AA'/XX'}$ = 2.2 Hz), 8.01 (AA'XX', 2H, J_{AX} = 8.8 Hz, $J_{AA'/XX'}$ = 2.3 Hz), 10.16 (exchangeable bs, 1H). ^{13}C-NMR (DMSO-d_6) δ (ppm): 42.42, 116.14 (d, J = 18.6 Hz), 116.37 (d, J = 3.5 Hz), 118.02 (d, J = 7.1 Hz), 128.99 (2C), 130.23 (2C), 132.68 (d, J = 3.7 Hz), 134.09, 138.20, 144.84 (d, J = 12.5 Hz), 151.44 (d, J = 243.8 Hz), 168.18, 200.93. HPLC analysis: retention time = 11.528 min; peak area, 97% (254 nm). Elemental analysis for $C_{19}H_{17}ClFNO_3$, calculated: % C, 63.08; % H, 4.74; % N, 3.87; found: % C, 62.90; % H, 5.10; % N, 3.48.

(4-Benzoylpiperidin-1-yl)(3-hydroxyphenyl)methanone (14). Off-white solid; 70% yield from **49a**, eluent *n*-hexane/EtOAc 3:7. ^{1}H-NMR (DMSO-d_6) δ (ppm): 1.43-1.56 (m, 2H), 1.68-1.95 (bm,

2H), 2.90-3.27 (bm, 2H), 3.59-3.72 (bm, 1H), 3.76 (tt, 1H, *J* = 11.2, 3.4 Hz), 4.37-4.54 (bm, 1H), 6.72-6.75 (m, 1H), 6.77 (dt, 1H, *J* = 7.8, 1.3 Hz), 6.81 (ddd, 1H, *J* = 8.2, 2.5, 1.2 Hz), 7.23 (t, 1H, *J* = 7.8 Hz), 7.51-7.58 (m, 2H), 7.65 (tt, 1H, *J* = 7.4, 1.5 Hz), 7.98-8.03 (m, 2H), 9.67 (exchangeable s, 1H). ^{13}C-NMR (DMSO-*d*$_6$) δ (ppm): 42.40, 113.38, 116.30, 117.08, 128.26 (2C), 128.88 (2C), 129.61, 133.28, 135.45, 137.49, 157.27, 168.93, 201.92. HPLC analysis: retention time = 10.185 min; peak area, 98% (254 nm). Elemental analysis for $C_{19}H_{19}NO_3$, calculated: % C, 73.77; % H, 6.19; % N, 4.53; found: % C, 73.43; % H, 6.54; % N, 4.22.

(1-(3-Hydroxybenzoyl)piperidin-4-yl)(*p*-tolyl)methanone (15). White solid; 86% yield from **49b**, eluent *n*-hexane/EtOAc 3:7. ^{1}H-NMR (DMSO-*d*$_6$) δ (ppm): 1.42-1.55 (m, 2H), 1.67-1.92 (bm, 2H), 2.38 (s, 3H), 2.90-3.27 (bm, 2H), 3.58-3.68 (bm, 1H), 3.72 (tt, 1H, *J* = 11.2, 3.5 Hz), 4.38-4.53 (bm, 1H), 6.72-6.75 (m, 1H), 6.77 (dt, 1H, *J* = 7.5, 1.2 Hz), 6.81 (ddd, 1H, *J* = 8.2, 2.5, 1.0 Hz), 7.23 (t, 1H, *J* = 7.8 Hz), 7.32-7.37 (m, 2H), 7.89-7.93 (m, 2H), 9.66 (exchangeable s, 1H). ^{13}C-NMR (DMSO-*d*$_6$) δ (ppm): 21.15, 42.27, 113.37, 116.29, 117.07, 128.40 (2C), 129.42 (2C), 129.62, 132.93, 137.51, 143.68, 157.27, 168.92, 201.41. HPLC analysis: retention time = 10.930 min; peak area, 99% (254 nm). Elemental analysis for $C_{20}H_{21}NO_3$, calculated: % C, 74.28; % H, 6.55; % N, 4.33; found: % C, 73.91; % H, 6.87; % N, 3.97.

(4-(4-Ethylbenzoyl)piperidin-1-yl)(3-hydroxyphenyl)methanone (16). White solid; 87% yield from **49c**, eluent *n*-hexane/EtOAc 4:6. ^{1}H-NMR (DMSO-*d*$_6$) δ (ppm): 1.20 (t, 3H, *J* = 7.6 Hz), 1.42-1.55 (m, 2H), 1.65-1.95 (bm, 2H), 2.68 (q, 2H, *J* = 7.6 Hz), 2.85-3.26 (bm, 2H), 3.55-3.76 (bm, 1H), 3.73 (tt, 1H, *J* = 11.4, 3.6 Hz), 4.35-4.55 (bm, 1H), 6.72-6.75 (m, 1H), 6.77 (dt, 1H, *J* = 7.5, 1.2 Hz), 6.81 (ddd, 1H, *J* = 8.2, 2.5, 1.0 Hz), 7.23 (t, 1H, *J* = 7.8 Hz), 7.38 (d, 2H, *J* = 8.4 Hz), 7.93 (d, 2H, *J* = 8.4 Hz), 9.65 (exchangeable s, 1H). ^{13}C-NMR (DMSO-*d*$_6$) δ (ppm): 15.17, 28.15, 42.27, 113.36, 116.28, 117.06, 128.24 (2C), 128.48 (2C), 129.59, 133.17, 137.49, 149.69, 157.25, 168.91, 201.41. HPLC analysis: retention time = 11.544 min; peak area, 97% (254 nm). Elemental analysis for $C_{21}H_{23}NO_3$, calculated: % C, 74.75; % H, 6.87; % N, 4.15; found: % C, 74.44; % H, 7.20; % N, 4.55.

(1-(3-Hydroxybenzoyl)piperidin-4-yl)(4-propylphenyl)methanone (17). White solid; 86% yield from **49d**, eluent *n*-hexane/EtOAc 4:6. ^{1}H-NMR ($CDCl_3$) δ (ppm): 0.95 (t, 3H, *J* = 7.4 Hz), 1.67 (sext, 2H, *J* = 7.5 Hz), 1.74-2.08 (bm, 4H), 2.65 (t, 2H, *J* = 7.6 Hz), 2.99-3.23 (bm, 2H), 3.48-3.59 (m, 1H), 3.80-3.99 (bm, 1H), 4.57-4.75 (bm, 1H), 6.83-6.91 (m, 2H), 6.93-6.97 (m, 1H), 7.23 (t, 1H, *J* = 7.9 Hz), 7.28 (d, 2H, *J* = 8.4 Hz), 7.87 (d, 2H, *J* = 8.3 Hz). ^{13}C-NMR (DMSO-d_6) δ (ppm): 13.57, 23.71, 37.11, 42.25, 113.35, 116.26, 117.04, 128.37 (2C), 128.78 (2C), 129.57, 133.18, 137.48, 148.10, 157.25, 168.89, 201.39. HPLC analysis: retention time = 12.121 min; peak area, 99% (254 nm). Elemental analysis for $C_{22}H_{25}NO_3$, calculated: % C, 75.19; % H, 7.17; % N, 3.99; found: % C, 75.38; % H, 6.78; % N, 3.62.

(1-(3-Hydroxybenzoyl)piperidin-4-yl)(4-isopropylphenyl)methanone (18). White solid; 77% yield from **49e**, eluent *n*-hexane/EtOAc 4:6. ^{1}H-NMR (DMSO-d_6) δ (ppm): 1.22 (d, 6H, *J* = 6.9 Hz), 1.40-1.56 (m, 2H), 1.63-1.96 (bm, 2H), 2.97 (sept, 1H, *J* = 6.9 Hz), 3.00-3.25 (bm, 2H), 3.58-3.78 (bm, 1H), 3.73 (tt, 1H, *J* = 11.1, 3.7 Hz), 4.36-4.54 (bm, 1H), 6.72-6.75 (m, 1H), 6.77 (dt, 1H, *J* = 7.5, 1.2 Hz), 6.81 (ddd, 1H, *J* = 8.2, 2.5, 1.0 Hz), 7.23 (t, 1H, *J* = 7.9 Hz), 7.41 (d, 2H, *J* = 8.2 Hz), 7.94 (d, 2H, *J* = 8.4 Hz), 9.66 (exchangeable s, 1H). ^{13}C-NMR (DMSO-d_6) δ (ppm): 23.45 (2C), 33.46, 42.24, 113.35, 116.26, 117.03, 126.77 (2C), 128.49 (2C), 129.57, 133.31, 137.47, 154.15, 157.24, 168.90, 201.37. HPLC analysis: retention time = 12.009 min; peak area, 99% (254 nm). Elemental analysis for $C_{22}H_{25}NO_3$, calculated: % C, 75.19; % H, 7.17; % N, 3.99; found: % C, 75.46; % H, 7.48; % N, 4.17.

(4-(4-Butylbenzoyl)piperidin-1-yl)(3-hydroxyphenyl)methanone (19). White solid; 82% yield from **49f**, eluent *n*-hexane/EtOAc 4:6. ^{1}H-NMR (DMSO-d_6) δ (ppm): 0.89 (t, 3H, *J* = 7.3 Hz), 1.30 (sext, 2H, *J* = 7.4 Hz), 1.41-1.52 (m, 2H), 1.57 (quint, 2H, *J* = 7.6 Hz), 1.65-1.93 (bm, 2H), 2.65 (t, 2H, *J* = 7.6 Hz), 2.88-3.06 (bm, 1H), 3.08-3.27 (bm, 1H), 3.56-3.80 (bm, 1H), 3.73 (tt, 1H, *J* = 11.3, 3.7 Hz), 4.36-4.54 (bm, 1H), 6.72-6.75 (m, 1H), 6.77 (dt, 1H, *J* = 7.4, 1.2 Hz), 6.81 (ddd, 1H, *J* = 8.2, 2.5, 1.0 Hz), 7.23 (t, 1H, *J* = 7.8 Hz), 7.26 (d, 2H, *J* = 8.4 Hz), 7.92 (d, 2H, *J* = 8.4 Hz), 9.66 (exchangeable s, 1H). ^{13}C-NMR (DMSO-d_6) δ (ppm): 13.71, 21.72, 32.71, 34.75, 42.55, 113.36,

116.27, 117.04, 128.39 (2C), 128.73 (2C), 129.57, 133.13, 137.48, 148.33, 157.26, 168.90, 201.37. HPLC analysis: retention time = 12.648 min; peak area, 99% (254 nm). Elemental analysis for $C_{23}H_{27}NO_3$, calculated: % C, 75.59; % H, 7.45; % N, 3.83; found: % C, 75.80; % H, 7.07; % N, 3.44.

(4-(4-Hydroxybenzoyl)piperidin-1-yl)(3-hydroxyphenyl)methanone (20). Beige solid; 40% yield from **49g**, eluent *n*-hexane/EtOAc 4:6. ^{1}H-NMR (DMSO-d_6) δ (ppm): 1.40-1.58 (m, 2H), 1.60-1.93 (bm, 2H), 2.85-3.25 (bm, 2H), 3.55-3.75 (m, 2H), 4.35-4.56 (bm, 1H), 6.72-6.75 (m, 1H), 6.77 (dt, 1H, J = 7.6, 1.2 Hz), 6.81 (ddd, 1H, J = 8.2, 2.5, 1.0 Hz), 6.86 (AA'XX', 2H, J_{AX} = 8.8 Hz, $J_{AA'/XX'}$ = 2.3 Hz), 7.23 (t, 1H, J = 7.8 Hz), 7.89 (AA'XX', 2H, J_{AX} = 8.8 Hz, $J_{AA'/XX'}$ = 2.4 Hz), 9.63 (exchangeable bs, 1H), 10.36 (exchangeable bs, 1H). ^{13}C-NMR (DMSO-d_6) δ (ppm): 41.85, 113.35, 115.36 (2C), 116.26, 117.04, 126.88, 129.58, 130.81 (2C), 137.51, 157.24, 162.12, 168.89, 199.92. HPLC analysis: retention time = 4.718 min; peak area, 99% (254 nm). Elemental analysis for $C_{19}H_{19}NO_4$, calculated: % C, 70.14; % H, 5.89; % N, 4.31; found: % C, 70.30; % H, 6.15; % N, 3.99.

(2,3-Dihydrobenzo[b][1,4]dioxin-6-yl)(1-(3-hydroxybenzoyl)piperidin-4-yl)methanone (21). Off-white solid; 50% yield from **49h**, eluent *n*-hexane/EtOAc 2:8. ^{1}H-NMR (DMSO-d_6) δ (ppm): 1.40-1.53 (bm, 2H), 1.63-1.90 (bm, 2H), 2.90-3.03 (bm, 1H), 3.10-3.23 (bm, 2H), 3.68 (tt, 1H, J = 10.2, 3.7 Hz), 4.27-4.35 (m, 4H), 4.40-4.51 (bm, 1H), 6.71-6.74 (m, 1H), 6.76 (dt, 1H, J = 7.8, 1.2 Hz), 6.81 (ddd, 1H, J = 8.1, 2.4, 0.9 Hz), 6.98 (d, 1H, J = 8.4 Hz), 7.22 (t, 1H, J = 7.9 Hz), 7.50 (d, 1H, J = 2.0 Hz), 7.54 (dd, 1H, J = 8.5, 2.1 Hz), 9.67 (exchangeable bs, 1H). ^{13}C-NMR (DMSO-d_6) δ (ppm): 41.93, 63.90, 64.52, 113.32, 116.24, 117.03, 117.21, 122.23, 128.93, 129.57, 137.48, 143.33, 147.93, 157.22 (2C), 168.87, 200.13. HPLC analysis: retention time = 10.153 min; peak area, 95% (254 nm). Elemental analysis for $C_{21}H_{21}NO_5$, calculated: % C, 68.65; % H, 5.76; % N, 3.81; found: % C, 69.05; % H, 5.37; % N, 4.20.

(1-(3-Hydroxybenzoyl)piperidin-4-yl)(4-morpholinophenyl)methanone (22). Off-white solid; 27% yield from **56**, eluent *n*-hexane/EtOAc 35:65. ^{1}H-NMR (DMSO-d_6) δ (ppm): 1.41-1.55 (m, 2H), 1.60-1.90 (bm, 2H), 2.85-3.24 (bm, 2H), 3.26-3.32 (m, 4H), 3.59-3.70 (m, 2H), 3.70-3.77 (m, 4H), 4.38-4.54 (bm, 1H), 6.72-6.75 (m, 1H), 6.77 (dt, 1H, J = 7.7, 1.2 Hz), 6.81 (ddd, 1H, J = 8.2, 2.5, 1.0

Hz), 6.96-7.03 (m, 2H), 7.23 (t, 1H, *J* = 7.9 Hz), 7.85-7.91 (m, 2H), 9.67 (exchangeable s, 1H). ^{13}C-NMR (DMSO-d_6) δ (ppm): 41.68, 46.75 (2C), 65.84 (2C), 113.12 (2C), 113.35, 116.26, 117.05, 125.24, 129.61, 130.15 (2C), 137.54, 154.09, 157.26, 168.89, 199.57. HPLC analysis: retention time = 9.805 min; peak area, 98% (254 nm). Elemental analysis for $C_{23}H_{26}N_2O_4$, calculated: % C, 70.03; % H, 6.64; % N, 7.10; found: % C, 70.40; % H, 7.01; % N, 6.78.

(1-(2-Fluoro-5-hydroxybenzoyl)piperidin-4-yl)(4-isopropylphenyl)methanone (23). Light yellow solid; 81% yield from **57**, eluent *n*-hexane/EtOAc 6:4. ^{1}H-NMR (DMSO-d_6) δ (ppm): 1.22 (d, 6H, *J* = 6.9 Hz), 1.38-1.54 (bm, 2H), 1.69-1.79 (bm, 1H), 1.84-1.94 (bm, 1H), 2.90-3.06 (m, 2H), 3.14-3.29 (bm, 1H), 3.43-3.53 (m, 1H), 3.67-3.80 (m, 1H), 4.45-4.54 (m, 1H), 6.64-6.70 (m, 1H), 6.80 (ddd, 1H, *J* = 9.0, 4.2, 3.1 Hz), 7.08 (t, 1H, *J* = 9.1 Hz),7.41 (d, 2H, *J* = 8.3 Hz), 7.94 (d, 2H, *J* = 8.4 Hz), 9.64 (exchangeable s, 1H). ^{13}C-NMR (DMSO-d_6) δ (ppm): 23.45 (2C), 28.28, 28.59, 33.46, 40.58, 42.10, 45.89, 113.94 (d, *J* = 3.7 Hz), 116.40 (d, *J* = 23.2 Hz), 117.19 (d, *J* = 7.8 Hz), 124.68 (d, *J* = 20.1 Hz), 126.77 (2C), 128.50 (2C), 133.30, 150.71 (d, *J* = 235.2 Hz), 153.73 (d, *J* = 1.5 Hz), 154.18, 163.79, 201.30. HPLC analysis: retention time = 12.274 min; peak area, 99% (254 nm). Elemental analysis for $C_{22}H_{24}FNO_3$, calculated: % C, 71.53; % H, 6.55; % N, 3.79; found: % C, 71.23; % H, 6.82; % N, 3.48.

(4-(4-Butylbenzoyl)piperidin-1-yl)(2-fluoro-5-hydroxyphenyl)methanone (24). Off-white solid; 87% yield from **58**, eluent *n*-hexane/EtOAc 55:45. ^{1}H-NMR (DMSO-d_6) δ (ppm): 0.90 (t, 3H, *J* = 7.4 Hz), 1.30 (sext, 2H, *J* = 7.5 Hz), 1.39-1.53 (bm, 2H), 1.57 (quint, 2H, *J* = 7.6 Hz), 1.69-1.79 (bm, 1H), 1.84-1.94 (bm, 1H), 2.65 (t, 2H, *J* = 7.8 Hz), 2.93-3.05 (m, 1H), 3.15-3.28 (bm, 1H), 3.43-3.54 (m, 1H), 3.67-3.79 (m, 1H), 4.45-4.55 (m, 1H), 6.64-6.70 (m, 1H), 6.80 (ddd, 1H, *J* = 8.9, 4.3, 3.1 Hz), 7.08 (t, 1H, *J* = 9.0 Hz), 7.36 (d, 2H, *J* = 8.3 Hz), 7.92 (d, 2H, *J* = 8.4 Hz), 9.64 (exchangeable bs, 1H). ^{13}C-NMR (DMSO-d_6) δ (ppm): 13.67, 21.68, 28.27, 28.59, 32.66, 34.71, 40.57, 42.08, 45.86, 113.92 (d, *J* = 3.5 Hz), 116.38 (d, *J* = 23.1 Hz), 117.17 (d, *J* = 7.6 Hz), 124.66 (d, *J* = 20.1 Hz), 128.37 (2C), 128.71 (2C), 133.10, 148.33, 150.70 (d, *J* = 235.2 Hz), 153.72 (d, *J* = 1.4 Hz), 163.77, 201.29. HPLC analysis: retention time = 12.889 min; peak area, 98% (254 nm). Elemental analysis for

$C_{23}H_{26}FNO_3$, calculated: % C, 72.04; % H, 6.83; % N, 3.65; found: % C, 72.28; % H, 7.19; % N, 3.86.

(1-(4-Fluoro-3-hydroxybenzoyl)piperidin-4-yl)(4-isopropylphenyl)methanone (25). White solid; 17% yield from **59**, eluent *n*-hexane/EtOAc 65:35. ^{1}H-NMR (DMSO-d_6) δ (ppm): 1.22 (d, 6H, *J* = 6.9 Hz), 1.43-1.57 (m, 2H), 1.70-1.92 (bm, 2H), 2.97 (sept, 1H, *J* = 6.9 Hz), 2.90-3.25 (bm, 2H), 3.65-3.80 (bm, 1H), 3.72 (tt, 1H, *J* = 11.4, 3.5 Hz), 4.24-4.60 (bm, 1H), 6.81 (ddd, 1H, *J* = 8.3, 4.3, 2.1 Hz), 6.96 (dd, 1H, *J* = 8.5, 2.1 Hz), 7.18 (dd, 1H, *J* = 11.3, 8.3 Hz), 7.41 (d, 2H, *J* = 8.2 Hz), 7.94 (d, 2H, *J* = 8.4 Hz), 10.12 (exchangeable bs, 1H). ^{13}C-NMR (DMSO-d_6) δ (ppm): 23.44 (2C), 33.44, 42.22, 116.05 (d, *J* = 18.9 Hz), 116.34 (d, *J* = 3.3 Hz), 117.97 (d, *J* = 7.0 Hz), 126.75 (2C), 128.48 (2C), 132.69 (d, *J* = 3.7 Hz), 133.31, 144.81 (d, *J* = 12.5 Hz), 151.41 (d, *J* = 243.6 Hz), 154.14, 168.15, 201.37. HPLC analysis: retention time = 12.239 min; peak area, 99% (254 nm). Elemental analysis for $C_{22}H_{24}FNO_3$, calculated: % C, 71.53; % H, 6.55; % N, 3.79; found: % C, 71.84; % H, 6.20; % N, 3.45.

(4-(4-Butylbenzoyl)piperidin-1-yl)(4-fluoro-3-hydroxyphenyl)methanone (26). White solid; 55% yield from **60**, eluent *n*-hexane/EtOAc 6:4. ^{1}H-NMR (DMSO-d_6) δ (ppm): 0.89 (t, 3H, *J* = 7.4 Hz), 1.30 (sext, 2H, *J* = 7.4 Hz), 1.44-1.55 (m, 2H), 1.57 (quint, 2H, *J* = 7.6 Hz), 1.70-1.90 (bm, 2H), 2.65 (t, 2H, *J* = 7.7 Hz), 2.83-3.37 (bm, 2H), 3.54-3.81 (bm, 1H), 3.72 (tt, 1H, *J* = 11.3, 3.5 Hz), 4.20-4.60 (bm, 1 H), 6.81 (ddd, 1H, *J* = 8.3, 4.3, 2.1 Hz), 6.96 (dd, 1H, *J* = 8.5, 2.1 Hz), 7.18 (dd, 1H, *J* = 11.1, 8.3 Hz), 7.35 (d, 2H, *J* = 8.4 Hz), 7.92 (d, 2H, *J* = 8.4 Hz), 10.11 (exchangeable bs, 1H). ^{13}C-NMR (DMSO-d_6) δ (ppm): 13.70, 21.72, 32.70, 34.75, 42.25, 116.11 (d, *J* = 18.7 Hz), 116.38 (d, *J* = 3.3 Hz), 118.00 (d, *J* = 6.9 Hz), 128.39 (2C), 128.73 (2C), 132.72 (d, *J* = 3.6 Hz), 133.17, 144.85 (d, *J* = 12.4 Hz), 148.33, 151.45 (d, *J* = 243.5 Hz), 169.18, 201.39. HPLC analysis: retention time = 12.863 min; peak area, 98% (254 nm). Elemental analysis for $C_{23}H_{26}FNO_3$, calculated: % C, 72.04; % H, 6.83; % N, 3.65; found: % C, 72.16; % H, 7.03; % N, 3.29.

(1-(2-Chloro-3-methoxybenzoyl)piperidin-4-yl)(4-chlorophenyl)methanone (31). 59% yield from 2-chloro-3-methoxybenzoic acid **27a** and **30**. ^{1}H-NMR ($CDCl_3$; asterisk denotes isomer peaks)

δ (ppm): 1.65-2.10 (m, 4H), 3.02-3.30 (m, 2H), 3.40-3.65 (m, 2H), 3.94* (s, 3H), 3.95 (s, 3H), 4.68-4.85 (m, 1H), 6.88 (dd, 1H, J = 7.6, 1.4 Hz), 6.92-7.00 (m, 1H), 7.27-7.34 (m, 1H), 7.45-7.51 (m, 2H), 7.89* (AA'XX', 2H, J_{AX} = 8.7 Hz, $J_{AA'/XX'}$ = 2.3 Hz), 7.90 (AA'XX', 2H, J_{AX} = 8.8 Hz, $J_{AA'/XX'}$ = 2.3 Hz).

(1-(2-Bromo-5-methoxybenzoyl)piperidin-4-yl)(4-chlorophenyl)methanone (32). 72% yield from 2-bromo-5-methoxybenzoic acid **28** and **30**. ^{1}H-NMR ($CDCl_3$; asterisk denotes isomer peaks) δ (ppm): 1.66-2.09 (m, 4H), 3.02-3.14 (m, 1H), 3.21-3.30 (m, 1H), 3.41-3.63 (m, 2H), 3.79* (s, 3H), 3.80 (s, 3H), 4.67-4.78 (bm, 1H), 6.76-6.83 (m, 2H), 7.41-7.48 (m, 3H), 7.85-7.90 (m, 2H).

(1-(3-Bromo-5-methoxybenzoyl)piperidin-4-yl)(4-chlorophenyl)methanone (33a). 70% yield from 3-bromo-5-methoxybenzoic acid **29a** and **30**. ^{1}H-NMR ($CDCl_3$) δ (ppm): 1.72-2.09 (bm, 4H), 2.97-3.26 (bm, 2H), 3.44-3.54 (m, 1H), 3.73-3.95 (bm, 1H), 3.81 (s, 3H), 4.50-4.75 (bm, 1H), 6.86 (dd, 1H, J = 2.2, 1.4 Hz), 7.08-7.12 (m, 2H), 7.46 (AA'XX', 2H, J_{AX} = 8.6 Hz, $J_{AA'/XX'}$ = 2.2 Hz), 7.88 (AA'XX', 2H, J_{AX} = 8.6 Hz, $J_{AA'/XX'}$ = 2.2 Hz).

(1-(3-Chloro-5-methoxybenzoyl)piperidin-4-yl)(4-chlorophenyl)methanone (33b). 65% yield from 3-chloro-5-methoxybenzoic acid **29b** and **30**. ^{1}H-NMR ($CDCl_3$) δ (ppm): 1.70-2.08 (bm, 4H), 2.93-3.25 (bm, 2H), 3.44-3.55 (m, 1H), 3.75-3.95 (bm, 1H), 3.82 (s, 3H), 4.55-4.75 (bm, 1H), 6.82 (dd, 1H, J = 2.3, 1.3 Hz), 6.92-6.97 (m, 2H), 7.46 (AA'XX', 2H, J_{AX} = 8.7 Hz, $J_{AA'/XX'}$ = 2.2 Hz), 7.89 (AA'XX', 2H, J_{AX} = 8.6 Hz, $J_{AA'/XX'}$ = 2.1 Hz).

(4-(4-Chlorobenzoyl)piperidin-1-yl)(3-fluoro-5-methoxyphenyl)methanone (33c). 67% yield from 5-fluoro-3-methoxybenzoic acid **29c** and **30**. ^{1}H-NMR ($CDCl_3$) δ (ppm): 1.72-3.05 (bm, 4H), 2.96-3.23 (bm, 2H), 3.44-3.54 (m, 1H), 3.74-3.93 (bm, 1H), 3.82 (s, 3H), 4.52-4.75 (bm, 1H), 6.63-6.71 (m, 2H), 6.71-6.75 (m, 1H), 7.46 (AA'XX', 2H, J_{AX} = 8.8 Hz, $J_{AA'/XX'}$ = 2.2 Hz), 7.89 (AA'XX', 2H, J_{AX} = 8.7 Hz, $J_{AA'/XX'}$ = 2.2 Hz).

(1-(4-Bromo-3-methoxybenzoyl)piperidin-4-yl)(4-chlorophenyl)methanone (33d). 77% yield from 4-bromo-3-methoxybenzoic acid **29d** and **30**. ^{1}H-NMR ($CDCl_3$) δ (ppm): 1.72-2.03 (bm, 4H), 3.01-3.22 (bm, 2H), 3.46-3.55 (m, 1H), 3.76-4.00 (bm, 1H), 3.92 (s, 3H), 4.54-4.75 (bm, 1H), 6.85

(dd, 1H, *J* = 8.0, 1.8 Hz), 6.97 (d, 1H, *J* = 1.8 Hz), 7.47 (AA'XX', 2H, J_{AX} = 8.7 Hz, $J_{AA'/XX'}$ = 2.2 Hz), 7.56 (d, 1H, *J* = 8.0 Hz), 7.89 (AA'XX', 2H, J_{AX} = 8.5 Hz, $J_{AA'/XX'}$ = 2.2 Hz).

(1-(4-Chloro-3-methoxybenzoyl)piperidin-4-yl)(4-chlorophenyl)methanone (33e). 63% yield from 4-chloro-3-methoxybenzoic acid **29e** and **30**. ^{1}H-NMR ($CDCl_3$) δ (ppm): 1.72-2.03 (bm, 4H), 2.98-3.23 (bm, 2H), 3.46-3.55 (m, 1H), 3.75-3.95 (bm, 1H), 3.93 (s, 3H), 4.51-4.76 (bm, 1H), 6.92 (dd, 1H, *J* = 8.0, 1.8 Hz), 7.01 (d, 1H, *J* = 1.8 Hz), 7.38 (d, 1H, *J* = 8.0 Hz), 7.46 (AA'XX', 2H, J_{AX} = 8.8 Hz, $J_{AA'/XX'}$ = 2.2 Hz), 7.89 (AA'XX', 2H, J_{AX} = 8.7 Hz, $J_{AA'/XX'}$ = 2.2 Hz).

(4-(4-Chlorobenzoyl)piperidin-1-yl)(4-fluoro-3-methoxyphenyl)methanone (33f). 73% yield from 4-fluoro-3-methoxybenzoic acid **29f** and **30**. ^{1}H-NMR ($CDCl_3$) δ (ppm): 1.72-2.07 (bm, 4H), 2.99-3.22 (bm, 2H), 3.45-3.55 (m, 1H), 3.81-4.02 (bm, 1H), 3.93 (s, 3H), 4.44-4.83 (bm, 1H), 6.94 (ddd, 1H, *J* = 8.2, 4.3, 2.0 Hz), 7.07 (dd, 1H, *J* = 8.0, 2.0 Hz), 7.09 (dd, 1H, *J* = 11.0, 8.2 Hz), 7.47 (AA'XX', 2H, J_{AX} = 8.6 Hz, $J_{AA'/XX'}$ = 2.2 Hz), 7.89 (AA'XX', 2H, J_{AX} = 8.7 Hz, $J_{AA'/XX'}$ = 2.2 Hz).

Methyl 2-chloro-5-methoxybenzoate (35a). 79% yield from 2-chloro-5-hydroxybenzoic acid **34a**. ^{1}H-NMR ($CDCl_3$) δ (ppm): 3.82 (s, 3H), 3.93 (s, 3H), 6.96 (dd, 1H, *J* = 8.9, 3.1 Hz), 7.33 (d, 1H, *J* = 3.2 Hz), 7.34 (d, 1H, *J* = 8.7 Hz).

Methyl 2-fluoro-5-methoxybenzoate (35b). 93% yield from 2-fluoro-5-hydroxybenzoic acid **34b**. ^{1}H-NMR ($CDCl_3$) δ (ppm): 3.82 (s, 3H), 3.93 (s, 3H), 7.02-7.07 (m, 2H), 7.38-7.42 (m, 1H).

Methyl 4-iodo-3-methoxybenzoate (35c). 99% yield from 3-hydroxy-4-iodobenzoic acid **34c**. ^{1}H-NMR ($CDCl_3$) δ (ppm): 3.92 (s, 3H), 3.94 (s, 3H), 7.37 (dd, 1H, *J* = 8.1, 1.8 Hz), 7.45 (d, 1H, *J* = 1.8 Hz), 7.85 (d, 1H, *J* = 8.0 Hz).

2-Chloro-5-methoxybenzoic acid (36a). 99% yield from **35a**. ^{1}H-NMR (acetone-d_6) δ (ppm): 3.86 (s, 3H), 7.11 (dd, 1H, *J* = 8.9, 3.1 Hz), 7.40 (d, 1H, *J* = 3.1 Hz), 7.42 (d, 1H, *J* = 8.9 Hz).

2-Fluoro-5-methoxybenzoic acid (36b). 99% yield from **35b**. ^{1}H-NMR ($CDCl_3$) δ (ppm): 3.84 (s, 3H), 7.15-7.20 (m, 2H), 7.40-7.44 (m, 1H).

4-Iodo-3-methoxybenzoic acid (36c). 95% yield from **35c**. ^{1}H-NMR ($CDCl_3$) δ (ppm): 3.96 (s, 3H), 7.45 (dd, 1H, *J* = 8.0, 1.8 Hz), 7.50 (d, 1H, *J* = 1.8 Hz), 7.90 (d, 1H, *J* = 8.0 Hz).

(1-(2-Chloro-5-methoxybenzoyl)piperidin-4-yl)(4-chlorophenyl)methanone (37a). 54% yield from **36a** and **30**. ^{1}H-NMR ($CDCl_3$; asterisk denotes isomer peaks) δ (ppm): 1.64-2.07 (m, 4H), 3.02-3.15 (m, 1H), 3.20-3.30 (m, 1H), 3.39-3.65 (bm, 2H), 3.80* (s, 3H), 3.81 (s, 3H), 4.65-4.78 (m, 1H), 6.78-6.89 (m, 2H), 7.24-7.32 (m, 1H), 7.43-7.49 (m, 2H), 7.85-7.91 (m, 2H).

(4-(4-Chlorobenzoyl)piperidin-1-yl)(2-fluoro-5-methoxyphenyl)methanone (37b). 39% yield from **36b** and **30**. ^{1}H-NMR ($CDCl_3$) δ (ppm): 1.74-1.88 (bm, 3H), 1.97-2.06 (m, 1H), 3.02-3.12 (m, 1H), 3.13-3.30 (bm, 1H), 3.42-3.54 (bm, 1H), 3.66-3.75 (m, 1H), 3.80 (s, 3H), 4.66-4.76 (m, 1H), 6.85-6.93 (m, 2H), 7.01 (td, 1H, J = 8.6, 0.7 Hz), 7.46 (AA'XX', 2H, J_{AX} = 8.7 Hz, $J_{AA'/XX'}$ = 2.2 Hz), 7.88 (AA'XX', 2H, J_{AX} = 8.7 Hz, $J_{AA'/XX'}$ = 2.2 Hz).

(4-(4-Chlorobenzoyl)piperidin-1-yl)(4-iodo-3-methoxyphenyl)methanone (37c). 75% yield from **36c** and **30**. ^{1}H-NMR ($CDCl_3$) δ (ppm): 1.72-2.08 (bm, 4H), 2.97-3.24 (bm, 2H), 3.45-3.55 (bm, 1H), 3.77-4.02 (bm, 1H), 3.91 (s, 3H), 4.55-4.76 (bm, 1H), 6.73 (dd, 1H, J = 7.9, 1.7 Hz), 6.88 (d, 1H, J = 1.6 Hz), 7.47 (AA'XX', 2H, J_{AX} = 8.7 Hz, $J_{AA'/XX'}$ = 2.2 Hz), 7.80 (d, 1H, J = 7.9 Hz), 7.89 (AA'XX', 2H, J_{AX} = 8.7 Hz, $J_{AA'/XX'}$ = 2.1 Hz).

Methyl 2-amino-3-methoxybenzoate (39a). 69% yield from 2-amino-3-methoxybenzoic acid **38a**. ^{1}H-NMR ($CDCl_3$) δ (ppm): 3.87 (s, 3H), 3.88 (s, 3H), 4.90-5.45 (bs, 2H), 6.63 (t, 1H, J = 8.0 Hz), 6.88 (dd, 1H, J = 7.9, 1.3 Hz), 7.49 (dd, 1H, J = 8.2, 1.4 Hz).

Methyl 3-amino-5-methoxybenzoate (39b). 97% yield from 3-amino-5-methoxybenzoic acid **38b**. ^{1}H-NMR ($CDCl_3$) δ (ppm): 3.80 (s, 3H), 3.88 (s, 3H), 6.41 (t, 1H, J = 2.2 Hz), 6.96-6.99 (m, 2H).

Methyl 2-iodo-3-methoxybenzoate (41a). 40% yield from **39a**. ^{1}H-NMR ($CDCl_3$) δ (ppm): 3.91 (s, 3H), 3.94 (s, 3H), 6.92 (dd, 1H, J = 8.2, 1.2 Hz), 7.22 (dd, 1H, J = 7.7, 1.4 Hz), 7.34 (t, 1H, J = 7.9 Hz).

Synthesis of methyl 2-bromo-3-methoxybenzoate (41b). To a solution of **39a** (190 mg, 1 equiv) in a mixture of water (0.8 mL) and 1,4-dioxane (0.8 mL) was added dropwise 48% hydrobromic acid (0.5 mL) at room temperature and stirred for 30 min. After cooling the mixture to -5 °C, a solution of sodium nitrite (1.08 equiv) in water (0.2 mL) was added dropwise and then the reaction mixture was

stirred for 30 min at the same temperature. Then a fresh solution of copper (I) bromide (1.49 equiv) in 48% hydrobromic acid (0.3 mL) was added quickly, the reaction mixture was warmed slowly to room temperature, then heated at 110 °C for 5 h. After cooling, the mixture was diluted with water and extracted with ethyl acetate. The combined organic layer was washed with water, saturated $NaHCO_3$ solution and brine, dried over Na_2SO_4, filtered, and evaporated in vacuo. The residue was purified by flash column chromatography (silica gel) to afford bromide **41b** (50% yield). ^{1}H-NMR ($CDCl_3$) δ (ppm): 3.92 (s, 3H), 3.93 (s, 3H), 7.01 (dd, 1H, *J* = 8.0, 1.6 Hz), 7.26 (dd, 1H, *J* = 7.7, 1.7 Hz), 7.32 (t, 1H, *J* = 7.9 Hz).

Methyl 2-iodo-5-methoxybenzoate (41c). 78% yield from **40**. ^{1}H-NMR ($CDCl_3$) δ (ppm): 3.82 (s, 3H), 3.93 (s, 3H), 6.75 (dd, 1H, *J* = 8.7, 3.1 Hz), 7.34 (d, 1H, *J* = 3.1 Hz), 7.83 (d, 1H, *J* = 8.7 Hz).

Methyl 3-iodo-5-methoxybenzoate (41d). 25% yield from **39b**. ^{1}H-NMR ($CDCl_3$) δ (ppm): 3.83 (s, 3H), 3.91 (s, 3H), 7.43 (dd, 1H, *J* = 2.5, 1.5 Hz), 7.51 (dd, 1H, *J* = 2.5, 1.3 Hz), 7.96 (t, 1H, *J* = 1.4 Hz).

2-Iodo-3-methoxybenzoic acid (42a). 99% yield from **41a**. ^{1}H-NMR ($CDCl_3$) δ (ppm): 3.92 (s, 3H), 6.97 (dd, 1H, *J* = 8.1, 1.4 Hz), 7.37 (t, 1H, *J* = 7.9 Hz), 7.44 (dd, 1H, *J* = 7.7, 1.3 Hz).

2-Bromo-3-methoxybenzoic acid (42b). 95% yield from **41b**. ^{1}H-NMR ($CDCl_3$) δ (ppm): 3.94 (s, 3H), 7.07 (dd, 1H, *J* = 8.2, 1.4 Hz), 7.36 (t, 1H, *J* = 8.0 Hz), 7.49 (dd, 1H, *J* = 7.8, 1.5 Hz).

2-Iodo-5-methoxybenzoic acid (42c). 64% yield from **41c**. ^{1}H-NMR ($CDCl_3$) δ (ppm): 3.84 (s, 3H), 6.80 (dd, 1H, *J* = 8.7, 3.1 Hz), 7.55 (d, 1H, *J* = 3.1 Hz), 7.89 (d, 1H, *J* = 8.7 Hz).

3-Iodo-5-methoxybenzoic acid (42d). 99% yield from **41d**. ^{1}H-NMR (acetone-d_6) δ (ppm): 3.88 (s, 3H), 7.53-7.56 (m, 2H), 7.93 (t, 1H, *J* = 1.4 Hz).

(4-(4-Chlorobenzoyl)piperidin-1-yl)(2-iodo-3-methoxyphenyl)methanone (43a). 60% yield from **42a** and **30**. ^{1}H-NMR ($CDCl_3$; asterisk denotes isomer peaks) δ (ppm): 1.65 -1.84 (m, 2H), 1.87-2.14 (m, 2H), 3.02-3.14 (m, 1H), 3.18-3.26 (m, 1H), 3.42-3.59 (m, 2H), 3.90* (s, 3H), 3.90 (s, 3H), 4.68-4.80 (m, 1H), 6.77-6.82 (m, 1H), 6.84 (dd, 1H, *J* = 7.5, 1.3 Hz), 7.34* (t, 1H, *J* = 7.6 Hz), 7.36 (t, 1H, *J* = 7.7 Hz), 7.43-7.48 (m, 2H), 7.85-7.90 (m, 2H).

(1-(2-Bromo-3-methoxybenzoyl)piperidin-4-yl)(4-chlorophenyl)methanone (43b). 57% yield from **42b** and **30**. ^{1}H-NMR ($CDCl_3$; asterisk denotes isomer peaks) δ (ppm): 1.65-2.07 (m, 4H), 3.01-3.26 (m, 2H), 3.40-3.60 (m, 2H), 3.91* (s, 3H), 3.92 (s, 3H), 4.67-4.81 (m, 1H), 6.83* (dd, 1H, *J* = 7.6, 1.3 Hz), 6.87-6.92 (m, 2H), 7.32* (t, 1H, *J* = 7.4 Hz), 7.34 (t, 1H, *J* = 7.9 Hz), 7.43-7.48 (m, 2H), 7.84-7.90 (m, 2H).

(4-(4-Chlorobenzoyl)piperidin-1-yl)(2-iodo-5-methoxyphenyl)methanone (43c). 43% yield from **42c** and **30**. ^{1}H-NMR ($CDCl_3$; asterisk denotes isomer peaks) δ (ppm): 1.65-2.14 (bm, 4H), 3.02-3.14 (bm, 1H), 3.21-3.29 (bm, 1H), 3.44-3.62 (bm, 2H), 3.80* (s, 3H), 3.83 (s, 3H), 4.66-4.78 (bm, 1H), 6.67* (dd, 1H, *J* = 8.8, 2.9 Hz), 6.67 (dd, 1H, *J* = 8.7, 3.0 Hz), 6.74* (d, 1H, *J* = 3.0 Hz), 6.79 (d, 1H, *J* = 3.0 Hz), 7.43-7.49 (m, 2H), 7.66 (d, 1H, *J* = 8.8 Hz), 7.69* (d, 1H, *J* = 8.7 Hz), 7.86-7.91 (m, 2H).

(4-(4-Chlorobenzoyl)piperidin-1-yl)(3-iodo-5-methoxyphenyl)methanone (43d). 50% yield from **42d** and **30**. ^{1}H-NMR ($CDCl_3$) δ (ppm): 1.72-2.08 (bm, 4H), 2.96-3.24 (bm, 2H), 3.44-3.54 (bm, 1H), 3.76-3.93 (bm, 1H), 3.80 (s, 3H), 4.53-4.74 (bm, 1H), 6.89 (dd, 1H, *J* = 2.3, 1.4 Hz), 7.27-7.31 (m, 2H), 7.46 (AA'XX', 2H, J_{AX} = 8.7 Hz, $J_{AA'/XX'}$ = 2.2 Hz), 7.89 (AA'XX', 2H, J_{AX} = 8.7 Hz, $J_{AA'/XX'}$ = 2.2 Hz).

Synthesis of 1-acetylpiperidine-4-carboxylic acid (45). Isonipecotic acid **44** (2 g) and pyridine (1.25 mL) were added to 3 mL of Ac_2O at room temperature. The reaction mixture was stirred at 140 °C for 2 h and then cooled down to room temperature. The excess Ac_2O was evaporated under vacuum and then 20 mL EtOAc/diethyl ether (1:1, v:v) was added to the residue. The resulting white solid was filtered and washed with 60 mL EtOAc/diethyl ether (1:1, v:v) to give pure compound **45** (85% yield). ^{1}H-NMR ($CDCl_3$) δ (ppm): 1.60-1.77 (m, 2H), 1.93-2.02 (m, 2H), 2.10 (s, 3H), 2.59 (tt, 1H, *J* = 10.6, 4.0 Hz), 2.80-2.91 (m, 1H), 3.10-3.22 (m, 1H), 3.74-3.84 (m, 1H), 4.35-4.46 (m, 1H).

1-(4-Benzoylpiperidin-1-yl)ethanone (46a). 72% yield from **45** and benzene. ^{1}H-NMR ($CDCl_3$) δ (ppm): 1.55-2.00 (bm, 4H), 2.13 (s, 3H), 2.73-3.00 (bm, 1H), 3.08-3.37 (bm, 1H), 3.51 (tt, 1H, *J* =

10.7, 4.0 Hz), 3.80-4.05 (bm, 1H), 4.36-4.67 (bm, 1H), 7.46-7.52 (m, 2H), 7.59 (tt, 1H, *J* = 7.4, 1.5 Hz), 7.92-7.96 (m, 2H).

1-(4-(4-Methylbenzoyl)piperidin-1-yl)ethanone (46b). 56% yield from **45** and toluene. ^{1}H-NMR ($CDCl_3$) δ (ppm): 1.57-1.74 (bm, 1H), 1.77-1.95 (bm, 3H), 2.11 (s, 3H), 2.42 (s, 3H), 2.77-2.88 (bm, 1H), 3.16-3.27 (bm, 1H), 3.47 (tt, 1H, *J* = 10.8, 4.0 Hz), 3.84-3.94 (bm, 1H), 4.52-4.60 (bm, 1H), 7.26-7.30 (m, 2H), 7.84 (AA'XX', 2H, J_{AX} = 8.2 Hz, $J_{AA'/XX'}$ = 1.9 Hz).

1-(4-(4-Ethylbenzoyl)piperidin-1-yl)ethanone (46c). 76% yield from **45** and ethylbenzene. ^{1}H-NMR ($CDCl_3$) δ (ppm): 1.27 (t, 3H, *J* = 7.6 Hz), 1.56-1.96 (bm, 4H), 2.12 (s, 3H), 2.72 (q, 2H, *J* = 7.7 Hz), 2.76-2.90 (bm, 1H), 3.15-3.29 (bm, 1H), 3.48 (tt, 1H, *J* = 10.7, 4.0 Hz), 3.85-3.95 (bm, 1H), 4.50-4.62 (bm, 1H), 7.31 (d, 2H, *J* = 8.2 Hz), 7.87 (d, 2H, *J* = 8.3 Hz).

1-(4-(4-Propylbenzoyl)piperidin-1-yl)ethanone (46d). 50% yield from **45** and *n*-propylbenzene. ^{1}H-NMR ($CDCl_3$) δ (ppm): 0.95 (t, 3H, *J* = 7.4 Hz), 1.67 (sext, 2H, *J* = 7.5 Hz), 1.73-1.96 (bm, 4H), 2.11 (s, 3H), 2.65 (t, 2H, *J* = 7.6 Hz), 2.76-2.91 (bm, 1H), 3.15-3.28 (bm, 1H), 3.48 (tt, 1H, *J* = 10.7, 4.0 Hz), 3.84-3.96 (bm, 1H), 4.50-4.63 (bm, 1H), 7.28 (d, 2H, *J* = 8.4 Hz), 7.86 (AA'XX', 2H, J_{AX} = 8.3 Hz, $J_{AA'/XX'}$ = 1.8 Hz).

1-(4-(4-Isopropylbenzoyl)piperidin-1-yl)ethanone (46e). 57% yield from **45** and cumene. ^{1}H-NMR ($CDCl_3$) δ (ppm): 1.27 (d, 6H, *J* = 6.9 Hz), 1.71-1.95 (bm, 4H), 2.12 (s, 3H), 2.76-2.92 (bm, 1H), 2.97 (sept, 1H, *J* = 6.8 Hz), 3.15-3.29 (bm, 1H), 3.48 (tt, 1H, *J* = 10.7, 4.1 Hz), 3.83-3.98 (bm, 1H), 4.49-4.62 (bm, 1H), 7.33 (d, 2H, *J* = 8.2 Hz), 7.88 (AA'XX', 2H, J_{AX} = 8.4 Hz, $J_{AA'/XX'}$ = 1.8 Hz).

1-(4-(4-Butylbenzoyl)piperidin-1-yl)ethanone (46f). 50% yield from **45** and *n*-butylbenzene. ^{1}H-NMR ($CDCl_3$) δ (ppm): 0.93 (t, 3H, *J* = 7.4 Hz), 1.36 (sext, 2H, *J* = 7.4 Hz), 1.62 (quint, 2H, *J* = 7.6 Hz), 1.59-1.97 (bm, 4H), 2.11 (s, 3H), 2.67 (t, 2H, *J* = 7.7 Hz), 2.75-2.90 (bm, 1H), 3.15-3.28 (bm, 1H), 3.48 (tt, 1H, *J* = 10.7, 4.0 Hz), 3.83-3.97 (bm, 1H), 4.50-4.63 (bm, 1H), 7.28 (d, 2H, *J* = 8.4 Hz), 7.86 (d, 2H, *J* = 8.3 Hz).

1-(4-(4-Methoxybenzoyl)piperidin-1-yl)ethanone (46g). 43% yield from **45** and anisole. ^{1}H-NMR ($CDCl_3$) δ (ppm): 1.57-1.96 (bm, 4H), 2.11 (s, 3H), 2.74-2.89 (m, 1H), 3.14-3.28 (m, 1H), 3.45 (tt,

1H, *J* = 10.6, 4.1 Hz), 3.83-3.98 (bm, 1H), 3.87 (s, 3H), 4.52-4.63 (m, 1H), 6.95 (AA'XX', 2H, J_{AX} = 9.0 Hz, $J_{AA'/XX'}$ = 2.5 Hz), 7.93 (AA'XX', 2H, J_{AX} = 9.0 Hz, $J_{AA'/XX'}$ = 2.5 Hz).

1-(4-(2,3-Dihydrobenzo[b][1,4]dioxine-6-carbonyl)piperidin-1-yl)ethanone (46h). 53% yield from **45** and benzo-1,4-dioxane. ^{1}H-NMR ($CDCl_3$) δ (ppm): 1.58-1.94 (bm, 4H), 2.13 (s, 3H), 2.76-2.93 (bm, 1H), 3.08-3.30 (bm, 1H), 3.36-3.45 (m, 1H), 3.84-4.00 (bm, 1H), 4.27-4.35 (m, 4H), 4.46-4.64 (bm, 1H), 6.92 (d, 1H, *J* = 8.8 Hz), 7.46-7.51 (m, 2H).

Phenyl(piperidin-4-yl)methanone (47a). 80% yield from **46a**. ^{1}H-NMR ($CDCl_3$) δ (ppm): 1.66-1.98 (m, 4H), 2.47-2.65 (bm, 2H), 2.79-2.90 (m, 1H), 3.20-3.30 (m, 1H), 3.44 (tt, 1H, *J* = 10.6, 3.7 Hz), 7.43-7.50 (m, 2H), 7.57 (tt, 1H, *J* = 7.4, 1.7 Hz), 7.90-7.96 (m, 2H).

Piperidin-4-yl(*p*-tolyl)methanone (47b). 66% yield from **46b**. ^{1}H-NMR ($CDCl_3$) δ (ppm): 1.64-1.77 (m, 2H), 1.81-1.93 (m, 2H), 2.42 (s, 3H), 2.74-2.84 (m, 2H), 3.16-3.25 (m, 2H), 3.39 (tt, 1H, *J* = 11.1, 3.7 Hz), 7.24-7.28 (m, 2H), 7.82-7.86 (m, 2H).

(4-Ethylphenyl)(piperidin-4-yl)methanone (47c). 91% yield from **46c**. ^{1}H-NMR ($CDCl_3$) δ (ppm): 1.26 (t, 3H, *J* = 7.6 Hz), 1.63-1.75 (m, 2H), 1.81-1.94 (bm, 2H), 2.71 (q, 2H, *J* = 7.6 Hz), 2.78 (td, 2H, *J* = 12.3, 2.8 Hz), 3.19 (dt, 2H, *J* = 12.6, 3.4 Hz), 3.39 (tt, 1H, *J* = 11.3, 3.7 Hz), 7.29 (d, 2H, *J* = 8.4 Hz), 7.87 (d, 2H, *J* = 8.3 Hz).

Piperidin-4-yl(4-propylphenyl)methanone (47d). 94% yield from **46d**. ^{1}H-NMR ($CDCl_3$) δ (ppm): 0.94 (t, 3H, *J* = 7.3 Hz), 1.66 (sext, 2H, *J* = 7.5 Hz), 1.79-1.90 (bm, 4H), 2.64 (t, 2H, *J* = 7.6 Hz), 2.77 (td, 2H, *J* = 12.3, 2.6 Hz), 3.19 (dt, 2H, *J* = 12.6, 3.4 Hz), 3.38 (tt, 1H, *J* = 11.3, 3.7 Hz), 7.26 (d, 2H, *J* = 8.4 Hz), 7.86 (AA'XX', 2H, J_{AX} = 8.3 Hz, $J_{AA'/XX'}$ = 1.8 Hz).

(4-Isopropylphenyl)(piperidin-4-yl)methanone (47e). 94% yield from **46e**. ^{1}H-NMR ($CDCl_3$) δ (ppm): 1.27 (d, 6H, *J* = 6.9 Hz), 1.63-1.74 (m, 2H), 1.80-1.89 (bm, 2H), 2.77 (td, 2H, *J* = 12.3, 2.6 Hz), 2.96 (sept, 1H, *J* = 6.9 Hz), 3.19 (dt, 2H, *J* = 12.5, 3.4 Hz), 3.39 (tt, 1H, *J* = 11.3, 3.7 Hz), 7.31 (d, 2H, *J* = 8.2 Hz), 7.88 (AA'XX', 2H, J_{AX} = 8.4 Hz, $J_{AA'/XX'}$ = 1.8 Hz).

(4-Butylphenyl)(piperidin-4-yl)methanone (47f). 94% yield from **46f**. ^{1}H-NMR ($CDCl_3$) δ (ppm): 0.93 (t, 3H, *J* = 7.3 Hz), 1.36 (sext, 2H, *J* = 7.4 Hz), 1.61 (quint, 2H, *J* = 7.6 Hz), 1.66-1.75 (m, 2H),

1.80-1.95 (m, 2H), 2.66 (t, 2H, *J* = 7.7 Hz), 2.77 (td, 2H, *J* = 12.2, 2.6 Hz), 3.19 (dt, 2H, *J* = 12.5, 3.3 Hz), 3.83 (tt, 1H, *J* = 11.2, 3.6 Hz), 7.27 (d, 2H, *J* = 8.2 Hz), 7.86 (d, 2H, *J* = 8.3 Hz).

(4-Methoxyphenyl)(piperidin-4-yl)methanone (47g). 81% yield from **46g**. ^{1}H-NMR ($CDCl_3$) δ (ppm): 1.64-1.78 (m, 2H), 1.79-1.90 (m, 2H), 2.78 (td, 2H, *J* = 12.2, 2.8 Hz), 3.20 (dt, 2H, *J* = 12.7, 3.5 Hz), 3.36 (tt, 1H, *J* = 11.3, 3.7 Hz), 3.87 (s, 3H), 6.94 (AA'XX', 2H, J_{AX} = 9.0 Hz, $J_{AA'/XX'}$ = 2.5 Hz), 7.93 (AA'XX', 2H, J_{AX} = 9.0 Hz, $J_{AA'/XX'}$ = 2.5 Hz).

(2,3-Dihydrobenzo[b][1,4]dioxin-6-yl)(piperidin-4-yl)methanone (47h). 95% yield from **46h**. ^{1}H-NMR ($CDCl_3$) δ (ppm): 1.63-1.97 (m, 4H), 2.30-2.56 (bm, 2H), 2.72-2.95 (bm, 1H), 3.13-3.39 (bm, 2H), 4.23-4.38 (m, 4H), 6.91 (d, 1H, *J* = 8.8 Hz), 7.44-7.52 (m, 2H).

(4-Benzoylpiperidin-1-yl)(3-methoxyphenyl)methanone (49a). 34% yield from **47a** and **48**. ^{1}H-NMR ($CDCl_3$) δ (ppm): 1.74-2.10 (bm, 4H), 2.98-3.22 (bm, 2H), 3.50-3.60 (bm, 1H), 3.78-3.95 (bm, 1H), 3.83 (s, 3H), 4.60-4.80 (bm, 1H), 6.92-6.99 (m, 3H), 7.31 (dd, 1H, *J* = 9.0, 7.5 Hz), 7.46-7.52 (m, 2H), 7.59 (tt, 1H, *J* = 7.4, 1.5 Hz), 7.92-7.98 (m, 2H).

(1-(3-Methoxybenzoyl)piperidin-4-yl)(*p*-tolyl)methanone (49b). 37% yield from **47b** and **48**. ^{1}H-NMR ($CDCl_3$) δ (ppm): 1.73-2.08 (bm, 4H), 2.42 (s, 3H), 2.97-3.21 (bm, 2H), 3.47-3.57 (bm, 1H), 3.83 (s, 3H), 3.83-3.95 (bm, 1H), 4.60-4.76 (bm, 1H), 6.92-6.99 (m, 3H), 7.26-7.34 (m, 3H), 7.83-7.87 (m, 2H).

(4-(4-Ethylbenzoyl)piperidin-1-yl)(3-methoxyphenyl)methanone (49c). 94% yield from **47c** and **48**. ^{1}H-NMR ($CDCl_3$) δ (ppm): 1.26 (t, 3H, *J* = 7.6 Hz), 1.73-2.07 (bm, 4H), 2.71 (q, 2H, *J* = 7.6 Hz), 2.96-3.24 (bm, 2H), 3.48-3.59 (bm, 1H), 3.78-3.95 (bm, 1H), 3.83 (s, 3H), 4.60-4.77 (bm, 1H), 6.92-6.99 (m, 3H), 7.28-7.34 (m, 3H), 7.88 (AA'XX', 2H, J_{AX} = 8.4 Hz, $J_{AA'/XX'}$ = 1.8 Hz).

(1-(3-Methoxybenzoyl)piperidin-4-yl)(4-propylphenyl)methanone (49d). 89% yield from **47d** and **48**. ^{1}H-NMR ($CDCl_3$) δ (ppm): 0.95 (t, 3H, *J* = 7.3 Hz), 1.67 (sext, 2H, *J* = 7.4 Hz), 1.73-1.87 (bm, 4H), 2.65 (t, 2H, *J* = 7.6 Hz), 2.97-3.20 (bm, 2H), 3.47-3.58 (m, 1H), 3.72-4.00 (bm, 1H), 3.82 (s, 3H), 4.58-4.79 (bm, 1H), 6.92-7.00 (m, 3H), 7.27-7.33 (m, 3H), 7.87 (d, 2H, *J* = 8.2 Hz).

(4-(4-Isopropylbenzoyl)piperidin-1-yl)(3-methoxyphenyl)methanone (49e). 92% yield from **47e** and **48**. ^{1}H-NMR ($CDCl_3$) δ (ppm): 1.27 (d, 6H, *J* = 6.9 Hz), 1.74-2.09 (bm, 4H), 2.97 (sept, 1H, *J* = 6.9 Hz), 2.99-3.21 (bm, 2H), 3.48-3.59 (m, 1H), 3.77-3.97 (bm, 1H), 3.83 (s, 3H), 4.58-4.77 (bm, 1H), 6.92-6.99 (m, 3H), 7.28-7.36 (m, 3H), 7.99 (d, 2H, *J* = 8.4 Hz).

(4-(4-Butylbenzoyl)piperidin-1-yl)(3-methoxyphenyl)methanone (49f). 97% yield from **47f** and **48**. ^{1}H-NMR ($CDCl_3$) δ (ppm): 0.93 (t, 3H, *J* = 7.3 Hz), 1.36 (sext, 2H, *J* = 7.3 Hz), 1.54-1.67 (m, 2H), 1.73-1.87 (m, 3H), 1.91-2.08 (bm, 1H), 2.67 (t, 2H, *J* = 7.8 Hz), 2.96-3.24 (bm, 2H), 3.47-3.58 (m, 1H), 3.74-3.97 (bm, 1H), 3.83 (s, 3H), 4.59-4.79 (bm, 1H), 6.92-7.00 (m, 3H), 7.26-7.34 (m, 3H), 7.87 (d, 2H, *J* = 8.3 Hz).

(4-(4-Methoxybenzoyl)piperidin-1-yl)(3-methoxyphenyl)methanone (49g). 33% yield from **47g** and **48**. ^{1}H-NMR ($CDCl_3$) δ (ppm): 1.70-2.10 (bm, 4H), 2.94-3.23 (bm, 2H), 3.44-3.56 (bm, 1H), 3.77-3.96 (bm, 1H), 3.82 (s, 3H), 3.88 (s, 3H), 4.59-4.80 (bm, 1H), 6.91-7.00 (m, 5H), 7.27-7.34 (m, 1H), 7.94 (AA'XX', 2H, J_{AX} = 8.9 Hz, $J_{AA'/XX'}$ = 2.4 Hz).

(2,3-Dihydrobenzo[b][1,4]dioxin-6-yl)(1-(3-methoxybenzoyl)piperidin-4-yl)methanone (49h). 71% yield from **47h** and **48**. ^{1}H-NMR ($CDCl_3$) δ (ppm): 1.71-2.06 (bm, 4H), 2.96-3.20 (bm, 2H), 3.41-3.51 (m, 1H), 3.78-3.92 (bm, 1H), 3.83 (s, 3H), 4.27-4.35 (m, 4H), 4.60-4.76 (bm, 1H), 6.91-6.98 (m, 4H), 7.31 (dd, 1H, *J* = 8.0, 7.5 Hz), 7.48-7.52 (m, 2H).

Synthesis of ethyl piperidine-4-carboxylate (50). Isonipecotic acid **44** (500 mg, 1 equiv) was dissolved in absolute ethanol (19.4 mL). The solution was cooled to 0 °C and $SOCl_2$ (4 eq) was added dropwise. The mixture was heated at 90 °C for 3 h, then the mixture was cooled to room temperature and the solvent was evaporated in vacuo. The residue was dissolved in EtOAc and washed with a 10% aqueous solution of NaOH and with brine. The organic layer was dried and evaporated. The residue furnished the pure ethyl ester **50** (74% yield). ^{1}H-NMR ($CDCl_3$) δ (ppm): 1.25 (t, 3H, *J* = 7.1 Hz), 1.54-1.66 (m, 2H), 1.83-1.91 (m, 2H), 2.40 (tt, 1H, *J* = 11.3, 3.9 Hz), 2.62 (td, 2H, *J* = 12.0, 2.5 Hz), 3.08 (dt, 2H, *J* = 12.7, 3.8 Hz), 4.13 (q, 2H, *J* = 7.1 Hz).

Synthesis of ethyl 1-benzoylpiperidine-4-carboxylate (51). Benzoyl chloride (1 equiv) was added dropwise with stirring to a cooled solution of ethyl isonipecotate **50** (700 mg, 1 equiv) and triethylamine (1.5 equiv) in 7 mL CH_2Cl_2. Following the addition, the reaction mixture was stirred overnight, then treated with water and stirred for an additional 10 min. The mixture was diluted with CH_2Cl_2 and the layers were separated, the organic extract was washed 0.5 M HCl and with saturated sodium bicarbonate solution. After drying over anhydrous sodium sulfate, the solution was concentrated and then the residue was purified by flash column chromatography to give compound **51** (93% yield). ^{1}H-NMR ($CDCl_3$) δ (ppm): 1.26 (t, 3H, J = 7.1 Hz), 1.60-2.13 (bm, 4H), 2.57 (tt, 1H, J = 10.8, 4.1 Hz), 2.96-3.14 (bm, 2H), 3.61-3.86 (bm, 1H), 4.16 (q, 2H, J = 7.1 Hz), 4.40-4.65 (bm, 1H), 7.35-7.44 (m, 5H).

Synthesis of 1-benzoylpiperidine-4-carboxylic acid (52). The ester **51** (1.1 g, 1 equiv) was redissolved in 70% aqueous ethanol (4.4 mL). Then ground NaOH pellets (2.5 equiv) were added into the above solution. The reaction mixture was stirred overnight, evaporated, diluted with water, then followed by addition of 1 N HCl and extraction with EtOAc. The organic phase was dried over anhydrous sodium sulfate, filtered and concentrated to give carboxylic acid **52** (99% yield). ^{1}H-NMR ($CDCl_3$) δ (ppm): 1.60-2.15 (bm, 4H), 2.63 (tt, 1H, J = 10.6, 4.1 Hz), 3.00-3.16 (m, 2H), 3.64-3.87 (bm, 1H), 4.40-4.64 (bm, 1H), 7.36-7.43 (m, 5H).

(1-Benzoylpiperidin-4-yl)(4-bromophenyl)methanone (53). 43% yield from **52** and bromobenzene. ^{1}H-NMR ($CDCl_3$) δ (ppm): 1.70-2.07 (bm, 4H), 2.96-3.23 (bm, 2H), 3.43-3.54 (m, 1H), 3.76-3.98 (bm, 1H), 4.58-4.79 (bm, 1H), 7.41 (s, 5H), 7.63 (AA'XX', 2H, J_{AX} = 8.7 Hz, $J_{AA'/XX'}$ = 2.1 Hz), 7.81 (AA'XX', 2H, J_{AX} = 8.6 Hz, $J_{AA'/XX'}$ = 2.1 Hz).

Synthesis of (1-benzoylpiperidin-4-yl)(4-morpholinophenyl)methanone (54). A solution of Pd_2dba_3 (0.02 equiv), XPhos (0.08 equiv), K_3PO_4 (1.4 equiv), morpholine (1.2 equiv) and compound **53** (150 mg, 1 equiv) in toluene (0.8 mL) was stirred at 100 °C under argon in a sealed vial for 20 h. The reaction mixture was allowed to cool to room temperature, then filtered through a small pad of Celite, washed with ethyl acetate and concentrated under vacuum. The obtained crude residue was

purified by flash column chromatography to give intermediate **54** (63% yield). ^{1}H-NMR ($CDCl_3$) δ (ppm): 1.70-2.10 (m, 4H), 2.95-3.20 (bm, 2H), 3.26-3.37 (m, 4H), 3.44-3.54 (m, 1H), 3.78-4.95 (m, 5H), 4.60-4.80 (bm, 1H), 6.88 (AA'XX', 2H, J_{AX} = 9.1 Hz, $J_{AA'/XX'}$ = 2.3 Hz), 7.41 (s, 5H), 7.90 (AA'XX', 2H, J_{AX} = 9.1 Hz, $J_{AA'/XX'}$ = 2.4 Hz).

(4-Morpholinophenyl)(piperidin-4-yl)methanone (55). 72% yield from **54**. ^{1}H-NMR ($CDCl_3$) δ (ppm): 1.60-1.74 (m, 2H), 1.76-1.86 (m, 2H), 2.76 (td, 2H, *J* = 12.2, 2.7 Hz), 3.18 (dt, 2H, *J* = 12.5, 3.2 Hz), 3.26-3.40 (m, 5H), 3.82-3.90 (m, 4H), 6.88 (AA'XX', 2H, J_{AX} = 9.1 Hz, $J_{AA'/XX'}$ = 2.4 Hz), 7.90 (AA'XX', 2H, J_{AX} = 9.0 Hz, $J_{AA'/XX'}$ = 2.4 Hz).

(1-(3-Methoxybenzoyl)piperidin-4-yl)(4-morpholinophenyl)methanone (56). 99% yield from **55** and **48**. ^{1}H-NMR ($CDCl_3$) δ (ppm): 1.70-2.08 (m, 4H), 2.94-3.21 (bm, 2H), 3.28-3.35 (m, 4H), 3.43-3.54 (bm, 1H), 3.83 (s, 3H), 3.84-3.90 (m, 5H), 4.61-4.77 (bm, 1H), 6.85-6.91 (m, 2H), 6.92-6.99 (m, 3H), 7.31 (dd, 1H, *J* = 9.0, 7.5 Hz), 7.87-7.93 (m, 2H).

(1-(2-Fluoro-5-methoxybenzoyl)piperidin-4-yl)(4-isopropylphenyl)methanone (57). Yellow solid; 93% yield from **47e** and **36b**, eluent *n*-hexane/EtOAc 7:3. ^{1}H-NMR ($CDCl_3$) δ (ppm): 1.28 (d, 6H, *J* = 6.9 Hz), 1.76-1.88 (bm, 3H), 1.98-2.06 (bm, 1H), 2.97 (sept, 1H, *J* = 7.0 Hz), 3.03-3.13 (m, 1H), 3.14-3.30 (bm, 1H), 3.46-3.58 (bm, 1H), 3.65-3.75 (m, 1H), 3.80 (s, 3H), 4.66-4.75 (m, 1H), 6.85-6.92 (m, 2H), 6.97-7.04 (m, 1H), 7.33 (d, 2H, *J* = 8.2 Hz), 7.88 (AA'XX', 2H, J_{AX} = 8.4 Hz, $J_{AA'/XX'}$ = 1.9 Hz). ^{13}C-NMR ($CDCl_3$) δ (ppm): 23.78 (2C), 28.70, 28.76, 34.39, 41.58, 43.22, 46.66, 56.02, 113.06, 116.68 (d, *J* = 23.7 Hz), 117.14, 124.66 (d, *J* = 19.9 Hz), 127.04 (2C), 128.67 (2C), 133.65, 152.49 (d, *J* = 240.3 Hz), 155.00, 156.15 (d, *J* = 2.0 Hz), 165.18, 201.33. HPLC analysis: retention time = 13.261 min; peak area, 99% (254 nm). Elemental analysis for $C_{23}H_{26}FNO_3$, calculated: % C, 72.04; % H, 6.83; % N, 3.65; found: % C, 71.68; % H, 7.14; % N, 4.01.

(4-(4-Butylbenzoyl)piperidin-1-yl)(2-fluoro-5-methoxyphenyl)methanone (58). 86% yield from **47f** and **36b**. ^{1}H-NMR ($CDCl_3$) δ (ppm): 0.93 (t, 3H, *J* = 7.3 Hz), 1.36 (sext, 2H, *J* = 7.4 Hz), 1.62 (quint, 2H, *J* = 7.6 Hz), 1.73-1.88 (bm, 3H), 1.97-2.07 (bm, 1H), 2.67 (t, 2H, *J* = 7.7 Hz), 3.03-3.13

(m, 1H), 3.14-3.30 (bm, 1H), 3.45-3.58 (bm, 1H), 3.66-3.75 (m, 1H), 3.80 (s, 3H), 4.66-4.75 (m, 1H), 6.85-6.93 (m, 2H), 6.96-7.04 (m, 1H), 7.29 (d, 2H, *J* = 8.3 Hz), 7.86 (d, 2H, *J* = 8.3 Hz).

(1-(4-Fluoro-3-methoxybenzoyl)piperidin-4-yl)(4-isopropylphenyl)methanone (59). 89% yield from **47e** and **29f**. ^{1}H-NMR ($CDCl_3$) δ (ppm): 1.28 (d, 6H, *J* = 6.9 Hz), 1.74-2.00 (bm, 4H), 2.98 (sept, 1H, *J* = 6.9 Hz), 3.04-3.21 (bm, 2H), 3.49-3.59 (m, 1H), 3.81-3.99 (bm, 1H), 3.91 (s, 3H), 4.50-4.75 (bm, 1H), 6.94 (ddd, 1H, *J* = 8.2, 4.4, 2.0 Hz), 7.05-7.12 (m, 2H), 7.34 (d, 2H, *J* = 8.2 Hz), 7.89 (d, 2H, *J* = 8.4 Hz).

(4-(4-Butylbenzoyl)piperidin-1-yl)(4-fluoro-3-methoxyphenyl)methanone (60). 89% yield from **47f** and **29f**. ^{1}H-NMR ($CDCl_3$) δ (ppm): 0.94 (t, 3H, *J* = 7.3 Hz), 1.36 (sext, 2H, *J* = 7.4 Hz), 1.62 (quint, 2H, *J* = 7.6 Hz), 1.74-2.07 (bm, 4H), 2.68 (t, 2H, *J* = 7.7 Hz), 3.02-3.20 (bm, 2H), 3.49-3.59 (m, 1H), 3.80-4.00 (bm, 1H), 3.92 (s, 3H), 4.40-4.80 (bm, 1H), 6.94 (ddd, 1H, *J* = 8.2, 4.3, 2.0 Hz), 7.05-7.13 (m, 2H), 7.29 (d, 2H, *J* = 8.4 Hz), 7.87 (d, 2H, *J* = 8.3 Hz).

2. Docking Calculations. The X-ray structure of MAGL (pdb code 3PE6[45]) was downloaded from the Protein Data Bank.[46] Hydrogen atoms were added to the ligand-protein complex, which was then minimized using Amber16 software[47] and ff14SB force field at 300 K. By using TIP3P explicit solvent model, a 10 Å water cap was generated around the complex, which was thus placed at the center of a rectangular parallelepiped box of explicit water molecules. Sodium ions were then added for the neutralization of the system. The system was subjected to two steps of energy minimization. In the first step, the coordinates of the protein were restrained using a harmonic potential of 500 kcal/mol•Å^2, thus minimizing only the position of the solvent molecules. During the second step, the whole system was minimized through 5000 steps of steepest descent followed by conjugate gradient (CG), until a convergence of 0.05 kcal/Å•mol. Maestro[48] was employed to build the ligands, while Macromodel[49] was used for their minimization in water environment performed with the CG method until a convergence value of 0.05 kcal/Å•mol, MMFFs force field and a distance-dependent dielectric constant of 1.0. AUTODOCK 4.0 software[50] was employed for molecular docking. The identification of the torsion angles in the ligands, the addition of the solvent model and the determination of protein

and ligand atomic charges was carried out using Autodock Tools. Kollmann charges were assigned to the protein and Gasteiger charges to the ligand. The docking site used for calculations was defined as a box of 82, 40, and 30 points in the x, y, and z directions centered on the center of mass of the reference inhibitor ZYH. A grid spacing of 0.375 Å and a distance-dependent function of the dielectric constant were used for the energetic map calculations. The compounds were subjected to a robust docking procedure by applying 200 runs of Autodock search, using the Lamarckian Genetic Algorithm with 10 000 000 steps of energy evaluations.[51] The number of individuals in the initial population was set to 500 and a maximum of 10 000 000 generations were simulated during each docking run. Cluster analysis was performed on the results using an RMS tolerance of 2.0 Å.

Chemicalize was used for prediction of log*P* and pK_a properties, Nov, 2018, https://chemicalize.com/ developed by ChemAxon (http://www.chemaxon.com).

3. MD Simulations. Molecular dynamic simulations were performed using AMBER, version 16[47] and were carried out using the ff14SB force field at 300 K. General Amber force field (GAFF) parameters were assigned to the ligands, while partial charges were calculated using the AM1-BCC method using the Antechamber suite of AMBER 16. By using TIP3P explicit solvent model, a 20 Å water cap was generated around the complexes, which were thus placed at the center of a rectangular parallelepiped box of explicit water molecules. Sodium ions were then added for the neutralization of the systems. Prior to MD simulations, two steps of energy minimization were performed with the same procedure described above. The minimized structures of the complexes were used as the starting conformations for the MD simulations, which were run using Particle Mesh Ewald (PME) electrostatics and periodic boundary conditions. The time step of the simulations was 2.0 fs with a cutoff of 10 Å for the nonbonded interaction, while SHAKE was employed to keep all bonds involving hydrogen atoms rigid. An initial MD step of 1.0 ns with constant-volume periodic boundary conditions was performed: in this step, the temperature of the system was raised from 0 to 300 K. Subsequently, a second step of constant pressure periodic boundary MD was run for 100 ns, keeping the temperature of the system at the constant value of 300 K with Langevin thermostat. A harmonic

potential of 10 kcal/mol•Å^2 was applied on all α carbons of the protein during both MD steps. The final structure of **23**-MAGL complex corresponded to the average of the last 80.0 ns of MD minimized by the CG method until a convergence of 0.05 kcal/mol•Å^2. The average structure was obtained using the Cpptraj program[52] implemented in AMBER 16.

4. Binding Energy Evaluation. The ligand-protein binding affinity of the four ligand-protein complexes and the pairwise per-residue free energy decomposition of **23**-MAGL complex were calculated with AMBER 16 using the MM-GBSA method. The trajectories corresponding to the last 80 ns of MD simulation were used for the evaluation, which was performed on a total of 400 MD frames (one every 200 ps). MOLSURF program and the MM-PBSA module of AMBER 16 were used to calculate nonpolar and polar energies, respectively, while SANDER module estimated van der Waals, electrostatic and internal contributions. The ligand's entropy was not taken into account in the calculation.

5. MAGL inhibition assay. Human recombinant MAGL, **2** and 4-nitrophenylacetate (4-NPA) substrate were purchased from Cayman Chemical. The IC_{50} values were generated in 96-well microtiter plates. The MAGL reaction was carried out at room temperature, at a final volume of 200 μL in 10 mM Tris buffer, pH 7.2, containing 1 mM EDTA and BSA 0.1 mg/mL. A total of 150 μL of 4-NPA 133.3 μM was added to 10 μL of DMSO containing the suitable amount of compound. The reaction was initiated by the addition of 40 μL of MAGL (11 ng/well) in such a way that the assay was linear over 30 min. After the reaction had proceeded for 30 min, absorbance values were then measured by using a Victor X3 Microplates Reader (PerkinElmer®) at 405 nm.[53] Two reactions were also run: one reaction containing no compounds and the second one containing neither compound nor MAGL. IC_{50} values were derived from experimental data using the Sigmoidal dose−response fitting of GraphPad Prism software. Final values were obtained from duplicates of three independent experiments. To remove possible false positive results, for each compound concentration a blank analysis was carried out, and the final absorbance results were obtained detracting the absorbance produced by the presence of all the components except MAGL in the same conditions. In the enzyme

kinetics experiments, compound **23** was tested in the presence of scalar concentrations of 4-NPA. It was added in scalar amounts (concentration range = 1–0.125 μM) to a reaction mixture containing scalar concentrations of 4-NPA (15–1400 μM). Finally, MAGL solution was added (11 ng/well). The MAGL activity was measured by recording the increase in 4-nitrophenol absorbance using the Victor X3 Microplates Reader (PerkinElmer®). The experimental data were analyzed by non-linear regression analysis with GraphPad Prism software, using a second order polynomial regression analysis, and by applying the mixed-model inhibition fit.

6. MAGL preincubation assay. The MAGL reaction was conducted in the same conditions reported above. A total of 150 μL of MAGL (11 ng/well) was added to 10 μL of DMSO containing the appropriate amount of compound. After 0 min, 30 min, and 60 min of incubation time the reaction was initiated by the addition of 40 μL of 4-NPA 500 μM. The enzyme activity was then measured according to the procedure described above. Final values were obtained from triplicates of two independent experiments.

7. MAGL dilution assay. The enzyme (880 ng in 75 μL of Tris buffer, pH 7.2) was incubated during 60 min at room temperature with 5 μL of compound **23** (concentration of 4 μM in the mixture) dissolved in DMSO. The MAGL-inhibitor mixture was then diluted 40-fold with the buffer. After 15 min of incubation, the reaction was initiated on a 160 μL aliquot by the addition of 40 μL of 4-NPA 500 μM and the enzyme activity was measured according to the procedure described above. Final values were obtained from triplicates of two independent experiments.

8. Enzyme Activity Assays. Enzyme activity assays were performed as previously described using cell homogenates of U937 cells (FAAH) and HEK-293 cells stably transfected with ABHD6 and ABHD12 (ABHD6 and ABHD12), and intact U937 cells (MAGL).[6] Briefly, FAAH activity was determined using U937 cell homogenates (1.0×10^6 cells per sample) which were diluted in 200 mL of Tris-HCl 10 mM, EDTA 1 mM, pH 8 containing 0.1% fatty acid-free BSA and pre-incubated with the compounds at different concentrations for 15 min at 37 °C. Then, 100 nM of AEA containing 1 nM of [ethanolamine-1-^{3}H]AEA were added to the homogenates and incubated for 15 min at 37 °C.

The reaction was stopped by the addition of 400 µL of ice-cold $CHCl_3$:MeOH (1:1) and samples were vortexed and rapidly centrifuged at 16000×g for 10 min at 4 °C. The upper aqueous phase was collected in scintillation tubes and mixed with 3 mL of Ultima Gold scintillation liquid (PerkinElmer Life Sciences). The radioactivity was measured for tritium content by liquid scintillation spectroscopy. *h*ABHD6 and *h*ABHD12 activity assays were performed using cell homogenates from *h*ABHD6 and *h*ABHD12 stably transfected HEK293 cells. Compounds at the screening concentration of 10 µM were pre-incubated with 40 µg of cell homogenate for 30 min at 37 °C in assay buffer (Tris 1 mM, EDTA 10 mM plus fatty acid-free 0.1% BSA, pH 7.6). WWL70 10 µM or THL 20 µM were used as positive controls, while DMSO as vehicle control. Then, 10 µM of 2-OG was added and incubated for 5 min at 37 °C. The reaction was stopped by the addition of 400 µL of ice-cold $CHCl_3$:MeOH (1:1) and samples were vortexed and centrifuged (16000×g, 10 min, 4 °C). Aliquots (200 µL) of the aqueous phase were assayed for tritium content by liquid scintillation spectroscopy. Blank values were recovered from tubes containing no enzyme, whereas basal 2-OG hydrolysis occurring in non-transfected HEK293 cells was subtracted. For MAGL activity assay 1.0×10^6 of intact U937 cells were suspended in 400 µL of assay buffer (Tris-HCl 10 mM, EDTA 1 mM plus fatty acid-free 0.1% BSA, pH 8) in plastic tubes and incubated with different concentrations of the screening compounds at 37 °C (co-incubation). Then, 10 µM of nonradioactive (2-OG) and a small tracer (0.5 nM) of [1,2,3-^{3}H]2-OG was added and cells were incubated for 5 min at 37 °C with shaking. The reaction was stopped by the addition of 800 µL of a methanol chloroform ice-cold mixture 1:1 (v/v) and, after vigorous vortexing, aqueous and organic phases were separated by centrifugation at 10000×g, for 10 min, at 4°C. Aliquots (400 µL) of both the aqueous and organic phases were transferred in scintillation tubes and mixed with 3 mL of Ultima Gold scintillation liquid. The radioactivity associated with the [^{3}H]glycerol formation for the aqueous phase and [^{3}H]2-OG for the organic phase was measured for tritium content by liquid scintillation spectroscopy. Compounds were tested in two independent experiments, each performed in triplicates.

9. MAGL activity assay in mouse brain membrane preparations. The assay was performed similarly to the MAGL assay in U937 cells (see paragraph above). Briefly, 100 μg of mouse brain membranes were used per each sample and diluted in 245 μL of assay buffer (Tris-HCl 10 mM, EDTA 1 mM plus fatty acid-free 0.1% BSA, pH 8). In each tube, the FAAH inhibitor **URB597** (1 μM) was added in order to avoid possible 2-OG hydrolysis by FAAH. The samples were incubated with DMSO (15 min), **JZL184** 1 μM (30 min) or compound **23** (15 min) at different concentrations (0.01-30 μM) at 37 °C under shaking (400 rpm). Afterwards, the 2-OG mix (final concentration of 2-OG 10 μM with 1 nM tracer of [1,2,3-^{3}H]2-OG) was added to each sample and the reaction was stopped after 2 min of incubation at 37 °C by adding 500 μL of ice-cold chloroform-methanol solution (1:1, v/v) and placing the tubes on ice. As blank, the 2-OG mixture was added in the assay buffer without mouse brain membranes and the chloroform-methanol solution was added. The tubes were centrifuged for 10 min at 10'000 rpm at 4 °C. For all samples, an aliquot (400 μL) of the aqueous phase was transferred in a scintillation tube and mixed with 3 mL of Ultima Gold scintillation liquid and shacked for 5 min. The radioactivity associated with the [^{3}H]glycerol formation for the aqueous phase was measured for tritium content by liquid scintillation spectroscopy.

10. CB1 and CB2 binding assay. Binding assay to cannabinoid receptor 1 and 2 (CB1 and CB2) were performed as previously described.[6] Briefly, clean membranes expressing *h*CB1 or *h*CB2 were re-suspended in binding buffer (50 mM Tris-HCl, 2.5 mM EDTA, 5 mM $MgCl_2$, 0.5% fatty acid-free bovine serum albumin (BSA), pH 7.4) and incubated with vehicle or compounds and 0.5 nM of [^{3}H]CP55,940 for 90 min at 30 °C. Non-specific binding was determined in the presence of 10 μM of WIN55,512. After incubation, membranes were filtered through a pre-soaked 96-well microplate bonded with GF/B filters under vacuum and washed twelve times with 150 μL of ice-cold binding buffer. The radioactivity was measured and the results expressed as [^{3}H]CP55,940 binding. Compounds were tested, at a screening concentration of 10 μM, in two independent experiments, each performed in triplicates.

11. Competitive Activity-Based Protein Profiling (ABPP). Activity-based protein profiling (ABPP) experiments were performed using mouse brain membrane preparations at a final concentration of 2 mg/mL in PBS. Sample preparations was performed as previously described.[6] Samples (19.5 µL) were preincubated with either DMSO (vehicle control), URB597 (4 µM), JZL184 (1 µM), WWL70 (10 µM) or compound **23** (different concentrations) for 25 minutes at 25 °C under shaking and then added with TAMRA-FP probe (125 nM final concentration) and incubated for 5 minutes at 25 °C under shaking. URB597, JZL184, and WWL70 were used as positive controls for FAAH, MAGL, and ABHD6 inhibition, respectively. The reaction was stopped by adding of 10 µL of 3x Laemmli buffer and the samples kept for 3 min at room temperature, boiled for 10 min at 90 °C, cooled down to room temperature and centrifuged at 10'000 g for 1 min. The samples were loaded on a 11% SDS-PAGE gel and resolved by electrophoresis at 120 V for 180 min. The gel was scanned with a Typhoon FLA 9500 using TAMRA settings at excitation wavelength of 542 nm and emission light wavelength 568 nm. After coomassie staining and destaining, the gels were scanned in Cy5 settings. The gels were analyzed using the software ImageJ and the quantification of band intensity was performed by normalizing the values obtained for FAAH (band 1), MAGL (bands 3 and 4) and ABHD6 (band 5) with the reference band (2). The intensities were compared to DMSO sample, which reflects 100% of enzyme activity respectively and thus no inhibition of the enzymes. Data are an average of three independent gels.

12. Cell viability assay. Human breast MDA-MB-231, colorectal HCT116 and ovarian CAOV3, OVCAR3 and SKOV3 cancer cells (from ATCC) were maintained at 37 °C in a humidified atmosphere containing 5% CO_2 according to the supplier. Cells (5×10^2) were plated in 96-well culture plates. The day after seeding, vehicle or compounds were added at different concentrations to the medium. Compounds were added to the cell culture at a concentration ranging from 200 to 0.02 µM. Cell viability was measured after 96 h according to the supplier (CellTiter-Glo® luminescence assay, Promega G7571) with a Tecan M1000 PRO instrument. IC_{50} values were calculated from

logistical dose response curves. Averages were obtained from two independent experiments, each performed in triplicates, and error bars are standard deviations.

13. LC-MS/MS quantification of AEA, 2-AG, arachidonic acid and prostaglandins *in vivo* after the administration of compound 23. Male, 8-10 weeks old C57BL6 mice were provided by Janvier Labs (St Berthevin, France) and housed in groups of five per cage in a selected pathogen-free unit under controlled 12-h light/12-h dark cycle, ambient temperature 21 °C ± 1 °C humidity 40% to 50% with free access to standard rodent chow and water in accordance with the Swiss Federal guidelines. The mice were acclimatized to the animal house for 1 week before the experiment and trained to i.p. injections for 4 days (with sterile saline solution). For the experiments, mice were injected intraperitoneal (i.p,) with compound **23** at the dose of 50 mg/kg or vehicle (DMSO). The animals were sacrificed 1 h post-injection for the vehicle group and 1 h or 2 h post-injection for compound **23**. Brain and plasma were collected immediately after death, rinsed in ice-cold PBS and snap-frozen using dry ice. Samples extraction was performed as previously described.[6] Briefly, brain or plasma were weighed and transferred to extraction tubes containing three steel beads and 0.1 M formic acid for mechanic homogenization. Afterwards, the homogenates were rapidly transferred into glass tubes containing 1.5 mL of ethyl acetate:hexane (9:1) 0.1% formic acid solution and spiked with internal standards. The samples were vortexed strongly for 30 s, sonicated in cold ultrasound bath for 10 min. In order to separate the phases, samples were centrifuged at 3000 rpm for 10 min at 4 °C and kept for 1 h at -20 °C to freeze the aqueous phase. The upper organic phase was transferred in plastic tubes, evaporated and the extracted samples reconstituted in 100 µL of ACN:H_2O (8:2). 10 µL of the solution were injected in the LC-MS/MS system (5500 QTrap, AbSciex with Exion UHPLC).

14. LC-MS/MS conditions. A hybrid triple quadrupole 5500 QTRAP mass spectrometer (AB Sciex) was used with a Exion UHPLC. The column for the UHPLC was a Reprosil-PUR C18 column (3 µm particle size; 2 × 50 mm, Dr. A. Maisch HPLC GmbH, Ammerbuch-Entringen, Germany) kept at 40 °C with a mobile phase flow rate of 0.3 mL/min using a gradient with increasing organic solvent. As mobile phase a composition mixture for the negative and positive mode has been used as followed:

Negative Mode: Water, 2 mM ammonium acetate and 0.1% formic acid and acetonitrile 0.1% formic acid. Positive Mode: Water, 2 mM ammonium acetate and methanol, 2 mM ammonium acetate.

As previously published,[6] the following MRM transitions were monitored and used for quantification of the analytes: PGE2, m/z 351→271, PGD2 351→189.1 (internal standard PGE2-d4 355→319), arachidonic acid (AA) 303→59 (internal standard AA-d8 311→59), 2-AG, m/z 379→203 (internal standard 2-AG-d5 384→287), AEA 348→62 (internal standard AEA-d4 352→66). Calibration was prepared by using eleven points calibrations in the appropriate matrix. To ensure constant background concentrations of the endogenous analytes, bulk tissues were homogenized and used for validation experiments (the background was subtracted to spiked concentration levels). For the calibration curve, the concentration range as well as the quantity of internal standards were specifically designed to quantify the analytes in the biological matrix of interest. For data analysis, the ratio (Peak area under the curve analyte/peak area under the curve of internal standard) was calculated and used to ensure linearity of the method. The slope, intercept and regression coefficient of each calibration line was determined. Analyte amounts were normalized to the tissue weight respectively to the microliter of plasma extracted.

SUPPORTING INFORMATION

MM-GBSA results for the four ligand-MAGL complexes; calculated log*P* values for the reported compounds; MD simulation and H-bond analysis of **23**; docking results of compounds **13d** into MAGL; cytochrome P450 prediction for compound **23**; quantification of arachidonic acid and prostaglandin levels in plasma and brain of C57BL6 mice treated with compound **23**; concentration-dependent inhibition of 2-OG hydrolysis of compound **23** in mouse brain membrane preparations; RP-HPLC traces of final compounds; ^{1}H and ^{13}C-NMR spectra of compounds **11d**, **13b-d**, **15-19**, **23-26**; Molecular Formula Strings.

ACKNOWLEDGMENTS

We are grateful to the University of Pisa (Progetti di Ricerca di Ateneo, prog. n. PRA-2017-51 and PRA-2018-18) for funding.

ABBREVIATIONS USED

ECS, endocannabinoid system; eCBs, endocannabinoids; MAGL, monoacylglycerol lipase; AEA, anandamide; 2-AG, 2-arachidonoylglycerol; FAAH, fatty acid amide hydrolase; ABHD6, α/β hydrolase-6; ABHD12, α/β hydrolase-12; MD, molecular dynamics; 2-OG, 2-oleoyl glycerol; 4-NPA, 4-nitrophenylacetate; 4-NP, 4-nitrophenol; GAFF, General Amber force field.

AUTHOR INFORMATION

Corresponding Author

*E-mail: tiziano.tuccinardi@unipi.it. Phone: +39-050-2219595.

REFERENCES.

(1) Matsuda, L. A.; Lolait, S. J.; Brownstein, M. J.; Young, A. C.; Bonner, T. I. Structure of a Cannabinoid Receptor and Functional Expression of the Cloned CDNA. *Nature* **1990**, *346* (6284), 561–564.

(2) Munro, S.; Thomas, K. L.; Abu-Shaar, M. Molecular Characterization of a Peripheral Receptor for Cannabinoids. *Nature* **1993**, *365* (6441), 61–65.

(3) Macedonio, G.; Stefanucci, A.; Maccallini, C.; Mirzaie, S.; Novellino, E.; Mollica, A. Hemopressin Peptides as Modulators of the Endocannabinoid System and Their Potential Applications as Therapeutic Tools. *Protein Pept. Lett.* **2016**, *23* (12), 1045–1051.

(4) Maccarrone, M.; Guzmán, M.; Mackie, K.; Doherty, P.; Harkany, T. Programming of Neural Cells by (Endo)Cannabinoids: From Physiological Rules to Emerging Therapies. *Nat. Rev. Neurosci.* **2014**, *15* (12), 786–801.

(5) Chicca, A.; Marazzi, J.; Nicolussi, S.; Gertsch, J. Evidence for Bidirectional Endocannabinoid

Transport across Cell Membranes. *J. Biol. Chem.* **2012**, *287* (41), 34660–34682.

(6) Chicca, A.; Nicolussi, S.; Bartholomäus, R.; Blunder, M.; Aparisi Rey, A.; Petrucci, V.; Reynoso-Moreno, I. del C.; Viveros-Paredes, J. M.; Dalghi Gens, M.; Lutz, B.; Schiöth, H. B.; Soeberdt, M.; Abels, C.; Charles, R.-P.; Altmann, K.-H.; Gertsch, J. Chemical Probes to Potently and Selectively Inhibit Endocannabinoid Cellular Reuptake. *Proc. Natl. Acad. Sci.* **2017**, *114* (25), E5006–E5015.

(7) Ahn, K.; McKinney, M. K.; Cravatt, B. F. Enzymatic Pathways That Regulate Endocannabinoid Signaling in the Nervous System. *Chem. Rev.* **2008**, *108* (5), 1687–1707.

(8) Bisogno, T.; Petrocellis, L.; Marzo, V. Fatty Acid Amide Hydrolase, an Enzyme with Many Bioactive Substrates. Possible Therapeutic Implications. *Curr. Pharm. Des.* **2002**, *8* (7), 533–547.

(9) Lichtman, A. H. Reversible Inhibitors of Fatty Acid Amide Hydrolase That Promote Analgesia: Evidence for an Unprecedented Combination of Potency and Selectivity. *J. Pharmacol. Exp. Ther.* **2004**, *311* (2), 441–448.

(10) Mulvihill, M. M.; Nomura, D. K. Therapeutic Potential of Monoacylglycerol Lipase Inhibitors. *Life Sci.* **2013**, *92* (8–9), 492–497.

(11) Tuo, W.; Leleu-Chavain, N.; Spencer, J.; Sansook, S.; Millet, R.; Chavatte, P. Therapeutic Potential of Fatty Acid Amide Hydrolase, Monoacylglycerol Lipase, and N-Acylethanolamine Acid Amidase Inhibitors. *J. Med. Chem.* **2017**, *60* (1), 4–46.

(12) Bedse, G.; Bluett, R. J.; Patrick, T. A.; Romness, N. K.; Gaulden, A. D.; Kingsley, P. J.; Plath, N.; Marnett, L. J.; Patel, S. Therapeutic Endocannabinoid Augmentation for Mood and Anxiety Disorders: Comparative Profiling of FAAH, MAGL and Dual Inhibitors. *Transl. Psychiatry* **2018**, *8* (1), 92.

(13) Pasquarelli, N.; Engelskirchen, M.; Hanselmann, J.; Endres, S.; Porazik, C.; Bayer, H.; Buck, E.; Karsak, M.; Weydt, P.; Ferger, B.; Witting, A. Evaluation of Monoacylglycerol Lipase as a Therapeutic Target in a Transgenic Mouse Model of ALS. *Neuropharmacology* **2017**, *124*,

157–169.

(14) Pasquarelli, N.; Porazik, C.; Bayer, H.; Buck, E.; Schildknecht, S.; Weydt, P.; Witting, A.; Ferger, B. Contrasting Effects of Selective MAGL and FAAH Inhibition on Dopamine Depletion and GDNF Expression in a Chronic MPTP Mouse Model of Parkinson's Disease. *Neurochem. Int.* **2017**, *110*, 14–24.

(15) Dvoracsko, S.; Stefanucci, A.; Novellino, E.; Mollica, A. The Design of Multitarget Ligands for Chronic and Neuropathic Pain. *Future Med. Chem.* **2015**, *7* (18), 2469–2483.

(16) Monti, L.; Stefanucci, A.; Pieretti, S.; Marzoli, F.; Fidanza, L.; Mollica, A.; Mirzaie, S.; Carradori, S.; De Petrocellis, L.; Schiano Moriello, A.; Benyhe, S.; Zádor, F.; Szűcs, E.; Ötvös, F.; Erdei, A. I.; Samavati, R.; Dvorácskó, S.; Tömböly, C.; Novellino, E. Evaluation of the Analgesic Effect of 4-Anilidopiperidine Scaffold Containing Ureas and Carbamates. *J. Enzyme Inhib. Med. Chem.* **2016**, *31* (6), 1638–1647.

(17) Stefanucci, A.; Macedonio, G.; Dvorácskó, S.; Tömböly, C.; Mollica, A. Novel Fubinaca/Rimonabant Hybrids as Endocannabinoid System Modulators. *Amino Acids* **2018**, *50* (11), 1595–1605.

(18) Mollica, A.; Pelliccia, S.; Famiglini, V.; Stefanucci, A.; Macedonio, G.; Chiavaroli, A.; Orlando, G.; Brunetti, L.; Ferrante, C.; Pieretti, S.; Novellino, E.; Benyhe, S.; Zador, F.; Erdei, A.; Szucs, E.; Samavati, R.; Dvorácskó, S.; Tomboly, C.; Ragno, R.; Patsilinakos, A.; Silvestri, R. Exploring the First Rimonabant Analog-Opioid Peptide Hybrid Compound, as Bivalent Ligand for CB1 and Opioid Receptors. *J. Enzyme Inhib. Med. Chem.* **2017**, *32* (1), 444–451.

(19) Scalvini, L.; Piomelli, D.; Mor, M. Monoglyceride Lipase: Structure and Inhibitors. *Chem. Phys. Lipids* **2016**, *197*, 13–24.

(20) Granchi, C.; Caligiuri, I.; Minutolo, F.; Rizzolio, F.; Tuccinardi, T. A Patent Review of Monoacylglycerol Lipase (MAGL) Inhibitors (2013-2017). *Expert Opin. Ther. Pat.* **2017**, *27* (12), 1341–1351.

(21) Butler, C. R.; Beck, E. M.; Harris, A.; Huang, Z.; McAllister, L. A.; am Ende, C. W.; Fennell,

K.; Foley, T. L.; Fonseca, K.; Hawrylik, S. J.; Johnson, D. S.; Knafels, J. D.; Mente, S.; Noell, G. S.; Pandit, J.; Phillips, T. B.; Piro, J. R.; Rogers, B. N.; Samad, T. A.; Wang, J.; Wan, S.; Brodney, M. A. Azetidine and Piperidine Carbamates as Efficient, Covalent Inhibitors of Monoacylglycerol Lipase. *J. Med. Chem.* **2017**, *60* (23), 9860–9873.

(22) McAllister, L. A.; Butler, C. R.; Mente, S.; O'Neil, S. V.; Fonseca, K. R.; Piro, J. R.; Cianfrogna, J. A.; Foley, T. L.; Gilbert, A. M.; Harris, A. R.; Helal, C. J.; Johnson, D. S.; Montgomery, J. I.; Nason, D. M.; Noell, S.; Pandit, J.; Rogers, B. N.; Samad, T. A.; Shaffer, C. L.; da Silva, R. G.; Uccello, D. P.; Webb, D.; Brodney, M. A. Discovery of Trifluoromethyl Glycol Carbamates as Potent and Selective Covalent Monoacylglycerol Lipase (MAGL) Inhibitors for Treatment of Neuroinflammation. *J. Med. Chem.* **2018**, *61* (7), 3008–3026.

(23) Schlosburg, J. E.; Blankman, J. L.; Long, J. Z.; Nomura, D. K.; Pan, B.; Kinsey, S. G.; Nguyen, P. T.; Ramesh, D.; Booker, L.; Burston, J. J.; Thomas, E. A.; Selley, D. E.; Sim-Selley, L. J.; Liu, Q. S.; Lichtman, A. H.; Cravatt, B. F. Chronic Monoacylglycerol Lipase Blockade Causes Functional Antagonism of the Endocannabinoid System. *Nat. Neurosci.* **2010**, *13* (9), 1113–1119.

(24) Long, J. Z.; Li, W.; Booker, L.; Burston, J. J.; Kinsey, S. G.; Schlosburg, J. E.; Pavón, F. J.; Serrano, A. M.; Selley, D. E.; Parsons, L. H.; Lichtman, A. H.; Cravatt, B. F. Selective Blockade of 2-Arachidonoylglycerol Hydrolysis Produces Cannabinoid Behavioral Effects. *Nat. Chem. Biol.* **2009**, *5* (1), 37–44.

(25) Muccioli, G. G.; Labar, G.; Lambert, D. M. CAY10499, a Novel Monoglyceride Lipase Inhibitor Evidenced by an Expeditious MGL Assay. *Chembiochem* **2008**, *9* (16), 2704–2710.

(26) King, A. R.; Dotsey, E. Y.; Lodola, A.; Jung, K. M.; Ghomian, A.; Qiu, Y.; Fu, J.; Mor, M.; Piomelli, D. Discovery of Potent and Reversible Monoacylglycerol Lipase Inhibitors. *Chem. Biol.* **2009**, *16* (10), 1045–1052.

(27) Wang, L.; Wang, G.; Yang, D.; Guo, X.; Xu, Y.; Feng, B.; Kang, J. Euphol Arrests Breast Cancer Cells at the G1 Phase through the Modulation of Cyclin D1, P21 and P27 Expression.

Mol. Med. Rep. **2013**, *8* (4), 1279–1285.

(28) Yousef, B.; Hassan, H.; Zhang, L.-Y.; Jiang, Z.-Z. Anticancer Potential and Molecular Targets of Pristimerin: A Mini- Review. *Curr. Cancer Drug Targets* **2017**, *17* (2), 100–108.

(29) Chicca, A.; Marazzi, J.; Gertsch, J. The Antinociceptive Triterpene β-Amyrin Inhibits 2-Arachidonoylglycerol (2-AG) Hydrolysis without Directly Targeting Cannabinoid Receptors. *Br. J. Pharmacol.* **2012**, *167* (8), 1596–1608.

(30) Hernández-Torres, G.; Cipriano, M.; Hedén, E.; Björklund, E.; Canales, A.; Zian, D.; Feliú, A.; Mecha, M.; Guaza, C.; Fowler, C. J.; Ortega-Gutiérrez, S.; López-Rodríguez, M. L. A Reversible and Selective Inhibitor of Monoacylglycerol Lipase Ameliorates Multiple Sclerosis. *Angew. Chemie - Int. Ed.* **2014**, *53* (50), 13765–13770.

(31) Patel, J. Z.; Ahenkorah, S.; Vaara, M.; Staszewski, M.; Adams, Y.; Laitinen, T.; Navia-Paldanius, D.; Parkkari, T.; Savinainen, J. R.; Walczyński, K.; Laitinen, J. T.; Nevalainen, T. J. Loratadine Analogues as MAGL Inhibitors. *Bioorg. Med. Chem. Lett.* **2015**, *25* (7), 1436–1442.

(32) Aghazadeh Tabrizi, M.; Baraldi, P. G.; Baraldi, S.; Ruggiero, E.; De Stefano, L.; Rizzolio, F.; Di Cesare Mannelli, L.; Ghelardini, C.; Chicca, A.; Lapillo, M.; Gertsch, J.; Manera, C.; Macchia, M.; Martinelli, A.; Granchi, C.; Minutolo, F.; Tuccinardi, T. Discovery of 1,5-Diphenylpyrazole-3-Carboxamide Derivatives as Potent, Reversible, and Selective Monoacylglycerol Lipase (MAGL) Inhibitors. *J. Med. Chem.* **2018**, *61* (3), 1340–1354.

(33) Granchi, C.; Rizzolio, F.; Palazzolo, S.; Carmignani, S.; Macchia, M.; Saccomanni, G.; Manera, C.; Martinelli, A.; Minutolo, F.; Tuccinardi, T. Structural Optimization of 4-Chlorobenzoylpiperidine Derivatives for the Development of Potent, Reversible, and Selective Monoacylglycerol Lipase (MAGL) Inhibitors. *J. Med. Chem.* **2016**, *59* (22), 10299–10314.

(34) Tuccinardi, T.; Granchi, C.; Rizzolio, F.; Caligiuri, I.; Battistello, V.; Toffoli, G.; Minutolo, F.; Macchia, M.; Martinelli, A. Identification and Characterization of a New Reversible MAGL Inhibitor. *Bioorganic Med. Chem.* **2014**, *22* (13), 3285–3291.

(35) Chang, J. W.; Niphakis, M. J.; Lum, K. M.; Cognetta, A. B.; Wang, C.; Matthews, M. L.; Niessen, S.; Buczynski, M. W.; Parsons, L. H.; Cravatt, B. F. Highly Selective Inhibitors of Monoacylglycerol Lipase Bearing a Reactive Group That Is Bioisosteric with Endocannabinoid Substrates. *Chem. Biol.* **2012**, *19* (5), 579–588.

(36) King, A. R.; Lodola, A.; Carmi, C.; Fu, J.; Mor, M.; Piomelli, D. A Critical Cysteine Residue in Monoacylglycerol Lipase Is Targeted by a New Class of Isothiazolinone-Based Enzyme Inhibitors. *Br. J. Pharmacol.* **2009**, *157* (6), 974–983.

(37) Pan, P.; Sun, H.; Liu, H.; Li, D.; Zhou, W.; Kong, X.; Li, Y.; Yu, H.; Hou, T. In Silico Exploration for Novel Type-I Inhibitors of Tie-2/TEK: The Performance of Different Selection Strategy in Selecting Virtual Screening Candidates. *Sci. Rep.* **2016**, *6* (1), 37628.

(38) Wang, L.; Chen, L.; Yu, M.; Xu, L. H.; Cheng, B.; Lin, Y. S.; Gu, Q.; He, X. H.; Xu, J. Discovering New MTOR Inhibitors for Cancer Treatment through Virtual Screening Methods and in Vitro Assays. *Sci. Rep.* **2016**, *6* (1), 18987.

(39) Shao, C.-Y.; Su, B.-H.; Tu, Y.-S.; Lin, C.; Lin, O. A.; Tseng, Y. J. CypRules: A Rule-Based P450 Inhibition Prediction Server. *Bioinformatics* **2015**, *31* (11), 1869–1871.

(40) Zaretzki, J.; Matlock, M.; Swamidass, S. J. XenoSite: Accurately Predicting CYP-Mediated Sites of Metabolism with Neural Networks. *J. Chem. Inf. Model.* **2013**, *53* (12), 3373–3383.

(41) Niphakis, M. J.; Cravatt, B. F. Enzyme Inhibitor Discovery by Activity-Based Protein Profiling. *Annu. Rev. Biochem.* **2014**, *83* (1), 341–377.

(42) Blankman, J. L.; Cravatt, B. F. Chemical Probes of Endocannabinoid Metabolism. *Pharmacol. Rev.* **2013**, *65* (2), 849–871.

(43) Baggelaar, M. P.; Janssen, F. J.; van Esbroeck, A. C. M.; den Dulk, H.; Allarà, M.; Hoogendoorn, S.; McGuire, R.; Florea, B. I.; Meeuwenoord, N.; van den Elst, H.; van der Marel, G. A.; Brouwer, J.; Di Marzo, V.; Overkleeft, H. S.; van der Stelt, M. Development of an Activity-Based Probe and In Silico Design Reveal Highly Selective Inhibitors for Diacylglycerol Lipase-α in Brain. *Angew. Chemie Int. Ed.* **2013**, *52* (46), 12081–12085.

(44) Bononi, G.; Granchi, C.; Lapillo, M.; Giannotti, M.; Nieri, D.; Fortunato, S.; Boustani, M. El; Caligiuri, I.; Poli, G.; Carlson, K. E.; Kim, S. H.; Macchia, M.; Martinelli, A.; Rizzolio, F.; Chicca, A.; Katzenellenbogen, J. A.; Minutolo, F.; Tuccinardi, T. Discovery of Long-Chain Salicylketoxime Derivatives as Monoacylglycerol Lipase (MAGL) Inhibitors. *Eur. J. Med. Chem.* **2018**, *157*, 817–836.

(45) Schalk-Hihi, C.; Schubert, C.; Alexander, R.; Bayoumy, S.; Clemente, J. C.; Deckman, I.; DesJarlais, R. L.; Dzordzorme, K. C.; Flores, C. M.; Grasberger, B.; Kranz, J. K.; Lewandowski, F.; Liu, L.; Ma, H.; Maguire, D.; Macielag, M. J.; McDonnell, M. E.; Haarlander, T. M.; Miller, R.; Milligan, C.; Reynolds, C.; Kuo, L. C. Crystal Structure of a Soluble Form of Human Monoglyceride Lipase in Complex with an Inhibitor at 1.35 Å Resolution. *Protein Sci.* **2011**, *20* (4), 670–683.

(46) Berman, H. M. The Protein Data Bank. *Nucleic Acids Res.* **2000**, *28* (1), 235–242.

(47) D.A. Case, V. Babin, J.T. Berryman, R.M. Betz, Q. Cai, D.S. Cerutti, T.E. Cheatham, III, T.A. Darden, R. E.; Duke, H. Gohlke, A.W. Goetz, S. Gusarov, N. Homeyer, P. Janowski, J. Kaus, I. Kolossváry, A. K.; T.S. Lee, S. LeGrand, T. Luchko, R. Luo, B. Madej, K.M. Merz, F. Paesani, D.R. Roe, A. Roitberg, C. S.; R. Salomon-Ferrer, G. Seabra, C.L. Simmerling, W. Smith, J. Swails, R.C. Walker, J. Wang, R.M. Wolf, X.; Kollman, W. and P. A. AMBER. version 16; University of California: San Francisco, CA, 2016.

(48) *Maestro*, version 9.0; Schrödinger Inc: Portland, OR, 2009.

(49) *Macromodel*, version 9.7; Schrödinger Inc: Portland, OR, 2009

(50) Morris, G. M.; Ruth, H.; Lindstrom, W.; Sanner, M. F.; Belew, R. K.; Goodsell, D. S.; Olson, A. J. AutoDock4 and AutoDockTools4: Automated Docking with Selective Receptor Flexibility. *J. Comput. Chem.* **2009**, *30* (16), 2785–2791.

(51) Poli, G.; Gelain, A.; Porta, F.; Asai, A.; Martinelli, A.; Tuccinardi, T. Identification of a New STAT3 Dimerization Inhibitor through a Pharmacophore-Based Virtual Screening Approach. *J. Enzyme Inhib. Med. Chem.* **2016**, *31* (6), 1011–1017.

(52) Roe, D. R.; Cheatham, T. E. PTRAJ and CPPTRAJ: Software for Processing and Analysis of Molecular Dynamics Trajectory Data. *J. Chem. Theory Comput.* **2013**, *9* (7), 3084–3095.

(53) Granchi, C.; Caligiuri, I.; Bertelli, E.; Poli, G.; Rizzolio, F.; Macchia, M.; Martinelli, A.; Minutolo, F.; Tuccinardi, T. Development of Terphenyl-2-Methyloxazol-5(4H)-One Derivatives as Selective Reversible MAGL Inhibitors. *J. Enzyme Inhib. Med. Chem.* **2017**, *32* (1), 1240–1252.

TABLE OF CONTENTS GRAPHIC